Hearing Loss and Schizophrenia-Relevant Cortical and Behavioral Abnormalities in a Mouse Model of 22q11.2 Deletion Syndrome

A thesis submitted to the University College London for the degree of
Doctor of Philosophy in Neuroscience

23 January, 2019

Fhatarah A. Zinnamon, ucbtfaz@ucl.ac.uk

Supervisors
Prof Jennifer Linden, j.linden@ucl.ac.uk
Dr Kuan Hong Wang, wkuan@mail.nih.gov

UCL/NIMH Joint Doctoral Training Program in Neuroscience
UCL Ear Institute and Division of Psychology and Language Sciences
Unit on Neural Circuits and Adaptive Behaviors, NIMH

Declaration

I, Fhatarah A. Zinnamon, confirm that the work presented in this thesis is my own. Where information has been derived from other sources, I confirm that this has been indicated in the thesis.

Signed: Date: 23/1/2019

Abstract

Patients with 22q11.2 Deletion Syndrome (22q11DS) have a 25-30% chance of developing schizophrenia and exhibit high rates of conductive hearing loss (HL). HL has been identified as a risk factor for schizophrenia, but the reasons for this association---and its relevance to developmental neuro-behavioral abnormalities in 22q11DS---are unknown.

In this thesis, I used the *Df1*/+ mouse model of 22q11DS to investigate interactions between genetic risk for schizophrenia, HL, and brain and behavioral abnormalities. *Df1*/+ mice have a multi-gene deletion analogous to human 22q11DS and ~60% of animals display conductive HL.

First, I asked whether genotype, HL or both affect sensorimotor gating, cortical auditory evoked potentials (AEPs), or parvalbumin-positive (PV+) inhibitory interneuron density in the primary auditory cortex (A1) using auditory brainstem response measurements (ABRs), prepulse inhibition of the acoustic startle response, auditory evoked potentials (AEPs) and immunohistochemistry. Results indicated that HL in *Df1*/+ mice was associated with altered central auditory gain, auditory sensorimotor gating and PV+ interneuron density in A1.

Next, I characterized the development of HL in *Df1*/+ mice over postnatal weeks 3-14.6 using ABRs and distortion product otoacoustic emissions. Results showed that HL onset and duration within *Df1*/+ animals were variable but more likely to be persistent (versus transient), first appearing during postnatal development as opposed to adulthood.

Lastly, I investigated the origins of synaptic projections to PV+ interneurons in A1 using modified retrograde rabies virus. Results revealed consistent projection patterns originating within the auditory thalamus and basal forebrain for both anterior and posterior A1 injection locations. This tracing approach holds promise for future experiments comparing projections to PV+ interneurons in wildtype and *Df1*/+ mice with and without HL.

Work presented in this thesis provides evidence for bottom-up neurobiological mechanisms through which HL arising from 22q11DS may promote the emergence of schizophrenia-relevant auditory brain and behavioral abnormalities.

Impact statement

22q11.2 Deletion Syndrome (22q11DS) is one of the most common congenital chromosomal abnormalities, occurring in 1 out of 4000 live births. It is also second highest risk factor for developing schizophrenia (only having a monozygotic twin or two schizophrenic parents increases the probability), as up to 30% of patients with 22q11DS develop schizophrenia. Thus, the disorder is of particular interest as a model of the pathogenesis of schizophrenia.

The *Df1*/+ mouse model of 22q11DS recapitulates many features of human 22q11DS and schizophrenia. These include abnormalities in auditory sensorimotor gating and increased susceptibility to middle ear inflammation (otitis media), which can cause conductive hearing loss. Hearing loss has been described as a "neglected risk factor for psychosis," as it increases the risk of developing psychosis and hallucinations. Additionally, an imbalance of excitation and inhibition in cortical circuits caused by deficits in inhibitory interneuron development is thought to play a role in the cause of psychosis and cognitive dysfunction in schizophrenia. This mouse model therefore has the potential to provide unparalleled insight into the nature of brain abnormalities associated with hearing loss and the emergence of brain abnormalities in 22q11DS and schizophrenia. The current study is the first to link a reduction in parvalbumin-positive inhibitory interneurons in the primary auditory cortex, hearing loss and altered cortical activity and behavior in a mouse model with elevated genetic risk for schizophrenia.

The potential implications of this study's link between conductive hearing loss and cortical interneuron density for both human 22q11DS patients and those who suffer from hearing loss during development are profound. Otitis media is the most common disease in young children across the world and occurs at least once before the age of two in 80% of infants. Approximately 40-70% of children with 22q11DS suffer from persistent ear inflammation due to otitis media. This work suggests that elevated hearing thresholds that result from conductive hearing loss can significantly alter response properties of neurons within the auditory cortex. Reasons for the association could include common

etiology, bottom-up changes in neuronal networks driven by loss of sensory input, and top-down changes in cognition driven by difficulty with social communication. Future studies based upon the results of this thesis could impact both academic and clinical schizophrenia fields.

The incidence of schizophrenia in 22q11DS during adulthood might be reduced by earlier and more aggressive treatment of chronic otitis media in childhood. Follow-up studies based upon this thesis can inform how hearing loss could be handled, perhaps with a focus on earlier detection. The *Df1*/+ mouse and other mouse models of 22q11DS may help to reveal how hearing loss alone or its interaction with other schizophrenia risk factors produce brain and behavioral abnormalities underlying psychiatric disease, and how to best handle their occurrence. In the long term, this project could contribute to development of medical interventions designed to correct abnormalities in cortical circuit function that underlie cognitive deficits in schizophrenia.

Declaration **2**

Abstract **3**

Impact statement **5**

Chapter 1: General introduction and literature review **12**
1.1 Schizophrenia and 22q11DS **12**
1.2 Genetics of 22q11DS **16**
1.2.1 *TBX1* 16
1.2.2 GWAS and CNVs 18
1.2.3 Genes within the 22q11.2 deleted region associated with schizophrenia 19
1.3 Schizophrenia hypotheses and parvalbumin-positive interneurons **22**
1.4 *Df1*/+ mouse model of 22q11DS **26**
1.5 Prepulse inhibition in schizophrenia, 22q11DS and the *Df1*/+ mouse **29**
1.6 Middle ear infection and hearing loss in schizophrenia, 22q11DS and *Df1*/+ mice **31**
1.7 Auditory Brainstem Responses (ABRs) and Auditory Evoked Potentials (AEPs) **36**
1.8 Viral-based neural tracing **39**
1.9 Aims **40**

Chapter 2: Materials and methods **42**
2.1 University College London (UCL) experiments **42**
2.1.1 Animals 42
2.1.2 Pilot experiments (referenced in appendix 1) 43
2.1.3 Auditory brainstem response (ABR) recording 43
2.1.4 Perfusion 45
2.1.5 Tympanic membrane scoring 45
2.1.6 Histology 46
2.1.7 Nissl staining 47
2.1.8 Parvalbumin staining 47
2.1.9 Anterior-posterior localisation of sections relative to Bregma 48
2.1.10 Imaging 49
2.1.11 Image processing and cell counting 49
2.1.12 Data analysis 51
2.1.13 Revision of M2 target locations based on Allen Brain Atlas and viral vector experiments 52
2.1.14 Identifying sections at the A-P locations M2 and A1 55
2.1.15 Automated cell counting 56
2.2 Follow up study: Hearing loss promotes schizophrenia-relevant brain and behavioral abnormalities in a mouse model of human 22q11.2 Deletion Syndrome **57**
2.2.1 Animals 57
2.2.2 Acoustic startle response (ASR) and prepulse inhibition (PPI) testing 57
2.2.3 Auditory brainstem response (ABR) and auditory evoked potential (AEP) recording 59
2.2.4 Histology, immunohistochemistry and microscopy 60
2.2.5 Data analysis 60
2.2.6 Startle data analysis 61
2.2.7 ABR/AEP data analysis 62
2.2.8 Quantification of cell counts 63
2.3 National Institute of Mental Health (NIMH) experiments **65**

2.3.1 Animals 65
2.3.2 Longitudinal hearing loss experiments 65
2.3.3 Distortion-product otoacoustic emissions (DPOAEs) and ABR recording 65
2.3.4 Monosynaptic retrograde tracing experiments 67
2.3.5 Viral vector injection and surgery 68
2.3.6 Histology, immunohistochemistry and microscopy 69
2.3.7 Quantification of viral vector cell counts 69

Chapter 3: Hearing loss promotes schizophrenia-relevant brain and behavioral abnormalities in a mouse model of human 22q11.2 Deletion Syndrome (under review at Journal of Neuroscience) 71
3.1 Introduction 71
3.2 Results 73
3.2.1 *Df1*/+ mice exhibit hearing loss in 60% of animals (54% of ears) 73
3.2.2 ABR Wave I amplitude reductions in *Df1*/+ mice with hearing loss are not maintained in cortical AEPs 75
3.2.3 *Df1*/+ mice with hearing loss show elevation of central auditory gain 80
3.2.4 *Df1*/+ mice exhibit abnormal PPI of ASR for prepulse cues with fixed absolute sound level, but not for cues adjusted relative to startle threshold 82
3.2.5 *Df1*/+ mice with hearing loss show reduced density of PV+ but not NeuN+ cells in auditory cortex 88
3.2.6 *Df1*/+ mice do not show abnormalities in PV+ or NeuN+ cell density in M2, nor changes in laminar distributions of PV+ cells in A1 90
3.3 Discussion 94
3.3.1 Hearing loss in mouse models of 22q11DS 94
3.3.2 Central auditory abnormalities in mouse models of 22q11DS 96
3.3.3 Auditory sensorimotor gating in mouse models of 22q11DS 98
3.3.4 Parvalbumin-positive cortical interneurons and hearing loss 99
3.3.5 Parvalbumin-positive cortical interneurons in mouse models of 22q11DS 100
3.3.6 Implications for schizophrenia research 101

Chapter 4: Characterization of hearing loss in *Df1*/+ mice 103
4.1 Introduction 103
4.2 Results 104
4.2.1 ABR click thresholds indicate that 76% of Df1/+ animals have hearing loss at any given point 104
4.2.2 No WT animals display elevated thresholds to ABR 8k tone stimuli, while approximately 62% of *Df1*/+ have hearing loss 106
4.2.3 16k ABR tone thresholds are elevated in approximately 54% of *Df1*/+ mice, WT display no hearing loss 108
4.2.4 ABR 32k tone thresholds indicate hearing loss in 14% of WT mice and 23% of *Df1*/+ mice 109
4.2.6 DPOAEs 116
4.3 Discussion 116
4.3.1 Otitis media in *Df1*/+ mice 117
4.3.2 DPOAEs vs ABRs 118
4.3.3 Duration of hearing loss in *Df1*/+ mice 119

Chapter 5: Viral-based neuronal tracing of PV+ neurons within the auditory cortex 121
5.1 Introduction 121
5.2 Results 124

5.2.1 Monosynaptic input tracing using PV-Cre/*Df1*/+ mice demonstrates basal forebrain and auditory thalamus projections to A1 124
5.2.2 Both A1 injection sites revealed a similar number of AAV stained PV+ cells 126
5.2.3 No difference was found in the amount of connections traced from the auditory thalamus in the anterior A1 injection site 127
5.3 Discussion 128

Chapter 6: Summary, limitations and future directions 130
6.1 Summary 130
6.2 Limitations of this PhD study 132
6.3 Future directions 133

Appendix 1: Pilot studies of hearing loss assessment and PV+ cortical interneuron density in *Df1*/+ mice 137
Introduction 137
Results 138
Tympanic membrane scoring and ABR measurements 138
PV+ cell counts in A1 139
PV+ cell counts in M2 141
PV+ cell counts in A24b 142
Implications for future study (Chapter 3) 143

References 146

List of Figures and Tables

Figure	Page
Figure 1.1 Typical and atypical deleted regions of 22q11DS	16
Figure 1.2 Parvalbumin positive interneurons exert spatiotemporal control upon pyramidal cells	24
Figure 1.3 Mouse models of 22q11DS	28
Figure 1.4 Prepulse inhibition paradigm	30
Figure 1.5 Otitis media with effusion	33
Figure 1.6 Anatomy of the ascending auditory pathway	37
Figure 2.1 Determination of ABR thresholds	45
Figure 2.2 Examples of tympanic membrane scoring	46
Figure 2.3 Example of A1 identification in Nissl-stained section	48
Figure 2.4 Example of frontal cortex (A24b, M2) identification in Nissl-stained sections	49
Figure 2.5 PV+ A1 counting area	50
Figure 2.6 PV+ frontal counting areas	51
Figure 2.7 Brightest fluorescence of viral vector in M2	54
Figure 2.8 Comparison of results from manual cell counting and automated cell counting algorithm	56
Table 2.1 Numbers of mice and brain hemispheres used for analyses of PV+ and NeuN+ cell density and laminar distribution	64
Table 2.2 Numbers of mice, hearing loss profile and A1 injection site used in analyses of monosynaptic retrograde tracing experiments	70
Figure 3.1 Elevated auditory brainstem response (ABR) thresholds in *Df1*/+ mice	74
Figure 3.2 Average ABR and auditory evoked potential (AEP) waveforms in WT and *Df1*/+ mice	76
Figure 3.3 Reductions in ABR wave I amplitude in *Df1*/+ mice with hearing loss are not maintained in cortical AEPs	77
Figure 3.4 No significant differences between *Df1*/+ and WT mice in ABR wave I latency or AEP P1, N1 or P2 latencies	79
Figure 3.5 Central auditory gain is elevated in Df1/+ mice with hearing loss	81
Figure 3.6 Example acoustic startle responses and prepulse inhibition (PPI) of startle in WT and Df1/+ mice	84
Figure 3.7 Population analysis of acoustic startle response and prepulse inhibition of startle in WT and Df1/+ mice	86
Figure 3.8 PV+ cell density is reduced in the auditory cortex but not the motor cortex of Df1/+ mice	89
Figure 3.9 NeuN+ cell density is not reduced in the auditory cortex or the motor cortex of Df1/+ mice	91
Figure 3.10 Df1/+ mice with hearing loss have minimal differences in laminar distribution of PV+ cells in A1 or M2	93
Figure 4.1 No WT mice and 76% of Df1/+ mice show hearing loss to click ABR stimuli that first appears more often during development and is persistent	106
Figure 4.2 Approximately 62% of Df1/+ mice have elevated 8k tone ABR thresholds that first appear during development and are persistent, WT animals show no hearing loss	107
Figure 4.3 No WT mice and approximately 54% of Df1/+ mice show hearing loss to 16k tone ABR stimuli that first appears more often during development and is persistent	109
Figure 4.4 ABR responses to 32k tones revealed approximately 14% of WT mice and 23% of Df1/+ mice show hearing loss	110
Figure 4.5 ABR responses to 40k frequency tones show that approximately 43% of WT mice and 23% of Df1/+ mice show hearing loss	112
Figure 4.6 Even WT thresholds are increased at higher tone frequencies	113
Figure 4.7 Df1/+ testing sessions indicate animals have hearing loss at all frequencies	114

Table 4.1 ABR thresholds increase with frequency tested	116
Figure 5.1 Diagram of TVA and RVdG viral injections and infection	122
Figure 5.2 BF and auditory thalamic neurons target both anterior and posterior A1 locations	125
Figure 5.3 TVA, RV infected and starter cell identification	126
Figure 5.4 No difference in numbers of TVA+, RV-infected or starter cells in anterior vs posterior injection site	127
Figure 5.5 No differences in the number of RV-labelled cells from the auditory thalamus or BF regardless of injection site	128
Table A.1 ABR thresholds were not correlated with tympanic membrane scores	139
Figure A.1 Results indicated a significant reduction in PV+ cell counts in A1 of Df1/+ mice relative to WT mice	140
Figure A.2 The reduction in A1 PV+ cell counts showed some correlation with increased ABR thresholds in the contralateral ear (in WT mice) and the ipsilateral ear (for Df1/+ mice)	140
Figure A.3 No significant difference between Df1/+ and WT mice was found for PV+ cell counts within the motor cortex	141
Figure A.4 Reductions in PV+ cell counts in M2 were not correlated with increased ABR thresholds in either the contralateral or ipsilateral ear	141
Figure A.5 No significant difference between Df1/+ and WT mice was found in PV+ cell counts within the cingulate cortex	142
Figure A.6 No significant correlation between PV+ cell counts in A24b and ABR thresholds in either the contralateral or ipsilateral ear	142
Figure A.7 ABRs were repeatable	145

Chapter 1: General introduction and literature review

1.1 Schizophrenia and 22q11DS

Schizophrenia is a severe brain disorder characterized by symptoms in three domains: negative symptoms (i.e., lack of motivation, lack of emotional reactivity, social withdrawal, flattening of affect, apathy, poverty of speech), positive symptoms (i.e., hallucinations, delusions, and dissociative thinking), and cognitive deficits (i.e., abnormal working memory, attention, and executive function) (Breedlove et al., 2010). Schizophrenia is one of the most devastating disorders of humankind and afflicts about 1% of the population worldwide, while another 2-3% of the general population have schizotypal personality disorder. As such, the disorder exacts a huge toll on those diagnosed, their loved ones, society and the economy as a whole. In 2002, the annual estimated cost of caring for patients with schizophrenia in the United States was $62.7 billion (McEvoy, 2007; Wu et al., 2005). It is estimated that approximately 30% of all the homeless people in the United States have schizophrenia (Kandel et al., 2000). Additionally, patients diagnosed with schizophrenia have a 2- to 3-fold increased risk of dying and die 12–15 years earlier than the average population due to comorbid conditions. This difference in mortality has been increasing in recent decades, causing the disease to result in more loss of lives than most cancers and physical illnesses (Saha et al., 2007). The high prevalence and exorbitant societal cost have led to increased efforts towards understanding the mechanisms of schizophrenia in order to develop effective treatments for all three domains of psychopathology.

Currently, despite the availability of antipsychotic therapy, cognitive impairment in schizophrenia remains largely untreatable. Patients with schizophrenia often have impairments in attention, memory and executive function, in addition to deficits on tasks related to frontal and temporal lobe functioning including processing speed, verbal fluency, verbal memory, and learning (Lesh et al., 2011). These cognitive deficits are present in schizophrenia regardless of illness stage, and the degree of neurocognitive function (secondary verbal memory, immediate memory, vigilance, and executive function) is one of the

best predictors of long-term functional outcome for patients with schizophrenia (Green et al., 2000; Lesh et al., 2011; Lewis et al., 2012). Cognitive symptoms therefore appear to be core to schizophrenia pathophysiology; however, no effective treatments for these symptoms currently exist. Most treatments for schizophrenia alleviate symptoms such as psychosis and anhedonia, but do not correct the pervasive cognitive deficits that are most predictive of adverse long-term outcomes in patients. Recently there has been an increase in the amount of research into the pathophysiological mechanisms underlying the aetiology of these symptoms and effective treatment options.

One of the most challenging aspects of schizophrenia research has been identifying its causes and understanding the disease process. Complex and variable combinations of environmental and genetic risk factors combine to alter the development, structure and function of the brain, which create the characteristic symptoms seen in schizophrenic patients. Traditional medical genetics approaches such as population, family, twin, and adoption studies combined with novel linkage analysis and allelic association studies have highlighted the high heritability of the disease. The first evidence of schizophrenia's heritability came from Franz Kallman in the 1930's. Kallman found that even though environmental factors vary greatly, the incidence of schizophrenia is 1% throughout the entire population of the world, but the incidence of schizophrenia among parents, children, and siblings of patients with the disease is about 15% (Kallmann, 1938). Through the study of monozygotic (identical twins that have essentially identical genomes and share almost 100% of each other's genes) and dizygotic twins (fraternal twins that have only half of their genes in common and are genetically equivalent to siblings), it was established that while the concordance, or tendency for twins to develop the same illness, for schizophrenia in monozygotic twins is about 45%, in dizygotic twins it is only about 15%. Twin adoptee studies further disentangled hereditary and experiential factors. A higher incidence of schizophrenia among first-order relatives as opposed to second-order or third-order relatives was found (Gottesman and Wolfgram, 1991). The risk of developing schizophrenia is proportional to how genetically related one is to an

affected individual (Lewis et al., 2005). The significantly higher rate of concordance among monozygotic twins and the higher incidence of schizophrenia in relatives of patients indicates a strong genetic factor, but the disease cannot be solely due to genetic causes since identical twins don't have identical incidence of the development of schizophrenia (Breedlove et al., 2010; Kandel et al., 2000; Lewis et al., 2005).

The reason for this non-Mendelian genetic transmission lies in the fact that the disease is polygenic, meaning that it involves multiple genes. The development of advanced genomic technologies and their applications to large samples have led to the identification of several genes involved in the susceptibility of schizophrenia. Genome wide association and copy number variant studies have identified several candidate genes. It has become apparent that the disease comes in many genetic forms, some inherited and some de novo mutations. However, the genetic abnormality most strongly associated with schizophrenia is located on chromosome 22.

22q11.2 Deletion Syndrome (22q11DS) is a genetic syndrome that results from a 1.5-3Mb congenital multigene deletion on the long arm (q) of chromosome 22 within the area 11.2 (Scambler, 2000). It is the second most common chromosomal disorder after Down's Syndrome, and occurs in 1:4,000 live births (Jonas et al., 2014). The deletion in children is associated with significantly higher levels of autism spectrum symptoms (in up to 40% of patients), attention deficit hyperactivity disorder, anxiety disorders, affective disorders such as bipolar disorder and depression and psychotic features (Arinami, 2006; Gothelf et al., 2004). Additionally, it is one of few cytogenetic abnormalities that occurs in tandem with a psychiatric disease and elevated risk of psychopathology (Paylor and Lindsay, 2006; Torres et al., 2016). In particular, 22q11DS is the second highest risk factor for developing schizophrenia (only having a monozygotic twin or two schizophrenic parents increases the probability, and both of these occurrences are very rare). Fully 25-30% of adults with 22q11DS develop schizophrenia during adolescence or adulthood (Sivagnanasundaram et al., 2007), and patients with schizophrenia are 20 to 80 times more likely to

have the 22q11.2 microdeletion relative to the general population (Arinami, 2006). Up to 6% of patients with childhood-onset schizophrenia have 22q11DS (Usiskin et al., 1999), and 22q11DS accounts for up to 1-2% of sporadic cases of schizophrenia (Jonas et al., 2014). Approximately 5-10% of deletions are inherited (Scambler, 2000). The schizophrenic phenotypes of individuals with and without the 22q11.2 deletion do not differ significantly (Bassett et al., 2003) and 22q11DS is considered as a genetic subtype of schizophrenia (Bassett and Chow, 1999; Torres et al., 2016). Thus, it is of particular interest as a model of the pathogenesis of schizophrenia.

22q11DS creates a constellation of phenotypes that can lead to multiple diagnoses including velocardiofacial syndrome (VCFS), DiGeorge syndrome (DGS), conotruncal anomaly face syndrome, Shprintzen syndrome, CATCH 22 syndrome, and Cayler cardiofacial syndrome among others. 22q11DS is accompanied by an array of over 100 different malformations and clinical presentations including, cognitive disorders and neurocognitive disabilities (affecting 80–100% of sufferers), palatal anomalies (69–100%) such as submucosal and hard palate clefts, velopharyngeal insufficiency, delay in speech, language and motor development, serious heart defects, immune compromise, auricular anomalies (such as small or round ears, external ear defects, and thick helices), chronic otitis media, and both conductive and sensorineural hearing loss, along with elevated rates of psychopathology and mental illness (Digilio et al., 1999; Fuchs et al., 2015; Long et al., 2006; Oskarsdottir et al., 2005; Papangeli and Scambler, 2013; Umlauf, 2008).

The deletion leaves sufferers with only one copy rather than two copies of certain genes. The majority of 22q11DS patients (around 85%) have the full 3Mb deletion which 90 genes are absent, while the remainder have either the smaller 1.5 Mb deletion that deletes only 28 genes, or atypical deletions (Guna et al., 2015; Torres et al., 2016). However, the size of the deletion does not correlate with the severity or penetrance of the disease (Papangeli and Scambler, 2013). Approximately 93% of cases are de novo, while 7% of patients have inherited the deletion (McDonald-McGinn et al., 2013). Genetic

association studies indicate that a number of genes deleted in 22q11DS are likely to contribute to both the key phenotypes of the syndrome as well as schizophrenia.

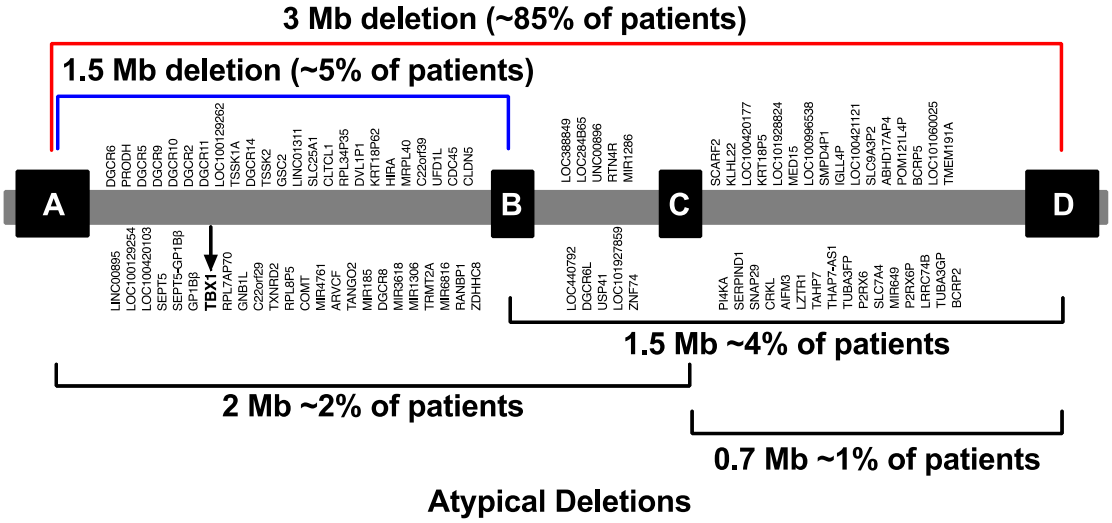

Figure 1.1 Typical and atypical deleted regions of 22q11DS

Genes deleted within the human 22q11.2 locus. 22q11.2 is one of the most structurally complex areas of the genome due to several large blocks of low copy repeats (LCRs) (McDonald-McGinn et al., 2015). These LCRs A, B, C, and D are common breakpoints on human chromosome 22q11.2 and are >96% identical, making the locus vulnerable to meiotic error. *TBX1* is highlighted in bold with an arrow, which is deleted in both the larger 3Mb deletion (highlighted in red) as well as the more common of the smaller 1.5Mb deletions (highlighted in blue). Original figure.

1.2 Genetics of 22q11DS

1.2.1 *TBX1*

TBX1 and plays an important role in the pathogenesis of 22q11DS. *TBX1* encodes DNA binding proteins that function as transcription factors important in many developmental processes, with multiple sites of expression and roles in a wide variety of tissues. This gene is a member of the T-Box gene family. Consisting of 17 genes, the family is highly conserved and is found in virtually all metazoan species (Douglas et al., 2015; Fernandez et al., 2015; Heike et

al., 2010). *TBX1* is deleted in both the 3Mb and the 1.5Mb common versions of the human 22q11.2 deletion, and therefore most patients display haploinsufficiency for *TBX1*. Haploinsufficiency occurs when a mutation in one copy of the gene leads to its inactivation, leaving only a single functional copy that is inadequate for normal functioning and leads to an altered phenotypic state (Douglas et al., 2015). The haploinsufficiency of *TBX1* is regarded as one of the major genetic causes of the 22q11DS and affects pharyngeal, heart, ear, skeletal and brain development during embryogenesis to cause the core physical malformations associated with 22q11DS in mice and humans, including abnormal facial features, cardiac defects, thymic hypoplasia, velopharyngeal insufficiency of the cleft palate, parathyroid dysfunction with hypocalcaemia (Douglas et al., 2015; Funke et al., 2007; Ma et al., 2007; Torres et al., 2016). *TBX1* is also implicated in abnormalities of the ear which can lead to increased incidence of hearing loss, which is discussed in later chapters. During development *TBX1* is expressed in nearly all of the affected areas in 22q11DS.

Although responsible for the major phenotypic features of 22q11DS, *TBX1* is not thought to be responsible for the cognitive and neuropsychiatric features common to the syndrome (Torres et al., 2016). Due to the possibility that 22q11DS and schizophrenia share some developmental origins, multiple studies have investigated whether *TBX1* plays a role in the development of schizophrenia. In a sample of Chinese schizophrenic patients, genetic polymorphisms within *TBX1* were screened and in fact do not correlate with increased susceptibility to schizophrenia (Ma et al., 2007). Another study matched white patients with diagnoses of schizophrenia, schizoaffective disorder, bipolar disorder, and major depressive disorder to controls and analyzed single nucleotide polymorphisms (SNPs) at the *TBX1* locus to discover no differences between those with psychiatric disorders compared to controls (Funke et al., 2007). (SNPs are a common genetic variation that occur in most people, and represent a difference in a single nucleotide in relevant DNA that can act as a biological marker when it occurs within a gene or a regulatory region near a gene and affects the gene's function.) Despite the fact

that neither study found that genetic variation of *TBX1* made a strong contribution to the etiology of the schizophrenia, these results are not definitive. In mice, *Tbx1* has been identified as one of two genes responsible for prepulse inhibition (PPI) deficits in heterozygous mice, an assay of sensorimotor gating and a schizophrenia phenotype (Paylor et al., 2006). Also, a recent study in mice showed that both *Tbx1* null mice and *Tbx1* heterozygous mice display disrupted cortical development (Flore et al., 2017). The *TBX1* protein is a transcription factor, meaning that it is possible for *TBX1* to act indirectly to cause some of the abnormalities seen in schizophrenia by regulating other genes. It is possible that these indirect changes, for example altered corticogenesis, could combine with other abnormalities that contribute to the symptoms of the disorder (refer to chapter 3 for discussion of how *Tbx1* haploinsufficiency causes hearing loss and could act as an indirect mode of producing abnormalities).

1.2.2 GWAS and CNVs

Attempts to investigate genetic causality in schizophrenia have increased with the recent development of genome-wide association studies (GWAS). This has mostly been through high-density genotyping of single nucleotide polymorphisms (SNPs) in large sets of data collected from cases and controls. These studies identify common yet low-risk variants. In the largest SNP study in recent years, over 108 distinct genome-wide significant loci have been identified as risk factors for schizophrenia (Consortium et al., 2014). (Interestingly, three loci were found on chromosome 22, yet none were within the commonly deleted region of 22q11DS.) Unfortunately, any single genetic alteration is only likely to contribute to a small proportion of the risk of developing schizophrenia, meaning that genetic association studies can only provide part of the answer.

Another genetic approach is to look at variants that are less common but have a larger effect size, like 22q11DS. GWAS tailored to examine these rare, high-risk variants search for copy number variants (CNVs, which are deletions,

duplications, insertions, inversions or recombinations within DNA). Such investigations have shown that 22q11DS is significantly associated with schizophrenia (Manolio et al., 2009). In two studies, deletions within the 22q11 chromosome were significantly associated with schizophrenia in 0.2% of cases vs. 0% of controls, (Stefansson et al., 2008) and had an odds ratio of 21.6 (Stone et al., 2008). This very large genetic risk associated with 22q11DS allows for unparalleled insight into the genesis of many of the structural abnormalities in schizophrenia and their developmental correlates.

1.2.3 Genes within the 22q11.2 deleted region associated with schizophrenia

COMT

The *catechol-O-methytransferase* (*COMT*) gene is another candidate gene in schizophrenia and 22q11DS research. *COMT* provides instructions for making membrane-bound catechol-O-methyltransferase (MB-COMT), which degrades catecholamine neurotransmitters, such as dopamine, epinephrine, and norepinephrine, particularly in the prefrontal cortex as well as soluble catechol-O-methyltransferase (S-COMT) which is produced by other tissues, including the liver, kidneys, and blood to control hormone levels (Prasad et al., 2008). Reductions in neurotransmitter degradation can lead to continued firing of the neuron and increased neurotransmitter levels (Fernandez et al., 2015). In 22q11DS there is only one functional copy of the *COMT* gene, which leads to reduced degradation of neurotransmitters (Fernandez et al., 2015).

The *COMT* gene contains a common and functional SNP, a valine-to-methionine variant ($Val_{108/158}$ Met) that alters the enzyme's activity and dopamine availability in brain areas where this neurotransmitter is released, such as the prefrontal cortex (Torres et al., 2016). This polymorphism is thought to be the main source of genetic variation in COMT activity. The dopamine hypothesis in schizophrenia has become very popular, and the relationship between dopamine and normal brain functioning has been observed to follow an inverted "U" –shaped pattern. As such, too much or too little dopamine have

negative effects, which is supported by positron emission tomography (PET), cognition, behavioral, and animal model studies. The Val allele causes higher enzyme activity, and Val allele's increased degradation of dopamine leads to decreased cortical dopamine availability and a homeostatic increase in D1 receptors. In healthy volunteers, Val/Val homozygotes were found to have higher dopamine D1 receptor binding (indexed by labeled ligand binding) in the cortex when compared to Met carriers using PET radiotracer (Slifstein et al., 2008).

Prefrontal dopamine also modulates the response of prefrontal neurons during working memory tasks. One of the first studies to report on cognitive effects of the high activity Val allele found that the allele impairs prefrontal executive cognition and working memory. Additionally, there was a significant increase in the transmission of the Val allele in schizophrenic families (Egan et al., 2001). A meta-analysis of the effects of the *COMT* gene on cognition found only small effects, but this is possibly due to the inverted "U" –shaped pattern of dopamine activity, which would explain the discrepancy between the studies (Barnett et al., 2008)

The $Val_{108/158}$ Met polymorphism is specific to humans, but there is evidence for high-activity and low-activity forms in mice. Mouse models of the *COMT* deletion showed that reduced COMT activity leads to significantly slower clearance of dopamine (notably in the frontal cortex), emotional reactivity impairment in the dark/light exploratory model of anxiety, and increased aggressive behavior in male mice (Gogos et al., 1998). Using three mouse models of altered *COMT* activity (over-expressed, under-expressed, and wildtype), results indicated a cognitive-affective trade-off. Lower *COMT* activity was associated with better cognitive function, but also increased anxiety-like behavior and greater stress reactivity. The opposite was true for increased *COMT* activity (Papaleo et al., 2008). Taken together, these studies show that the Val/Met polymorphism influences dopamine at levels that are physiologically and behaviorally relevant. This is particularly important

considering that dopamine is thought to play a key role in the pathophysiology of psychosis (de Koning et al., 2012).

PRODH

The proline dehydrogenase (*PRODH*) gene encodes the enzyme proline dehydrogenase protein (also know as proline oxidase, found primarily in the brain, liver, and kidneys), which breaks down proline by starting the reaction that converts it to pyrroline-5-carboxylate in mitochondria. A subsequent step converts this intermediate product to glutamate, the primary neurotransmitter in the cerebral cortex (Fernandez et al., 2015; Torres et al., 2016). It is a key gene deleted in 22q11DS and thought to be involved in schizophrenia, as it is involved in metabolic functions that alter brain function and behavior. A reduction in *PRODH* leads to an increase in the amino acid proline, which can cause severe learning, cognitive and motor impairments in extreme cases (Jacquet et al., 2003). Approximately half of 22q11DS patients have elevated proline levels (Karayiorgou et al., 2010). In schizophrenic families, *PRODH* variations were associated with impaired performance on the Tower of Hanoi problem solving task reflecting planning capacity, a neurocognitive trait characteristic of the disorder (Li et al., 2008). Another study showed that *PRODH* variations that altered enzyme activity and schizophrenia risk was associated with decreased striatal gray matter volume, while a protective *PRODH* variant increased frontal lobe volume (Kempf et al., 2008). A mouse model of *PRODH* deficiency showed impairments in fear memory and tests of sensory motor gating (Gogos et al., 1999). Interestingly, there has been evidence for an epistatic compensatory relationship between *COMT* and *PRODH*, with PRODH-deficient mice showing COMT upregulation in the prefrontal cortex (Torres et al., 2016; Weinberger and Harrison, 2010).

GNB1L

The guanine-nucleotide-binding protein (G protein) β-polypeptide 1-like gene (*GNB1L*) encodes a G-protein beta-subunit-like polypeptide, although it's function is unknown. In addition to *TBX1*, *GNB1L* was also found to be one of

the genes responsible for PPI deficits in heterozygous mice (Paylor et al., 2006). A study in schizophrenic patients linked allelic variances in *GNB1L* to psychosis in males with 22q11DS (Williams et al., 2008).

DGCR8

DGCR8 microprocessor complex subunit (*DGCR8*) is a protein coding gene that encodes for an RNA - binding moiety of the microRNA "microprocessor" complex essential for microRNA production, a class of small non-coding RNAs that regulates gene expression by inhibiting or promoting microRNA expression, translation or stability. *DGCR8* creates microRNAs that help regulate production of different proteins. Impaired microRNA formation contributes to some of the behavioral and neuronal phenotypes of 22q11DS (Fénelon et al., 2011; Stark et al., 2008). Mice heterozygously deleted for *Dgcr8* (*Dgcr8 +/-* mice) show that a sole deletion in this gene leads to altered microRNA expression just as in mouse models of the larger 22q11 deletion (Stark et al., 2008). A later study in *Dgcr8 +/-* mice showed reductions in cortical layer 2/4 neurons, smaller dendritic spines in layer 5 pyramidal neurons along with deficits in synaptic potentiation, short-term plasticity, and working memory-dependent learning tasks mirroring deficits learning and memory observed in 22q11DS (Fénelon et al., 2011). Post-mortem brain tissue of schizophrenia patients show a dysregulation of microRNAs, including *DGCR8* (Moreau et al., 2011). Disruptions in *Dgcr8* also cause pathogenic thalamocortical deficiencies that disrupt glutamatergic synaptic transmission to the auditory cortex, sensitivity to antipsychotics and deficits in acoustic startle responses in 22q11DS mice that are associated with schizophrenia and psychosis in humans (Chun et al., 2014).

1.3 Schizophrenia hypotheses and parvalbumin-positive interneurons

Neuropsychological impairments in schizophrenia that are also observed in 22q11DS include but are not limited to deficits in executive function, verbal working memory, intelligence and sustained attention (Lewandowski et al.,

2007). Cognitive and behavioural deficits are hypothesized to arise from functional abnormalities within cortical circuitry. An imbalance of excitation and inhibition in cortical circuits, caused by disruption of dopaminergic pathways and deficits in inhibitory interneuron development, is thought to be the root cause of psychosis and cognitive dysfunction in schizophrenia.

For decades, the dopamine hypothesis has been a pervasive schizophrenia theory. Dopamine has been found to mediate working memory, attention, reward pathways, motor and sensorimotor coordination (Weinberger and Harrison, 2010). It is posited that increased levels of subcortical presynaptic dopamine (increased synthesis and release) and elevated dopamine receptor sensitivity lead to the positive symptoms of psychosis while hypoactive dopamine in the dorsolateral prefrontal cortex contribute to cognitive symptoms (Guillin et al., 2007). Current antipsychotic drugs act on dopamine receptors, although these are not effective for all schizophrenia symptoms. This highlights the fact that the dopamine hypothesis is not sufficient to explain the complexity of the disorder.

Another hypothesis regarding the pathophysiology of schizophrenia is the glutamate hypothesis. Glutamate is the primary excitatory neurotransmitter in the brain and N-methyl-D-aspartate (NMDA) receptors are a major subtype of glutamate receptor (Weinberger and Harrison, 2010). Evidence of their involvement with schizophrenia comes from the initial discovery of psychotogenic effects of dissociative anesthetics such as ketamine and phencyclidine (PCP) that induce schizophrenia-like symptoms in healthy individuals and exacerbate symptoms in patients with schizophrenia (Moghaddam and Javitt, 2012). Additionally, NMDA receptors play an essential role in neural plasticity and pruning during adolescence, linking them to the altered developmental process during a period critical to schizophrenia onset (Selemon, 2013).

Adding to the complexity, γ–aminobutyric acid (GABA) neurons are the primary moderators of glutamatergic activation and are responsible for the balancing of

excitation and inhibition and network oscillations (Nakazawa et al., 2012; Shu et al., 2003). GABAergic interneurons expressing the Ca2+ buffer parvalbumin (called parvalbumin-positive, PV+ inhibitory interneurons) are the most numerous GABAergic subtype in the cortex. These include chandelier and basket cells, which target the soma and axon hillock of cortical pyramidal cells. Pyramidal cells are glutamatergic, excitatory projection neurons that specialize in transferring information between cortical areas and from cortical areas to other regions of the brain (Marín, 2012; Meechan, Tucker, Maynard, & LaMantia, 2009). PV+ basket cells project to the perisomatic area that controls the synchronized firing of pyramidal neurons (see figure 1.2).

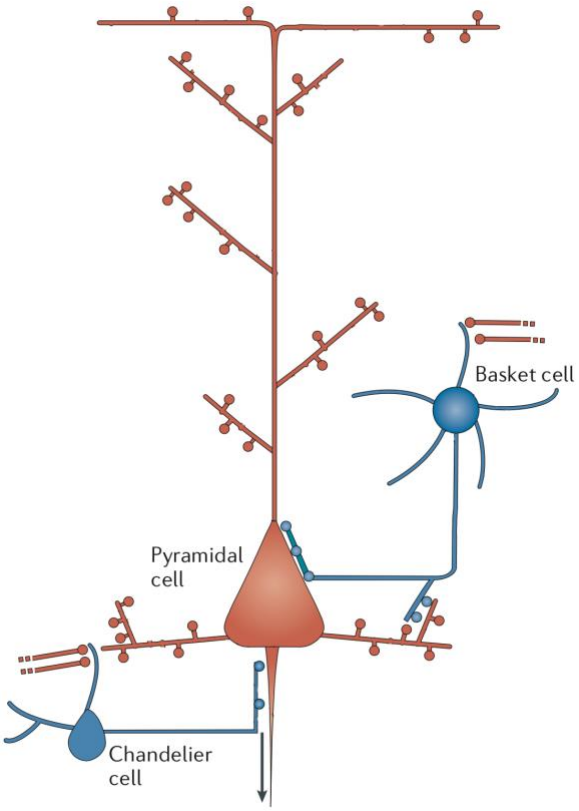

Figure 1.2 Parvalbumin positive interneurons exert spatiotemporal control upon pyramidal cells

In blue are PV+ interneurons as chandelier and basket cells which inhibit pyramidal cells, the primary excitation units of the mammalian prefrontal cortex and the corticospinal tract. Adapted from Marín, 2012.

When pyramidal neurons receive excitatory input, PV+ cells are then discharged synchronously via both neurotransmitter and electrical (gap junction) activity. The interneurons are fast-spiking and regarded as the most reliable, fastest, and most efficient sources of inhibition in the cortex (Nakazawa et al., 2012; Rossignol, 2011). PV+ cells are highly interconnected with each other and form a network of synchronous inhibition of pyramidal cells.

PV+ interneurons play a key role in balancing excitation and inhibition by preventing overexcitation and guiding information flow within the cortex. For example, basket cells are the target of thalamocortical axons responsible for feed-forward inhibition and the thalamocortical input of sensory responses (Rudy et al., 2011). Post mortem brain analyses of schizophrenic patients reveal reductions in PV+ (and calbindin) interneurons in the prefrontal cortex as well as reduced density of interneurons expressing mRNA for glutamic acid decarboxylase (GAD), the enzyme that synthesizes GABA, particularly the 67kDA isoform and GAD 1 mRNA (Beasley et al., 2002; Hashimoto et al., 2003). These reductions are largely composed of PV+ interneurons (Lewis et al., 2005).

PV+ interneurons control spatiotemporal activity of pyramidal neurons, which synchronizes network activity and creates rhythms (Rudy et al., 2011). This glutamatergic-GABAergic interaction modulates the gain of cortical output, and drives oscillations in the gamma frequency range (30 – 100 Hz) (Buzsáki and Draguhn, 2004; Marín, 2012). Gamma band oscillations are thought to arise from the synchronized inhibition of pyramidal neurons and they are measured through electroencephalogram (EEG) or magnetoencephalogram (MEG). The dendritic fields of pyramidal cells are well-aligned, allowing for the voltages generated by the simultaneous postsynaptic potentials to be easily summated, which produce the EEG field. The summated postsynaptic activity of neurons, called electromagnetic activity, is then recorded from the surface of the scalp. Although EEG also detects the activity of many different nerve cells and ongoing brain functions, specific brain activity can be isolated and visualized. For example, all activity recorded after the repeated presentation of a stimulus

would be time-locked and stable across trials. Through repeated averaging, these time-locked brain responses highlight brain activity related to this specific stimulus event, and all activity not related to the stimulus can be averaged out. This creates an event-related potential (ERP) waveform. Alternatively, a time-frequency analysis can be created by visualizing the oscillations of ERPs in different frequency bands, and this is how gamma oscillations are measured (Weinberger and Harrison, 2010).

Abnormalities in gamma oscillations have been linked to attention, working memory and executive function deficits in both humans and rodents. In schizophrenia there are reported abnormalities in PV+ interneurons, which are thought to cause patterns of activation within cortical projection neurons to become more variable and less reliable. Reductions in gamma oscillations are reported in schizophrenia patients with deficits in working memory and executive function (Rossignol, 2011). Deficits seen in gamma synchrony within the frontal cortex have been linked to cognitive control impairments in schizophrenic patients (Cho et al., 2006). Cognitive and executive brain function is heavily influenced by synchronous oscillatory activity at the gamma frequency and nearly all schizophrenia patients have deficits in attention, reasoning, verbal memory, working memory, problem solving and processing speed (Nakazawa et al., 2012). Thus, abnormalities in PV+ cortical interneuron networks in schizophrenia are thought to be a critical mechanism underlying observed abnormalities in gamma oscillations and contributing to cognitive deficits.

1.4 *Df1*/+ mouse model of 22q11DS

Most genes in the 22q11 deletion region in humans are conserved together in mice, which has allowed the generation of multiple mouse models of the disorder. Mouse chromosome 16 is orthologous to human chromosome 22, and with the exception of clathrin heavy polypeptide-like 1 (*CLTCL1*), nearly all genes deleted in human 22q11DS are conserved with minor changes in gene order on mouse chromosome 16. One minor difference is that only humans

carry a duplication in the functional genes DiGeorge syndrome critical region 6 (*DGCR6*) and *DGCR6*-like (*DGCR6L*) (Arinami, 2006; Karayiorgou et al., 2010). The clinical features seen in people with the 1.5Mb deletion and the 3Mb deletion are indistinguishable, meaning that the key genes involved in the disease are contained within the 1.5Mb region (Earls and Zakharenko, 2014). As such, most mouse models center on the 1.5Mb deletion seen in human 22q11DS.

The *Lgdel+/−* and *Df(16)A+/−* mice carry a slightly larger deletion between the genes *Dgcr2* and *Hira*, while *Df(16)1+/−* mice (also referred to as deficiency 1-knockout mouse, *Df1/+* mouse throughout this paper) have gene deletion between *Dgcr2* and *Ufd1l* gene (Earls and Zakharenko, 2014; Karayiorgou et al., 2010; Lindsay et al., 1999). Despite small differences in the number of genes deleted, all of these models are considered equivalent to the 1.5Mb deletion in humans. There have also been many other mouse strains with smaller and single-gene mutations and deletions that have been created to highlight the specific genes and regions responsible for particular phenotypes seen in 22q11DS. For example, the *TBX1* gene has been found to be one of the major causative factors of the physical features associated with 22q11DS through studies of murine models. Loss of function mutations of the gene in mice were found to cause heterozygotes to display defects in development of the thymus and aortic arch artery while homozygotes displayed the full range of defects seen in human 22q11DS including cleft palate (Paylor et al., 2001; Paylor & Lindsay, 2006). Additionally, humans with *TBX1* mutations without 22q11DS have been shown to have the typical phenotype of the syndrome (Fernandez et al., 2015).

The first mouse engineered to have a 22q11.2-like deletion (and the mice used in this thesis) was the *Df1/+* mouse heterozygous for the deleted region, developed by Lindsay and colleagues through Cre/loxP engineering (1999). The *Df1/+* deletion consists of a 1.2 Mb region, which encompasses 18 of the protein-encoding genes deleted in the human syndrome, one of which is *Tbx1* (Paylor et al., 2001; Long et al., 2006; Funke et al., 2007). Despite the fact that

the genetic deletion is not exactly identical to the minimum human 22q11.2 deletion, these mice have been found to recapitulate many of the phenotypes of 22q11DS including deficits in sensorimotor gating, learning and memory, cognitive and social impairment, cortical circuit dysfunction, and cardiovascular abnormalities associated with 22q11DS (Paylor et al., 2001; Paylor & Lindsay, 2006).

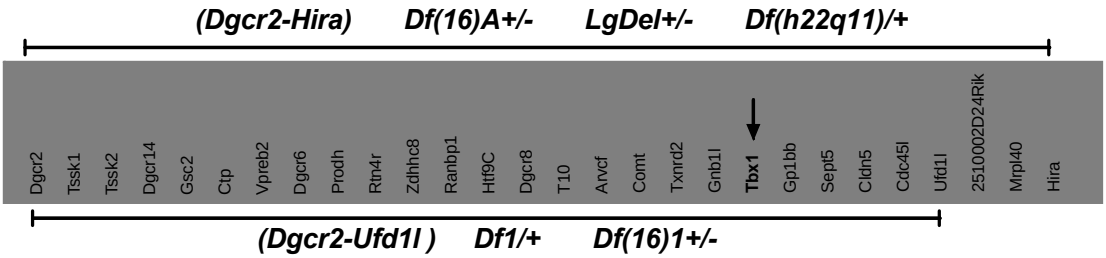

Figure 1.3 Mouse models of 22q11DS

Various mouse models of 22q11DS exist, all considered equivalent to the 1.5Mb deletion in humans. Throughout the literature mice with a deletion from Dgcr2 to Ufd1l are called *Df(16)1+/−* or *Df1/+* mice, while those with a deletion between Dgcr2 and Hira are called *Df(16)A+/-*, *LgDel+/-*, and *Df(h22q11)/+.* All animals have *Tbx1* (in bold identified with an arrow) within the deleted region. Original figure.

Unfortunately, studies examining which neuroanatomical changes seen in human 22q11DS through steriologic study or MRI are recapitulated in mice have yet to emerge. However, multiple cellular studies have recently been conducted to investigate neurobiological abnormalities in the mouse models. Meechan and colleagues (2009) found that corticogenesis and subsequent differentiation of the cerebral cortex in *Lgdel+/-* mice is disrupted. PV+ interneurons are not expressed in the developing cortex, but investigators found that the distribution of calbindin, another type of interneuron expressed in migrating interneurons, was altered in mutant embryos. In postnatal mice carrying the deletion, there was a 20% reduction in the number of basal progenitor cells that develop in the cortical subventricular zone and give rise to layer 2-3 pyramidal projection neurons, leading to reduced proportion of supragranular neurons. In the medial portion of the cortex, there was a similar

20% reduction in layer 2-3 pyramidal neurons. Further analysis showed misplacement and aberrant distribution of PV+ interneurons in upper and lower cortical layers at the level of the anterior commissure. However, the number of PV+ interneurons overall was not diminished. Another study by Fenelon and colleagues (2013) showed that *Df(16)A+/−* mice exhibit a reduction in layer 5 PV+ interneurons within the prelimbic area of the medial prefrontal cortex, but this reduction was modest (Fenelon et al., 2013). A more recent study in *Lgdel+/-* mice found a deficit in hippocampal activity which was causally linked to reduced excitability of PV+ interneurons (Marissal et al., 2018). No study to date has assessed PV+ interneuron cell numbers or density in the auditory cortex of *Df1/+* or similar mice.

1.5 Prepulse inhibition in schizophrenia, 22q11DS and the *Df1/+* mouse

Due to the complexity of psychiatric disorders, many of behavioural abnormalities in humans with schizophrenia are difficult to reproduce in mice. However, inhibition of the acoustic startle reflex can easily be studied in both humans and mice. The startle reflex is a response to a sudden, relatively intense stimulus, and is usually classified as a defensive response (Swerdlow & Geyer, 1998). A startle response relies upon sensory processing and is used as a measure of sensorimotor gating and preattentive processing (Drew et al., 2011; Gogos et al., 1999). A startle-evoking stimulus should be attenuated with the preceding presentation of a weaker auditory stimulus (called a prepulse). Normally, a subject should learn to prepare for the strong, startle-evoking auditory stimulus after the warning prepulse, and should thus be able to modulate their sensitivity to the incoming sensory stimuli. Prepulse inhibition (PPI) of the startle response is a measure of inhibitory “sensorimotor gating” as subjects should be able to filter or “gate” what they learn to be irrelevant sensory stimuli. PPI is characteristically diminished in neurological and psychiatric disorders, particularly schizophrenia. Additionally, while the physical manifestations within 22q11DS vary greatly, the neurocognitive profile is much more consistent, with decreased PPI and prefrontal influences on subcortical

and brainstem processing presented as keystones (McCabe et al., 2014; Sobin et al., 2004).

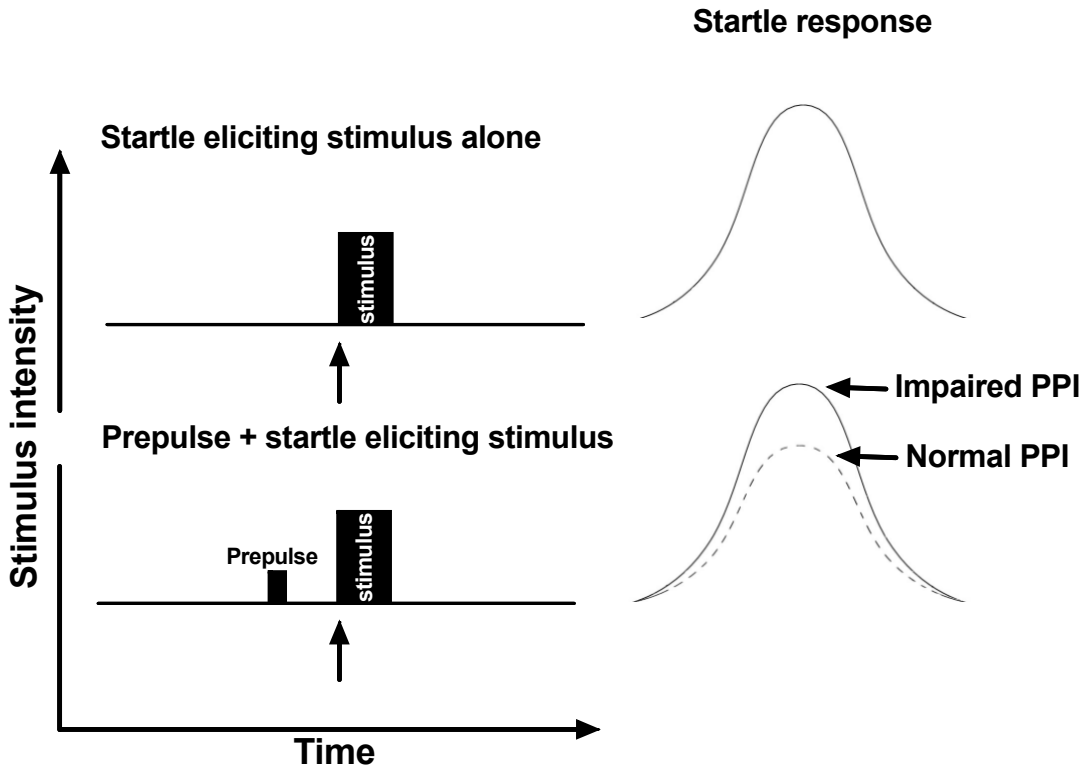

Figure 1.4 Prepulse inhibition paradigm

A preceding stimulus or "prepulse" presented before a startle eliciting stimulus attenuates the startle response. Normally, a reduction or inhibition of the startle response occurs (normal PPI), but in cases of impaired inhibition of the startle response to a prepulse, similar startle responses are still apparent (impaired PPI). Original figure.

Prepulse inhibition of acoustic startle is mediated by brain stem and forebrain circuits including the prefrontal cortex, thalamus, hippocampus, amygdala, nucleus accumbens, striatum, ventral pallidum, and globus pallidus (Zebardast et al., 2013). As such, it is considered preconscious or automatic inhibition. PPI deficits imply that both sensory and cognitive abnormalities (Swerdlow, Weber, Qu, Light, & Braff, 2008). In the prefrontal cortex, dopamine transmission is thought to be a modulating factor of decreased PPI based on dopamine agonist/antagonist studies in rats and humans (Swerdlow et al., 2003).

Although PPI is not diagnostic of schizophrenia in humans, the conservation across species makes it a robust and reliable quantitative phenotype useful for probing one of schizophrenia's core symptoms.

Reductions in PPI have consistently been found in mouse models of both schizophrenia and 22q11DS. Findings related to startle testing in 22q11DS mice suggest that genes in the deleted region play an important role in modulation of PPI such as *Prodh* (Gogos et al., 1999), *Comt* (Paterlini et al., 2005), *Tbx1*(Paylor et al., 2006), *Dgcr8* (Stark et al., 2008), and *Gnb1l* (Ishiguro et al., 2010).

The PPI test relies heavily on the ability to hear the stimulus tones presented. Although *Df1*/+ mice show hearing loss, to my knowledge, no study has yet to control for possible hearing loss confounds (although see Didriksen et al. 2017 for PPI studies with ABR testing in another mouse model of 22q11DS). Paylor and colleagues (2006) demonstrated decreased PPI in *Df1*/+ mice, yet failed to adequately characterize the hearing loss common to this mouse model. Experimenters demonstrated normal distortion-produce otoacoustic emissions (DPOAEs) in a small sample of mice (6 animals), though it was unclear whether these were the same animals used for PPI testing. Additionally, DPOAEs only show outer and middle ear problems and inner ear problems affecting the outer hair cells, and are not sensitive to problems with inner hair cells or with brainstem processing. Ideally, mice should have been screened for elevated hearing thresholds through auditory brainstem response measurement prior to PPI testing.

1.6 Middle ear infection and hearing loss in schizophrenia, 22q11DS and *Df1*/+ mice

Hearing loss and deafness have been experimentally and clinically associated with the development of paranoid symptoms, with moderate to severe deficits affecting approximately 40% of late-onset schizophrenia patients (Weinberger and Harrison, 2010). Hearing loss is also a predisposing factor for

schizophrenia, with 1.8 times higher diagnoses among those with severe hearing loss (David, 1995). More recently, Mason and colleagues (2008) found an odds ratio of 3.68 of middle-ear disease that predates schizophrenia in patients and revealed that auditory hallucinations were associated with middle-ear disease. History of ear disease was obtained from general practice records and hearing was only examined at one time to detect a hearing deficit. Auditory hallucinations have been associated with deafness and improvements in psychotic symptoms have been reported after fitting of a hearing aid (Weinberger and Harrison, 2010). A meta-analysis and review showed that hearing impairment increases the risk of all psychosis outcomes (hallucinations, delusions, psychotic symptoms and delirium), and early exposure to hearing impairment elevated the risk of schizophrenia by an odds ratio of 3.15. These findings highlight the link between middle ear disease, hearing loss and auditory hallucinations, but these results have yet to be revisited and extended. It would be interesting to assess patterns of hearing loss in 22q11DS longitudinally from birth (considering MEI are common in children) and how this correlates with psychosis and psychotic symptoms. It has been proposed that middle ear disease might predispose one to schizophrenia through inflammatory damage to the overlying temporal lobe (Mason et al., 2008); other mechanisms relating more directly to consequences of deafferentation have also been postulated (Linszen et al., 2016).

A key deficit seen in 22q11DS is the increased probability of middle ear infection/disease (MEI/MED). MEDs manifest most commonly through the form of otitis media, which results in inflammation of the middle ear causing pain and hearing loss. In otitis media with effusion, the Eustachian tube also becomes blocked and the middle ear retains fluid, which disrupts the air-to-fluid impedance-matching function of the tympanic membrane and middle ear. There is no cure for otitis media; however antibiotics can help deal with the infection although they cannot reduce the conditions that trigger infection (Yost, 2007). In 22q11DS, there is an increased vulnerability to MEIs (Oskarsdottir et al., 2005) and the majority of patients suffer from chronic otitis media (Liao et al., 2004). Other consistent phenotypes include auricular anomalies (such as

small or round ears, external ear defects, and thick helices), chronic otitis media, and both conductive and sensorineural hearing loss (Digilio et al., 1999; Long et al., 2006; Oskarsdottir et al., 2005; Papangeli and Scambler, 2013; Umlauf, 2008). A 30-40% incidence rate of hearing loss is associated with the syndrome (Paylor & Lindsay, 2006).

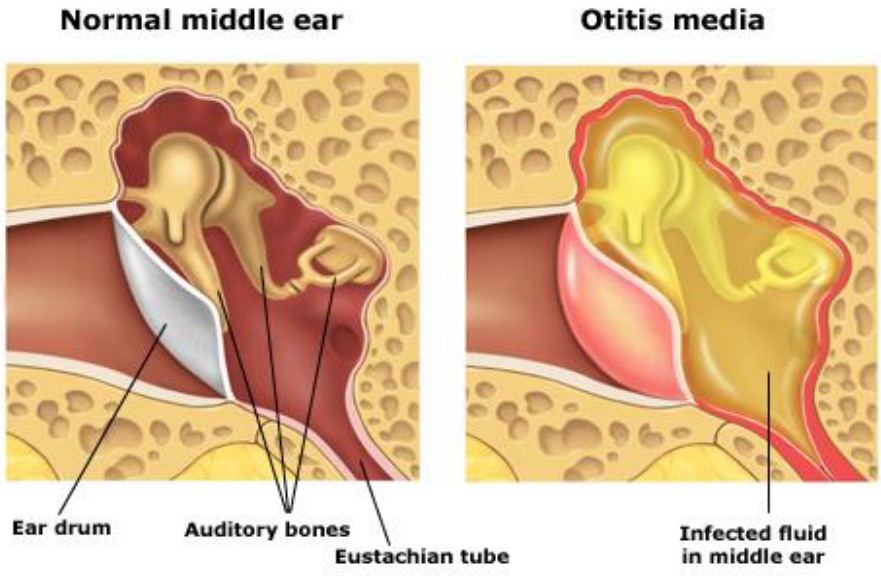

Figure 1.5 Otitis media with effusion

A normal middle ear has an air-filled middle ear (left), but in otitis media the middle ear is filled with fluid or inflammation. This can reduce mobility of the ear drum and middle ear bones (ossicles) and lead to increased hearing thresholds (hearing loss). Image from ent-surgery.com.au.

The increased incidence of middle ear disease/infection seen in *Df1*/+ animals mimics the phenotype seen in 22q11DS patients. Studies on the deletion have shown that conductive hearing loss is prevalent in 45% of patients and is primarily related to middle ear infection, as recurrent otitis media was shown in 58% of patients with hearing loss (Digilio et al., 1999). In another study, 88% patients with Velocardialfacial Syndrome and a 22q11 deletion (confirmed by DNA probing and fluorescence in situ hybridization) were found to have otitis media, 53% had conductive hearing loss and 39% needed pressure equalization tubes implanted to decrease the frequency of ear infections by allowing air into the middle ear and helping fluid to drain into the throat (Ford et

al., 2000). Our findings (Fuchs et al. 2013 and this thesis) recapitulate the deficits seen in human studies of 22q11DS, as we observe that the primary cause of the hearing loss in *Df1*/+ mutants is otitis media.

Two main types of hearing loss exist: conductive, where sound is not conducted efficiently from the outer and middle to the inner ear, and sensorineural, where there is damage to the sensory transduction mechanisms in the inner ear (cochlea) or the nerve pathways from the inner ear to the brain. The outer ear (OE) consists of the pinna, concha and external auditory meatus, which gathers sound energy and focuses it on the tympanic membrane of the middle ear (ME). The ME functions to transmit sound energy from the relatively low-impedance medium of air in the outer ear to higher impedance fluid of the inner ear (IE). Within the ME, the tympanic membrane is connected to the IE via three ossicles, the malleus, incus and stapes; the stapes is then connected to the oval window on the cochlea. The Eustachian tube connecting the ME to the pharynx allows for proper pressure balance across the tympanic membrane. The impedance-matching function of the ME is achieved primarily through two mechanisms. First, the difference in area between the tympanic membrane and the oval window produces pressure amplification; sound energy impinging on the large tympanic membrane is transmitted through the ossicles and concentrated on the smaller oval window. Second, the ossicular chain produces a lever action, which achieves a multiplication of force and drives the dense fluids of the IE to overcome the impedance mismatch due to the fluids and tissues of the IE (Kandel et al., 2000; Purves et al., 2008; Yost, 2007). See Figure 1.6 for a description of the ascending auditory pathway.

Otitis media is one of the most common childhood diseases, where an infection occurs between the tympanic membrane and the IE (including the Eustachian tube). The infection inflames the middle ear and leaves behind scar tissue which can restrict or immobilize the tympanum or ossicles. Otitis media often occurs with effusion, a condition in which the middle ear contains fluid. Both types of blockage of the Eustachian tube hinder pressure balance and cause hearing loss (Kandel et al., 2000; Yost, 2007). Generally, otitis media leads to

a 20-28 dB elevation of hearing thresholds, although in severe cases it can increase thresholds by up to 50 dB (Takesian et al., 2009).

Results from our previous study (Fuchs et al., 2013) confirmed hearing loss in 48% of *Df1*/+ mutant ears tested and linked the deficit to a higher incidence of opportunistic MEI (otitis media). Our conclusion that the hearing loss was due to a peripheral, conductive cause was reinforced by the fact that we found mice with monaural hearing deficits, which is a more typical symptom of conductive than sensorineural hearing loss. A more recent study by our collaborators examined the underlying cause of the hearing loss seen in *Df1*/+ mice. Middle ear infection in *Df1*/+ mice was found to arise from low-penetrance, frequently monaural developmental defects within the muscles that line the Eustachian tube (Fuchs et al., 2015). Normally, the Eustachian tube links the middle ear to the nasopharynx and drains mucus from the middle ear. In *Df1*/+ mice, abnormal development of the surrounding muscle of the Eustachian tube produces susceptibility to otitis media and consequently, hearing loss. Fuchs et al. (2015) further showed that this muscle abnormality in *Df1*/+ mice arises from haploinsufficiency (heterozygosity) for *Tbx1*; *Tbx1*/+ mice displayed a very similar pattern of susceptibility to otitis media and developmental abnormality in pharyngeal muscle.

Hearing loss can lead to changes in the primary auditory cortex. This is true for both sensorineural and conductive hearing loss. Sensorineural hearing loss can lead to alterations in thalamocortical and intracortical excitatory/inhibitory balance in A1 (Kotak et al., 2005). It alters both passive and active membrane properties, enhances synaptic excitation, and reduces synaptic inhibition. Decreased synaptic inhibition is thought to indicate that the strength of GABAergic synapses is decreased after hearing loss (Kotak et al., 2005). Conductive hearing loss also significantly alters temporal properties of auditory cortex synapses and spikes (Xu et al., 2007), and the cortex does not compensate for the loss of inhibition, but rather further reduces inhibitory drive (Sanes and Kotak, 2011). Additionally, inhibitory synapse function is more affected by juvenile, but not adult, hearing loss highlighting a developmental

aspect (Takesian et al., 2012). A study in a mouse model of age-related hearing loss (presbycusis) showed that hearing loss is also associated with a decline in PV+ interneurons in the primary auditory cortex (A1) (del Campo, Measor, & Razak, 2012).

Abnormalities in A1 are also detected with unilateral hearing loss, the effects of which can be just as, if not more dramatic and may also depend on the precise developmental stage at which it is experienced (Keating and King, 2013). Disruption of binaural input near the onset of hearing in mice has been shown to interfere with the normal coregistration of frequency-receptive fields between the contralateral and ipsilateral ears and cortical interaural level difference sensitivity, both of which affect sound localization. Conductive hearing loss confers specific and lasting changes upon cortical representation of sound features that underlie spatial hearing (Polley et al., 2013). Unilateral conductive hearing loss significantly reduces glucose activity in the contralateral inferior colliculus, reduces activity in the contralateral auditory cortex (Hutson et al., 2008), and alters the central encoding of perceptual abilities as well as spatial location (Thornton et al., 2014). Conductive impairment is purposed to contribute to potential cognitive dysfunctions related to processing sounds and speech (Vila and Lieu, 2015).

1.7 Auditory Brainstem Responses (ABRs) and Auditory Evoked Potentials (AEPs)

To assess auditory function and hearing loss, brain potentials in response to time-locked auditory stimuli, or event-related potentials, are typically used. Event-related potentials are a form of electroencephalography (EEG) signals, measured through the scalp. To be able to discern event-related activity from background EEG activity, large numbers of stimuli are presented repeatedly and the recordings averaged to obtain a higher signal-to-noise ratio for the stimulus-evoked potential (Luck, 2014). Auditory event-related potentials can assess the components that span the full length of the auditory pathway (see Figure 1.6 for a description of the ascending auditory pathway) and are divided

into subsets of latency-defined components that correspond to the progression of brain activity ascending the auditory pathway. Auditory brainstem responses (ABRs) represent the earliest components recorded within the initial 10ms after stimulus onset. This includes the auditory nerve and brainstem responses. Wave I of the ABR is commonly attributed to the activity within the auditory nerve. There is debate about the exact origin of later waves (and these origins are also thought to differ between mice and humans), but it is agreed that the signal then moves from the cochlear nucleus, through the superior olivary complex, into the lateral leminiscus and finally through to the inferior colliculus (Willott, 2001). A mid-latency component frequently studied is the first major positive deflection, P1 which is thought to correspond to the activation of the auditory thalamus and the auditory cortex (Picton et al., 1974). The first major negative peak, N1, is localized to the auditory cortex and the second major positive peak, P2, to the cortical association areas (Willott, 2001).

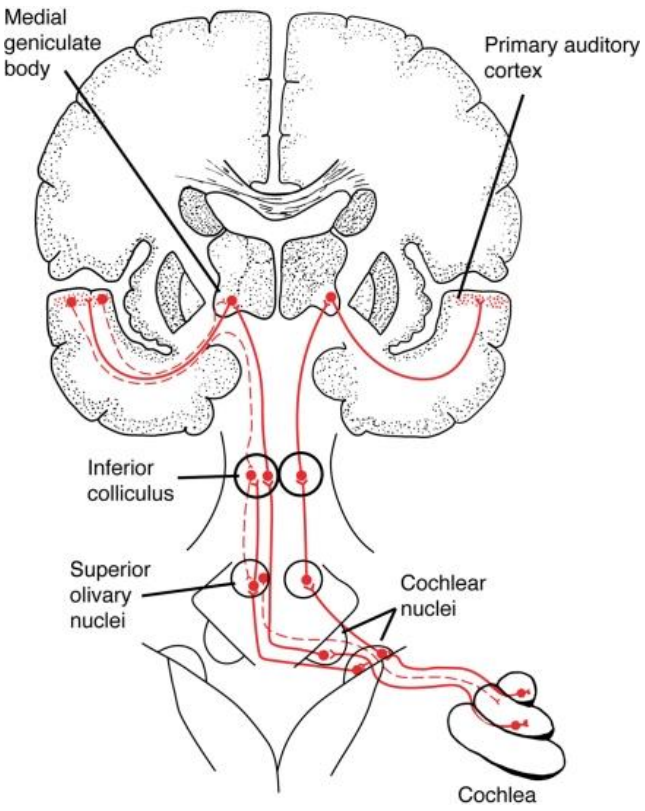

Figure 1.6 Anatomy of the ascending auditory pathway

Sound passes from the outer ear to the middle ear through the tympanic membrane. Vibrations are sent to the inner ear and hair cells of the cochlea. From the cochlea, neurons synapse onto the auditory nerve and then the

cochlear nucleus of the brainstem. At this point the auditory pathway sends information to both the ipsilateral and contralateral hemisphere, though more information tends to go to the contralateral side. The pathway emerging from the cochlear nucleus projects to the superior olivary nuclei, onto the inferior colliculus of the midbrain to the medial geniculate body of the thalamus and into the auditory cortex. (From homeschoolingforfree.org)

Impairments of auditory evoked potentials have been extensively studied as an endophenotypic marker of schizophrenia. ABR studies of schizophrenia patients have produced mixed results, in some cases suggesting increased wave latencies, reduced amplitudes or total absence of ABR waves (Hayashida et al., 1986; Källstrand et al., 2014; Nielzén et al., 2008). Studies focusing on hearing deficits within 22q11DS patients typically use either ABR or audiograms to characterize the type of hearing loss (for example whether it is conductive or sensorineural) and the extent of the hearing deficit (Digilio et al., 1999; Verheij et al., 2017). While there have been a few studies to test threshold deficits in 22q11DS patients (Digilio et al., 1999; Jiramongkolchai et al., 2016; Verheij et al., 2017), to my knowledge there are no studies that characterize specific ABR wave deficits in 22q11DS.

Other auditory event-related potentials such as the auditory steady state response (ASSR), an electrophysiologic response to a rapid auditory stimulus, and cortical AEPs, where responses are observed higher up the auditory pathway into the cortex, can be used to assess auditory function (Korczak et al., 2012). Within cortical AEPs N1 is consistently reduced in SCZ patients as well as first-degree relatives (Foxe et al., 2011; Rosburg et al., 2008). ASSR is also reduced in 22q11DS patients (Larsen et al., 2018) and N1 and P2 responses in cortical AEPs show varying impairments, which correspond to altered auditory processing (Rihs et al., 2013). While both ASSR and cortical AEPs can reliably reflect auditory function, cortical AEPs may be more robust estimates that are less influenced by the degree of hearing loss and display less variability (Tomlin et al., 2006). While there are many human 22q11DS studies, few reports have examined auditory abnormalities in mouse models of

the disease. Two studies have found that both auditory cortical activity and sound-evoked auditory thalamic responses are altered in mouse models of 22q11DS (Chun et al., 2014; Didriksen et al., 2017). Only one of them (Didriksen et al., 2017) considered and controlled for hearing loss. The *Df1*/+ mouse offers an unparalleled opportunity to understand the interaction between hearing loss and genetic risk factors for schizophrenia on cortical auditory function.

1.8 Viral-based neural tracing

Since studies have shown that there may be abnormal PV+ interneuron distribution or function within mouse models of 22q11DS, I wondered whether there would be abnormalities in the areas that project onto these interneurons as well (Fenelon et al., 2013; Marissal et al., 2018; Meechan et al., 2009). I decided to look at two areas that target A1, the auditory thalamus and the basal forebrain (BF).

The medial geniculate complex (MGC) of the thalamus is a relay station for all ascending auditory information on its way to the cortex (Purves et al., 2008). In the auditory cortex PV+ interneuron networks have faster response latencies than non-PV+ neurons, suggesting they enhance the timing and reliability of pyramidal responses and dampen the spread of excitation (Moore and Wehr, 2013). In chapter 3 I show that *Df1/+* animals display hearing loss which is linked with a reduction in the density of PV+ interneurons in the auditory cortex. In chapter 5 I ask whether there are differences in the projections to PV+ interneurons from the auditory thalamus.

The BF is not as well characterized as the auditory thalamus. A recent study found that the majority of A1 afferents from the striatum project to the BF and then go on to affect auditory cortical processing (Chavez and Zaborszky, 2017). The BF provides primarily cholinergic input to the entire cortex, A1 included, and is implicated in cognition including learning and attention. Specifically within A1, cholinergic inputs play an important role in auditory processing and

plasticity, but their precise projections to glutamatergic versus GABAergic neurons are less studied (Lin et al., 2015). The BF is heterogenous and both cholinergic and non-cholinergic projection neurons are interspersed, which has made selective tracing, monitoring and manipulation difficult (Lin et al., 2015; Nelson and Mooney, 2016). Only recently have cholinergic neurons been recorded during behavior (Hangya et al., 2015) and modified rabies tracing has been used to image different cellular projections (Nelson and Mooney, 2016). Mooney and colleagues (2016) discovered that BF axons can excite excitatory and inhibitory neurons, including PV+ interneurons, within A1 which both facilitate and suppress auditory responsiveness. However, these BF-A1 connections have never been examined in mouse models of 22q11DS. Also, the BF is part of the PPI circuit (Zebardast et al., 2013), and since mouse models of 22q11DS display impaired PPI it remains unknown whether *Df1*/+ animals with or without PPI deficits would also have altered BF-A1 circuitry.

To test whether the approach used by Nelson and Mooney (2016) was replicable and could be applied to *Df1*/+ mice with and without hearing loss, I conducted a viral monosynaptic neural tracing study in A1 to analyze projections from the BF to A1 (chapter 5).

1.9 Aims

The aim of this thesis is to examine the relationship between hearing loss and susceptibility to schizophrenia-relevant brain and behavioral abnormalities within a mouse model of 22q11DS, using a combination of behavioral, electrophysiological, immunohistochemical and viral-tracing techniques.

Given that (1) PV+ interneuron abnormalities are a common *post-mortem* finding in schizophrenia patients, (2) both 22q11DS patients and *Df1*/+ have conductive hearing loss, and (3) PV+ interneurons are reduced in density in A1 of mice with age-related hearing loss, I wondered whether conductive hearing loss in *Df1*/+ mice would affect PV+ cell density in A1. I begin with a pilot experiment investigating different techniques for characterizing hearing loss in

Df1/+ mice (ABR vs tympanic membrane scoring) and using both PV immunohistochemistry and Nissl cell body staining to assess cell counts within frontal cortices and A1 (appendix 1). I also trialed automated cell counting algorithms for the next study but decided to count by hand for accuracy and to save time. To find the brain area most likely to contain the most PV+ interneuron cell projections from A1 to analyze in the next set of experiments, I completed a set of viral tracing studies.

After pilot experiments, I then investigated the relationship between acoustic startle response, prepulse inhibition of the acoustic startle response, auditory brainstem response measurements of hearing loss, cortical auditory evoked potentials, and PV+ inhibitory interneuron cell density and laminar distribution in A1 and the secondary motor cortex (chapter 3).

Since no study had addressed when hearing loss in *Df1*/+ mice occurs or whether it is permanent or transient I then set out to characterize the hearing deficit in these animals. I did this by testing both distortion product otoacoustic emissions and auditory brainstem responses to clicks and different tone frequencies throughout development (chapter 4).

Finally, in chapter 5 I pilot a viral retrograde tracing study of projections to A1 PV+ interneurons in both *Df1*/+ and wildtype mice. Chapter 6 provides a summary of results including limitations of the present thesis and future directions.

Chapter 2: Materials and methods

Due to the nature of my joint degree program, experiments were split between the Linden Lab at University College London, United Kingdom and the Wang Lab at the National Institute of Mental Health in Bethesda, Maryland, USA. The first set of experiments were completed in the Linden Lab at UCL. Pilot experiments here included histology and immunohistochemistry to complete data collection partially collected by another member of the Linden Lab. Auditory brainstem response recordings and tympanic membrane scoring had been previously collected. Upon the completion of the pilot study, I injected viral vectors into the primary auditory cortex (A1) of animals to find the A-P Bregma location within the secondary motor cortex (M2) that would likely receive the most projections from A1. I also collaborated with the Gatsby Computational Unit at UCL to trial an automated cell counting code. In the next set of experiments, I added tests of auditory sensorimotor gating and auditory evoked potentials and continued to assess cell counts via immunohistochemistry and used ABR to assess hearing in *Df1*/+ animals and their wildtype littermates.

After collecting data at UCL, I then moved to NIMH for the remainder of the experiments. In the Wang Lab I analyzed the UCL data and performed my last two sets of experiments. First, I completed a longitudinal study to assess the nature of conductive hearing loss seen in *Df1*/+ animals using ABR with additional stimuli and distortion product otoacoustic emissions. The final set of experiments was a monosynaptic retrograde tracing study to examine projections to A1 interneurons.

2.1 University College London (UCL) experiments

2.1.1 Animals

All mice used in the experiments reported in this thesis were bred from a genetically modified line established previously on the C57BL/6J background (Lindsay et al., 1999). Breeding at University College London (UCL) was maintained by crossing Df1/+ males from within the colony with wildtype (WT) C57BL/6J females either from within the colony or from Charles River UK.

Back-crossing into the C57BL/6J strain had been maintained for well over 10 generations at the start of the experiments. Mice were maintained in standard cages and mouse housing facilities, on a standard 12 h on, 12 h off light/dark cycle. All experiments were performed in accordance with a Home Office project license approved under the United Kingdom Animal Scientific Procedures Act of 1986.

2.1.2 Pilot experiments (referenced in appendix 1)

Pilot data for the experiments reported in this thesis were collected by myself and Sandra Wenas, a former master's student in the Linden laboratory. A total of 24 mice (11 *Df1/+* mice and 13 of their WT littermates) were analyzed for this initial study. Of these 24, I completed coronal slicing, Nissl and immunohistochemical staining and analysis for 15 animals and re-imaged and analyzed the remaining 9 mice.

2.1.3 Auditory brainstem response (ABR) recording

To screen mice for hearing loss I recorded the auditory brainstem response (ABR), an electroencephalographic signal measured through the use of scalp electrodes which allows for the detection and visualization of sound-evoked potentials generated by neuronal circuits in the ascending auditory pathway (Willott, Carlson, and Chen 1994). ABR recordings were performed in a sound isolation booth (Industrial Acoustics Company, Inc.). Auditory stimuli were generated at a sample rate of 195,312.5 Hz using a digital signal processor (Tucker-Davis Technologies, TDT RX6), attenuated as needed (TDT PA5), amplified (TDT SA1), and presented using a free-field speaker (TDT FF1) positioned 17-18 cm from the ear directed toward the speaker. Speaker output was calibrated to within 2 dB of target values before each set of experiments using a Brüel & Kjær ¼ inch microphone (4939), placed at the location of the ear to be tested. Data was acquired at a 24,414 Hz sample rate (TDT RX5) using a low impedance headstage and signal amplifier (TDT RA4LI and RA16SD, 20x gain overall, 2.2 Hz - 7.5kHz filtering) along with a custom low-pass filter designed to remove attenuation switching transients (100 kHz cutoff).

Stimulus presentation and data acquisition was controlled using software from TDT (Brainware) and custom software written in MATLAB (Mathworks).

Mice were anaesthetized via intraperitoneal injection of a ketamine-medetomidine cocktail (0.003-0.01 ml/g body weight of 10mg/ml ketamine, 0.083 mg/ml metetomidine). Body temperature was maintained at 37-38°C using a homeothermic blanket (Harvard Apparatus). Mice were typically kept hydrated with subcutaneous injection of sterile saline or Ringer's solution (0.1ml S.C.), and ophthalmic ointment was applied to the eyes to prevent drying of the corneas. Subdermal needle electrodes (Rochester Medical) were inserted under the skin at the vertex (positive), at the bulla behind the ear directed toward the speaker (negative), and over the olfactory bulb (ground). In a few animals for which ABRs but not AEPs were recorded, I instead placed the ground electrode behind the bulla opposite the tested ear. ABR thresholds were determined in the left and right ears in turn in most animals. The animal was re-oriented between recordings to direct the ear being tested toward the speaker, but I avoided altering the positions of the subdermal electrodes by switching electrodes at the input of the pre-amplifier whenever possible. ABR stimuli were 50 μs monophasic clicks ranging in sound level from 0 to 90 dB SPL in 5 dB steps, repeated 500 times at an inter-click interval of 50 ms. Tests were monaural. Initial tests were completed with an earplug placed in the opposite ear, but results showed no difference in ABR thresholds with or without plugging of the opposite ear, so no earplug was used in subsequent experiments. ABR waveforms were repeatable and consistent upon repeated tests in the same animal (see Figure A.7).

Thresholds were subjectively defined to be the lowest sound intensity evoking a clear and characteristic deflection of the ABR wave. See Figure 2.1 for an example of ABR threshold determination. All threshold determination was performed blind to genotype. Auditory ABR thresholds were determined to be the lowest intensity at which an ABR waveform could be detected.

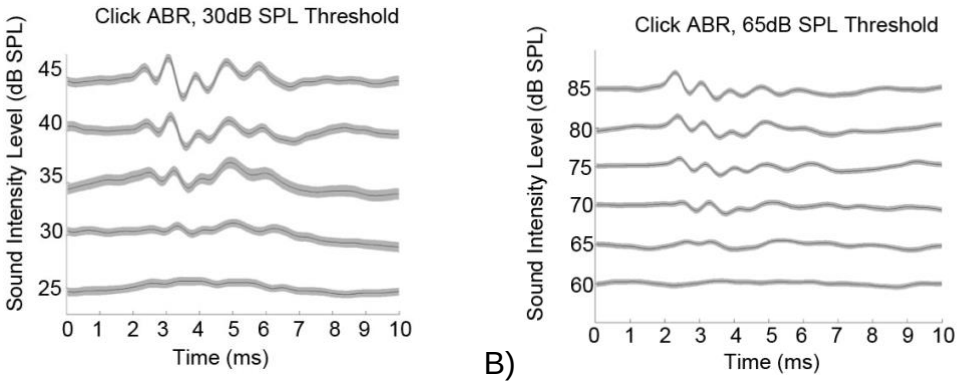

A) B)

Figure 2.1 Determination of ABR thresholds

ABRs produce wave voltages from the auditory nerve through the auditory midbrain. ABRs were presented at ascending intensities in 5 dB steps. The threshold was determined to be the lowest intensity at which a characteristic ABR can be discerned. The standard error can be seen in grey shading surrounding the mean amplitude of the waveform. (A) 25 – 45 dB SPL click stimuli were presented. The threshold for this WT mouse was defined as 30 dB SPL. (B) 60 – 85 dB SPL click stimuli presented. The threshold for this *Df1/+* mouse was defined as 65 dB SPL.

2.1.4 Perfusion

Mice were euthanized using an overdose of sodium pentobarbital (0.1-0.2 ml of 20 mg/ml Euthatal; Rhône Mérieux, Essex, UK) and were perfused transcardially with at least 30 ml 4% paraformaldehyde (Merck, Dorset, UK) using a peristaltic pump.

2.1.5 Tympanic membrane scoring

A total of 17 animals underwent tympanic membrane inspection where the appearance of the tympanic membrane was assessed to be either air filled (normal) or fluid filled (infected with OM). The tympanic membrane was given a score of 0 (normal), 1 (filled with air bubbles, or 2 (opaque and filled with a pus-like substance) and scored based on photos from a collaborator's previous study (see Figure 2.2). To obtain sufficient access to the tympanic membrane for this detailed visual inspection, the scoring had to be performed after the

outer ear had been removed. These scores were obtained following euthanasia and perfusion.

A) 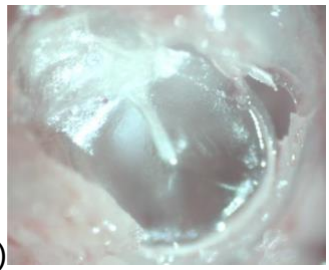 B) 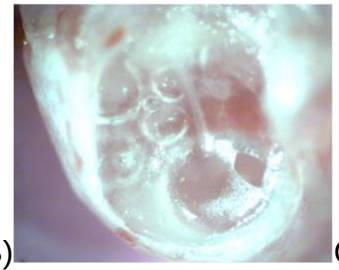 C) 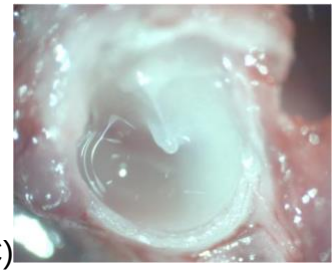

Figure 2.2 Examples of tympanic membrane scoring

(A) Normal middle ear with air-filled space behind the tympanic membrane. Middle ears like this were given a score of 0. (B) Middle ear with air bubbles behind the tympanic membrane, indicating partial filling of the middle ear cavity with effusion. Middle ears like this were given a score of 1. (C) Middle ear with complete effusion, made opaque by the quantity of pus-like substance behind the tympanic membrane. Middle ears like this were given a score of 2.

Photos courtesy of Jennifer Fuchs and Abigail Tucker, King's College London.

2.1.6 Histology

Following perfusion (and tympanic membrane scoring where performed), brains were removed and fixed in 4% paraformaldehyde before being stored in a 4°C refrigerator until histology could be completed. Brains were placed in increasing concentrations of sucrose solution (15% followed by 30%) until the brain sank to the bottom of the container to cryoprotect them from damage while freezing and slicing. Brains were processed in gender-matched, age-matched or genotype-matched pairs initially, but for the second round of immunohistochemistry brains were only paired through genotype (one of each). For increased adherence to the mounting block of the cryostat, the olfactory bulb and cerebellum were cut off with a razor blade. To differentiate each hemisphere after slicing, a needle was passed caudal to rostral through the hippocampus of one side of the cortex. The brains were embedded in OTC medium (TissueTek) and flash frozen before 50µm sections were sectioned coronally on a cryostat (Bright, Huntingdon, UK). Alternate slices were placed in phosphate buffered saline (PBS) to be stained with either cresyl violet (Nissl

staining) to identify frontal and auditory cortices or primary and secondary antibodies to parvalbumin (PV) to identify PV+ cells.

2.1.7 Nissl staining

For Nissl staining, sections were transferred to slides and allowed to dry overnight. Dried slides containing the sections were placed in 100% Ethanol, 95% Ethanol, 80% Ethanol, and 70% Ethanol for 20-60 seconds each, followed by 20 seconds in distilled water. Slides were then placed in Cresyl Violet dye for 20-30 minutes, followed by distilled water for 20 seconds. Slides were placed in 70% Ethanol followed by 80% Ethanol for 3-5 minutes. Sections were placed in baths containing 95% for 5 minutes each, followed by two baths of 100% Ethanol for 10 minutes each. Sections were then washed in two baths of Histoclear and coverslipped using DPX Mounting Media (Thermo Scientific) under a fume hood.

2.1.8 Parvalbumin staining

For parvalbumin staining, PBS solution was removed from each well and refilled with 0.5% Triton solution and left on a shaker for 20 minutes at room temperature. Sections were then placed in a blocking solution containing 60% PBS, 30% 0.5% Triton and 10% goat serum and incubated for 40 minutes on a shaker at room temperature. After the blocking mixture was removed, wells were filled with mouse anti-PV (diluted 1:8000 with blocking mixture, Sigma-Aldrich) and left on a shaker in a 4°C refrigerator overnight (approximately 17 hours). Primary anti-PV was removed and sections were then rinsed with PBS and placed on a shaker at room temperature for five minutes a total of five times. Sections were then incubated in a goat anti-mouse secondary antibody (diluted 1:200 with blocking mixture, Sigma-Aldrich) at room temperature for one hour on a shaker, covered. Aluminum foil and Styrofoam lids were used to avoid exposure to light when sections were not in the process of being manipulated from this stage forward. Sections were then rinsed again in PBS five times for five minutes and placed on a shaker at room temperature. Before being transferred to slides, sections were rinsed in distilled water before being

transferred to slides. Sections were mounted with Fluoromount-G (Southernbiotech) and coverslipped.

2.1.9 Anterior-posterior localisation of sections relative to Bregma

To identify the auditory and prefrontal cortex in each coronal section, the Franklin and Paxinos mouse atlas (2012) was referenced and each Nissl-stained coronal section was compared to atlas images. This atlas depicts A1 as located -2.18 and -3.64mm anterior-posterior (A-P) relative to Bregma. To avoid inclusion of the primary sensory cortex (S1), A1 cell counts were taken at Bregma -2.54mm A-P. A1 was identified by examining cortical thickness, changes in cell density, the structure of the hippocampus and rhinal fissure landmarks in the Nissl stained sections. See Figure 3 for an example of A1 identification. Cingulate cortex A24b counts were obtained at Bregma +1.70mm A-P and secondary motor cortex M2 counts were performed at the same A-P location. Bregma +1.70mm was chosen as the counting location for A24b as it was in the middle of the span of the cingulate cortex between 1.42 and 2.10mm A-P. This location was identified by the shape of the forcept minor of the corpus callosum (fmi), the shape and size of the lateral ventricle (LV), and the shape and width from the cortical surface to the midline. See Figure 4 for an example of frontal cortex identification.

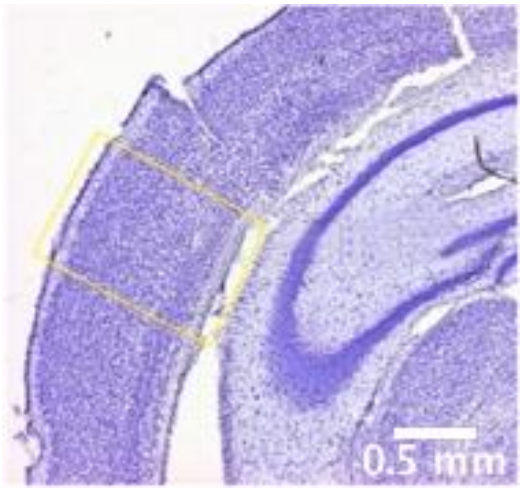

Figure 2.3 Example of A1 identification in Nissl-stained section

Example confocal image of a coronal section through primary auditory cortex (A1) stained with Nissl.

A) 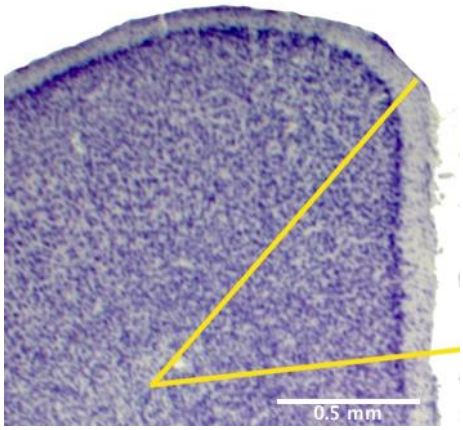

B) 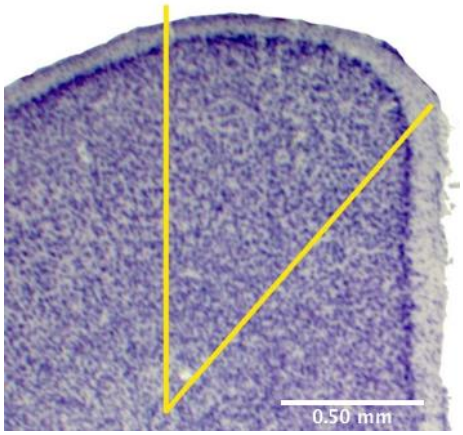

Figure 2.4 Example of frontal cortex (A24b, M2) identification in Nissl-stained sections

Example confocal image of a coronal section through the frontal cortex stained Nissl. (A) Cingulate cortex area (A24b). (B) Secondary motor cortex (M2).

2.1.10 Imaging

Nissl stained sections were viewed at magnifications ranging from 2.5x to 5x on a Zeiss AxioPlan 2 Imaging microscope. Once the appropriate representation of A1, A24b and M2 was observed, images were taken at 5x or 10x. Individual photos of each hemisphere were taken. For the final analysis, all section locations were reidentified and images retaken by the same experimenter for consistency.

2.1.11 Image processing and cell counting

ImageJ was used to enhance the contrast of images to identify cells for manual counting. The mouse brain atlas served as a guide for measurements of the shape and size of each area of the cortex. For each counted area, one known measurement was taken directly from the mouse atlas and applied to the taken image. This measurement was then set as a known distance so all other measurements would be normalized as ratios with respect to this known measurement. Further measurements and angles were then drawn.

Using the mouse atlas, it was established that the depth of A1 from pia to white matter is depicted as approximately 1mm and the height (dorsoventral) 0.6mm.

Using the Straight Line Selection Tool in ImageJ, a line was drawn from the pial surface to the white matter and set as a known distance of 1000. A perpendicular line was then drawn to reach a length of 600 (the same ratio as depicted in the atlas). See Figure 2.5 for an example image.

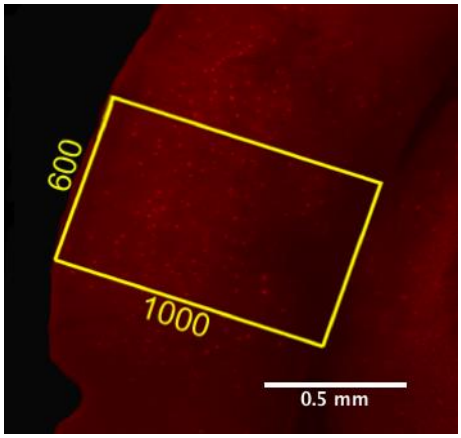

Figure 2.5 PV+ A1 counting area

Example confocal image of a coronal section through primary auditory cortex (A1) stained with an antibody against the inhibitory interneuron marker parvalbumin (PV). Numbers indicate normalized distances.

For A24b, the mouse atlas depicts a perpendicular line from the midline as approximately 0.75mm. This line was redrawn on the taken image and set as a known distance of 750. A line at the angle of 67 degrees was then drawn to complete the counting area outline. See Figure 2.6 for an example image.

M2 borders the cingulate cortex area (A24b) that was previously measured. To outline M2, a 17 degree angle from the top border of A24b was drawn from the pia to white matter. See Figure 2.6 for an example image.

A) 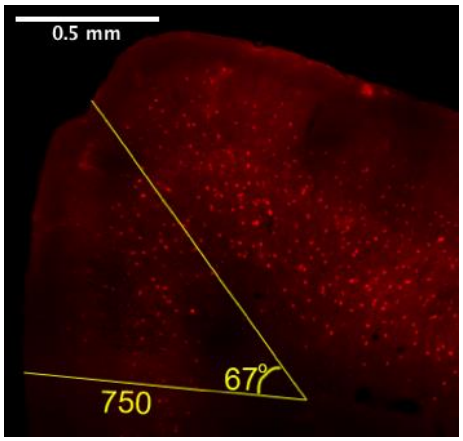

B) 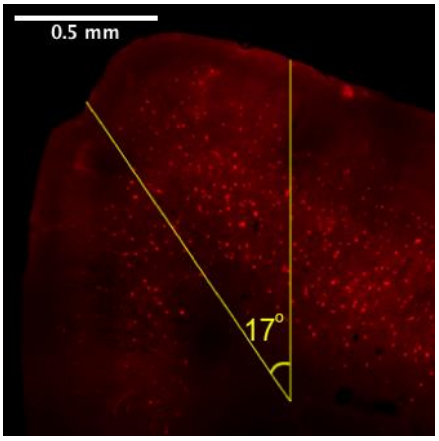

Figure 2.6 PV+ frontal counting areas

Example confocal image of a coronal section through primary auditory cortex (A1) stained with an antibody against the inhibitory interneuron marker parvalbumin (PV). (A) Cinguate cortex area (A24b). Numbers indicate normalized distance. (B) Secondary mortor cortex (M2).

Once the region of fixed size depicting the appropriate representation of each brain area was drawn on each image in both hemispheres, areas outside of this targeted area were blacked out. Manual counting was performed by painting dots over each cell and using ImageJ's counting function and double checked manually. Counting was performed blind to genotype in a total of 23 brains. Data was then transferred to Microsoft Excel and Matlab for analysis.

2.1.12 Data analysis

In the pilot study, data from 24 animals was included in analysis (n = 13 wildtype, n = 11 *Df1/+* animals; n = 9 wildtype tympanic membrane scores, n = 8 *Df1/+* tympanic membrane scores, n = 18 wildtype ABR ear scores, n = 16 *Df1/+* ABR ear scores).

For analysis of ABR data, non-parametric tests were used wherever possible, as the assumptions of normal distributions and equal variances inherent in t-tests and ANOVAs were violated by the threshold distributions of Df1/+ animals. The Wilcoxon rank-sum test (non-parametric t-test) was used to analyze the significance of the differences in median threshold between two groups. To

determine whether ABR thresholds were age or gender-related, a regression of thresholds against each was performed; the regression slope was not significantly different from zero in the current data.

2.1.13 Revision of M2 target locations based on Allen Brain Atlas and viral vector experiments

A study by Meechan and colleagues (2015) showed altered PV+ cell distribution in the medial prefrontal cortex in a similar mouse model of 22q11DS, which correlated with behavioral deficits in a visually guided discrimination task. However, these cell density measurements were conducted using brain sections from a more posterior A-P location (Bregma +0.25mm) than I had originally used for M2 based on the Franklin and Paxinos (2012) mouse atlas (Bregma +1.70mm). For further investigations I reconsidered this approach, and decided to identify optimal M2 locations for analysis based on density of projections from A1 to M2.

The Allen Brain Atlas mouse connectivity map and Brain Explorer 2 were used to visualize projections from A1 to M2. The online mouse connectivity brain map was searched to display the experiment in which axonal projections labeled by rAAV tracers were primarily injected in A1 of a C57BL/6J mouse and visualized in the target structure M2 using serial two-photon tomography. Data was exported to Brain Explorer 2, an application that allows users to view brain anatomy and gene expression data in three dimensions through the framework of the Allen Reference Atlas. By viewing the 3-D representation of the neuronal projections from A1 to M2, the projection point in M2 with the highest density and intensity of fluorescence was chosen. This was achieved by controlling projection visibility by setting thresholds on projection signal values to the highest intensity and density until projections in M2 were visible. This point was annotated as the secondary motor area layer 2/3, with an intensity of 705.1, a density of 0.05424 and a location of 5.401, 0.7818, 6.398. This area corresponded to image 53 in the Allen Mouse Brain Atlas. Using reference structures such as the crossing of the corpus callosum and the merging of the

left and right lateral ventricles, the slice was approximated to a location of Bregma +0.2 using The Mouse Brain in Stereotaxic Coordinates Third Edition by Franklin and Paxinos.

Additionally, I conducted my own anterograde viral vector injection experiments in A1, and quantified fluorescence in M2 by eye. Three mice were anaesthetized with 4% isofluorane and shortly thereafter injected with 0.2ml/g 1.2% Avertin via intraperitoneal injection. The skull was then secured using an ear bar and 100ul of 2% Lidocane was injected at the crown of the head under the skin. The skin covering the skull was incised to expose Lambda and Bregma for stereotaxic approximation. The target injection site of 2.6mm posterior from Bregma and 2.9mm lateral to Bregma was marked and a 0.5-1mm diameter circle was drilled through the skull. Once the brain was exposed and the level of anesthesia was reassessed, 1-2ul of viral vector was injected at the target site at a 24 degree injection trajectory. I trialed two types of viral vector, AAV1-GFP in two mice and AAV9-GFP in the third mouse. The vector was injected slowly between 4.3mm and 3.7mm deep into the cortex using an electronic syringe pump. Silicone gel was placed over the window in the skull for protection and the skin sutured together. Mice were placed back in their holding cages for two weeks before virus expression was analyzed. Of the three mice that received viral injections, A1 was targeted well and images were of sufficient quality in one mouse (injected with AAV1-GFP). Brains were fixed and sliced in 100µm slices, with every other slice imaged using a two-photon microscope (FV1000 multi-photon laser scanning microscope). DAPI mounting medium was used to stain cell bodies and visualize key structures to be used with an accompanying mouse brain atlas. The brightest fluorescence was apparent at an approximate A-P location of Bregma +0.3mm. See Figure 2.7 for images of GFP and DAPI stained sections deemed the brightest.

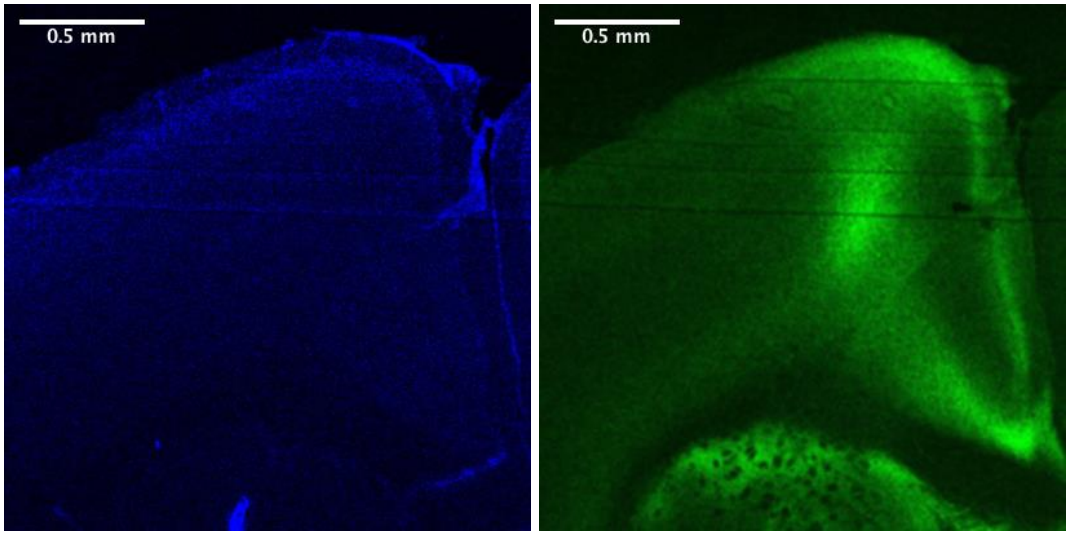

Figure 2.7 Brightest fluorescence of viral vector in M2

DAPI (left) and GFP (right) confocal images from the same coronal slice at Bregma 0.3mm that was injected with a fluorescent viral vector in the primary auditory cortex (A1).

I decided to take the difference between the M2 locations derived from the Allen Brain Atlas and my own viral vector experiments and selected a target location of Bregma +0.25mm (4.04mm Interaural). This coronal location will be referred to as M2target (M2tar).

I also wanted an additional A-P location to count cells where there are no projections from A1 to M2 in order to be able to quantify neuronal populations in a more anterior area of M2. Using the Mouse Brain in Stereotaxic Coordinates Third Edition by Franklin and Paxinos I chose the second most anterior brain slice that contains M2, which has an A-P location of Bregma +2.34mm (6.14 Interaural) and will be referred to as M2anterior (M2ant). The Brain Explorer 2 did not show any projections at this location. It is important to note that the most anterior projection site in M2 from A1 is at approximately Bregma +1.70/1.78mm. This is where I was initially counting for PV+ cells in M2, and thus it seemed possible that the reason I did not see a significant difference in PV+ interneuron density was that there are very few PV+ cells that receive direct projection from A1 in this location.

A point between the anterior M2 counting site and the posterior counting site was chosen to enable analysis of the gradient of PV+ distribution across the A1-to-M2 projection within M2. The midpoint between Bregma +2.34mm and +0.25mm is Bregma +1.30mm, which will be referred to as M2gradient (M2gra).

Primary auditory cortex (A1) on the Mouse Brain in Stereotaxic Coordinates Third Edition by Franklin and Paxinos lies between Bregma -2.18mm and -3.64mm. To avoid overlap with the primary somatosensory cortex, I chose Bregma -2.54 mm, which is posterior enough not to contain the primary somatosensory cortex region.

2.1.14 Identifying sections at the A-P locations M2 and A1

Since sections were sliced at 50µm thickness, I used the number of sections to count the mm from where the corpus callosum (cc) crosses the midline at 1.10mm Bregma. This is a beneficial marker to use, as it is very easy to see in both Nissl and DAPI stained sections as well as PV+ stained sections. Once the crossing of the cc was located in PV slides, the distance between the crossing of the cc and the intended Bregma location was calculated and identified.

M2

M2target (M2tar) was identified as Bregma 0.25mm, which is 0.85mm away from the crossing of the cc. With each section sliced at 50µm thickness, M2tar should be 17 slices posterior to the crossing of the cc.

A1

As in previous experiments, A1 was identified by comparing hippocampal and rhinal fissure landmarks to the Franklin and Paxinos (2012) atlas. See Figure 2.3 for previous example. Sections identified as A1tar were those with landmarks corresponding most closely to those typical of atlas sections at Bregma -2.54mm.

2.1.15 Automated cell counting

An automated cell counting algorithm was created by collaborators at the Gatsby Computational Unit at UCL (Pachitariu et al., 2013). I trialed the use of the automated cell counter, and planned to adopt its use for further analysis in the later dataset. After the algorithm learns to detect cells, it then gives each potential cell detected in the image a "cell-likeness" score. The smaller the number, the more likely it is a cell. Cell counting was initially done by hand to compare what threshold of "cell-likeness" from the algorithm consistently corresponds to the amount of cells counted manually. See Figure 2.8 for an example of thresholds trialed within the algorithm.

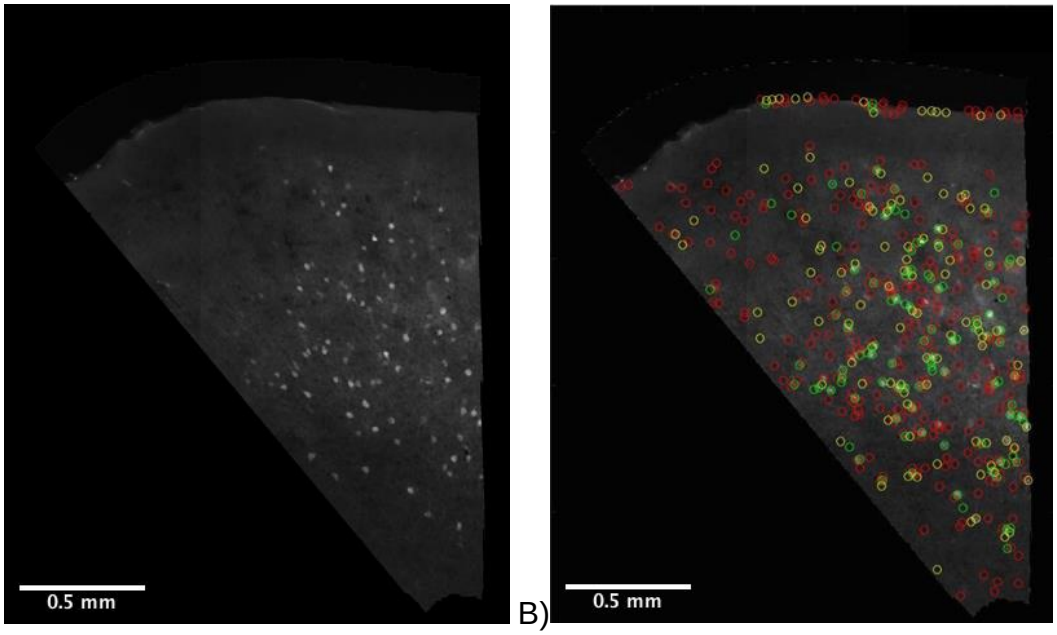

Figure 2.8 Comparison of results from manual cell counting and automated cell counting algorithm

(A) Cells counted by hand within cortical area M2. The total counted number of cells in this image was 108. (B) Automated cell counting within the same cortical area using different "cell-likeness" thresholds. For the most permissive threshold setting, the number of "cells" identified in this section was 500 (red circles); increasingly more strict thresholds produced cell counts of 209 (yellow circles) and 107 (green circles).

I found that the optimal "cell-likeness" threshold setting (which produced the best match between automated cell counts and manually determined cell

counts) varied considerably from image to image. Therefore, optimizing the parameters for automated cell counting proved to be much more time-consuming than expected. Rather than devoting time to honing the algorithm, I decided to count cells manually for the experiments described in this thesis.

2.2 Follow up study: Hearing loss promotes schizophrenia-relevant brain and behavioral abnormalities in a mouse model of human 22q11.2 Deletion Syndrome

2.2.1 Animals

Mice were maintained as described previously for the pilot study. Experiments described below were conducted in Df1/+ mice and wildtype littermates that were 6 to 19 weeks of age (mean 13, SD 4.49 weeks).

2.2.2 Acoustic startle response (ASR) and prepulse inhibition (PPI) testing

To test auditory sensorimotor gating in Df1/+ and WT mice, I measured the acoustic startle response (ASR) and prepulse inhibition (PPI) of the ASR. Startle experiments were conducted using a custom-built startle measurement system consisting of four piezoelectric sensors mounted underneath a circular platform 12.5 cm in diameter, housed within a dark acoustic isolation booth lined with acoustical foam. The platform was encircled by a removable cylindrical plastic tube approximately 13 cm in diameter and 30 cm high, to prevent the mice from jumping off. Infrared lighting outside the visible range of the mouse and a webcam (Logicam) were used to monitor the animals during testing. If a mouse tried to climb up the cylinder, the testing session was paused, the animal was returned to the platform and the recording restarted. A speaker (Peerless Vifa XT25TG30-04) was mounted in the ceiling of the booth, approximately 40 cm above the platform and centered over the opening of the cylindrical platform enclosure.

Sensor signals were acquired at a 30 kHz sample rate from the analog inputs on an Open Ephys data acquisition board using Open Ephys GUI software (www.open-ephys.org), then downsampled to 1 kHz for analysis. Acoustic stimuli were generated at a 96000 Hz sample rate using a professional sound

card (RME HDSPe AIO) and custom Python software (“StimControl”, by Arne F. Meyer). Stimuli were delivered to the speaker via either a Rotel RB-971 speaker amplifier or a Tucker-Davis Technologies SA5 speaker amplifier. Speaker output was calibrated using a ¼-inch free-field microphone, preamplifer and amplifier (G.R.A.S. 40BF, 26AC and 12AA) before the experiments began, to ensure that noise levels for cue and startle stimuli were within 2 dB of target levels. Measurements of speaker output were made with the microphone positioned in the center of the platform at the approximate height of the animals’ ears during testing.

Acoustic startle and prepulse inhibition data were typically collected from each mouse in two repeated 25-30 min testing sessions on different days, separated by 2 days. An additional testing session was conducted on a third day if a previous session had been unsuccessful (e.g., if there had been technical problems or difficulty keeping the animal on the measurement platform). Each session involved two types of behavioral tests: startleIO tests and startlePPI tests.

In startleIO tests, the ASR input/output function was measured, recorded, and also visually inspected online to choose prepulse cue levels used for subsequent startlePPI tests. StartleIO tests involved presentation of a 65 dB SPL continuous white noise background sound, overlaid with 20 ms noise bursts with sound levels ranging from 55 or 60 dB SPL to 95 dB SPL in 5 dB steps. Noise bursts of different sound levels were presented in pseudorandom order, with randomly varied inter-burst intervals that typically ranged from 1.67 s to 8 s (average 5 s). A typical startleIO test lasted 225 s and involved presentation of 5 repeats of each noise burst sound level. An initial online analysis of startle magnitude as a function of noise burst intensity level was performed to choose the two or three loudest sound levels that did not evoke a startle response, for use in subsequent startlePPI tests.

In startlePPI tests, prepulse inhibition of the acoustic startle response was assessed. Like startleIO tests, startlePPI tests were conducted with a

continuous 65 dB SPL white noise background. Approximately 20-25% of startlePPI trials were uncued trials, in which a 40 ms, 95 dB SPL startle-eliciting stimulus was presented in the middle of the 20 s trial. On the remaining 75-80% of trials (cued trials), the startle-eliciting stimulus was preceded by a 20 ms prepulse noise burst at one of the sound levels chosen to be below the startle threshold in the startleIO tests. The delay between the onset of the prepulse cue and the onset of the startle-eliciting stimulus alternated randomly between 50 ms and 100 ms; however, PPI proved to be more robust in both Df1/+ and WT mice using the shorter delay, and so only data collected using the 50 ms delay is presented here. A typical startlePPI test lasted 1000 s and involved pseudorandom presentations of 10 repeats of each of 4 possible cue conditions (2 sound levels x 2 delays) and 10 repeats of the uncued condition.

Within 1-2 days of the final behavioral testing session, mice that underwent startle testing were anaesthetized for auditory brainstem response and auditory evoked potential recordings, and then immediately terminated and perfused for immunohistochemical analysis.

2.2.3 Auditory brainstem response (ABR) and auditory evoked potential (AEP) recording

ABR recordings for this more complete set of experiments were recorded as described above for pilot experiments.

In a subset of animals, I collected further ABR recordings in combination with auditory cortical evoked-potential (AEP) recordings. To measure AEP signals, additional subdermal electrodes were placed at locations corresponding approximately to the left and right auditory cortices, and referenced to the same ground (at the olfactory bulb) as for the ABR recordings. Stimuli were 80 dB SPL clicks presented 1000 times at an inter-click interval of 300 ms. The longer inter-click interval allowed for resolution of late cortical AEP waves as well as the earlier ABR signals.

2.2.4 Histology, immunohistochemistry and microscopy

Perfusion and histology for this more complete set of experiments were recorded as described above for pilot experiments.

In some animals, alternate sections were used for Nissl staining and parvalbumin (PV) immunohistochemistry. In other animals, sections were triple-stained for PV, NeuN and DAPI. Nissl staining was performed on mounted sections using cresyl violet, as described previously for pilot experiments. For PV and NeuN staining, sections were incubated with 0.5% Triton and blocked with 0.5% Triton and goat serum blocking solution before being incubated in mouse anti-PV monoclonal antibody (1:2000, Sigma-Aldrich) and mouse anti-NeuN polyclonal antibody (1:2000, Sigma-Aldrich) at 4°C overnight. Sections were then rinsed in PBS and incubated with goat anti-mouse secondary antibody (1:200, Sigma-Aldrich) for one hour at room temperature on a shaker. Sections were then rinsed again in PBS. Slides were mounted with DAPI Flouromount-G (Southernbiotech) and coverslipped. Appropriate control staining protocols were included (the primary antibody was left out to control for non-specific staining and displayed no staining.

Sections stained for Nissl were viewed at 2.5x to 5x magnifications on a Zeiss Axio Scan 2 Imaging microscope. Single-plane images of appropriate A1 and M2 sections were taken at 5x to 10x magnification, with individual images for each hemisphere. Sections immunostained for PV were viewed and captured at 10x magnification on a Zeiss Axio Scan 2 Imaging microscope. All images were obtained at a resolution of 720 pixels/inch.

2.2.5 Data analysis

A total of 32 *Df1*/+ mice (11 male, 21 female) and 39 WT littermates (20 male, 19 female) were used in these experiments. All data analyses were conducted blind to the genotype of the animal. I performed comparisons between two groups with the unpaired t-test, and comparisons between multiple groups with the ANOVA followed by Fisher's LSD tests where group differences were

significant. Non-parametric tests were used where required; for random permutation tests the data were randomly permuted 10,000 times and the actual difference between the means of the groups were compared against the randomized distribution. Unless otherwise indicated, all statistical tests were two-tailed with $\alpha=0.05$.

2.2.6 Startle data analysis

Startle analysis was performed on data from 17 *Df1*/+ mice and 14 WT mice that completed startle testing successfully and also underwent subsequent ABR testing to assess hearing sensitivity. The time-varying startle signal was defined at each 1-ms time point as the square root of the sum of squared outputs from the four piezoelectric force sensors embedded beneath the startle platform. The startle response was defined as the sum of these sample-by-sample startle signals over the 0-65 ms period following the onset of the startle-eliciting noise burst. To determine the threshold for the startle response for each mouse, data from startleIO behavioral sessions were pooled across repeated sessions. The startle response threshold was then defined as the lowest noise burst level for which its startle response was significantly greater than the startle response elicited by a 60 dB SPL noise burst (Wilcoxon rank-sum test, $p<0.01$), and for which all noise burst levels above the threshold sound level also elicited a significantly stronger startle response than the 60 dB SPL reference. Mice for which no startle response threshold could be identified due to the mice escaping from the platform (2 *Df1*/+, 5 WT) were excluded from the population analysis shown in Figure 3.7.

The uncued startle response was determined using data from startlePPI behavioral sessions, and computed as the mean startle response to a 95 dB SPL noise burst on uncued trials from each behavioral session, averaged across repeated behavioral sessions for each animal. A behavioral session was included in this and other PPI analyses only if the uncued startle response was significantly different from the background startle response computed over a period 0–65 ms before the noise burst occurred (Wilcoxon sign-rank test,

$p<0.01$). For startlePPI sessions meeting this criterion, the cued startle response was then computed for each cue type, as the mean startle response to the 95 dB SPL noise burst on cued trials in each behavioral session averaged across repeated behavioral sessions for each animal. Prepulse inhibition (PPI) was then defined for each behavioral session and each cue type as follows:

PPI (%) = 100 * (1 - [cued startle response / uncued startle response]).

For population analysis, PPI values for each cue type and each behavioral session were averaged across behavioral sessions to obtain a single PPI measure for each animal. Cue conditions in which the cue itself evoked a significant startle response (i.e., significant difference in background startle response 0–65 ms before startle noise onset between cued and uncued trials; Wilcoxon rank-sum test, $p<0.01$) were excluded from the population analysis.

2.2.7 ABR/AEP data analysis

ABR recordings were performed in 25 *Df1*/+ (9 male, 16 female) and 26 WT (13 male, 13 female) mice. A total of 104 ABR threshold measurements (50 *Df1*/+, 52 WT) were obtained; each mouse contributed two separate ABR measurements, one for each ear. In the majority of animals, I collected ABR recordings in combination with auditory cortical evoked-potential (AEP) recordings. Combined ABR/AEP recordings were obtained from 79 ears and contralateral hemispheres (40 *Df1*/+, 39 WT); 20 *Df1*/+ mice and 19 WT mice each contributed separate ABR/AEP measurements for both of the two possible ear / contralateral hemisphere combinations, while 1 WT mice died after only one ABR/AEP recording had been completed. Separate measurements from the same animal obtained during auditory stimulation of left versus right ears were treated as independent measurements in our data analysis.

The differential ABR signal for a given ear (vertex electrode signal minus ipsilateral ear electrode signal) was averaged across 500 trials for each click

intensity, and analyzed to extract ABR waveform components as in previous studies (Fuchs et al. 2013). The ABR threshold was defined as the lowest sound intensity at which at least one of the characteristic deflections in the ABR waveform could be distinguished upon visualization of the ABR signal across all sound intensity levels (see Fuchs et al., 2013 for examples and details).

Since AEP signals were stronger over the contralateral than ipsilateral hemisphere, the single-ended AEP signal was derived from the temporal lobe electrode contralateral to the ear directed at the speaker subtracted from the ground electrode at the olfactory bulb. The AEP wave components were characterized as in Maxwell et al., 2004: P1, or P20, was defined as the maximum peak 15-30 ms after stimulus onset; N1, or N40, was defined as the maximum negative deflection 25-60 ms post-onset; and P2, or P80, was defined as the maximum peak 60-110 ms post-onset.

Wave amplitudes were defined for an 80 dB SPL click stimulus, as the difference in ABR/AEP signal amplitudes between baseline at the start of the recording and peak for ABR wave I; between the peak and subsequent trough for AEP P1-N1 complex; and between the trough and subsequent peak for AEP N1-P2 complex (see Figure 3.2). Wave latencies were defined as peak or trough times relative to stimulus onset. All amplitude and latency analyses were performed blind to mouse genotype and ABR threshold. Central auditory gain was defined as the amplitude of the AEP wave complex (P1-N1 or N1-P2) divided by the amplitude of ABR wave I.

2.2.8 Quantification of cell counts

PV+ and NeuN+ cell counts and laminar distributions in A1 and M2 were estimated for images from both hemispheres in each mouse when possible. Immunohistochemical data from some hemispheres and animals were lost due to problems with perfusion, damage to sections, or aberrant fluorescence in images. See Table 2.1 for details of number of mice and hemispheres used for different comparisons shown in Figure 3.8, Figure 3.9 and Figure 3.10 within

chapter 3. Only data from animals that had undergone ABR testing prior to immunohistochemistry were used for comparisons between *Df1*/+ mice with hearing loss, *Df1*/+ mice without hearing loss, and WT mice.

Cell type	Area	All WT	All *Df1*/+	WT with ABR	*Df1*/+ with ABR
PV+	A1	19 mice, 32 hems	19 mice, 34 hems	14 mice, 22 hems	14 mice, 24 hems (*Df1*/+ NHL: 6 mice, 10 hems; *Df1*/+ HL: 8 mice, 14 hems)
PV+	M2	25 mice, 43 hems	21 mice, 36 hems	19 mice, 31 hems	16 mice, 28 hemispheres (*Df1*/+ NHL: 7 mice, 11 hems; *Df1*/+ HL: 9 mice, 17 hems)
NeuN+	A1	14 mice, 25 hems	12 mice, 20 hems	14 mice, 25 hems	12 mice, 20 hems (*Df1*/+ NHL: 6 mice, 10 hems; *Df1*/+ HL: 6 mice, 10 hems)
NeuN+	M2	7 mice, 10 hems	10 mice, 15 hems	7 mice, 10 hems	10 mice, 15 hems (*Df1*/+ NHL: 4 mice, 6 hems; *Df1*/+ HL: 6 mice, 9 hems)

Table 2.1 Numbers of mice and brain hemispheres used for analyses of PV+ and NeuN+ cell density and laminar distribution

All mice were included in comparisons of WT and *Df1*/+ mice (chapter 3, Figure 3.8B,E, Figure 3.9B,E and Figure 3.10A,C). Only data from mice which underwent ABR testing were included in comparisons of WT animals and *Df1*/+ mice with and without hearing loss (Figure 3.8C,F, Figure 3.9C,F and Figure 3.10B,D). Hems = hemispheres

As previously described above for pilot experiments, cortical areas of interest were defined by overlaying the section image with the Franklin and Paxinos (2012) mouse atlas image of the corresponding coronal location relative to bregma, using Adobe Photoshop Elements (Adobe Systems Inc). Using ImageJ, dots were centered over the cells, cell centroid locations recorded (X,Y coordinates, in pixels), and data transferred to MATLAB for analysis of cell counts. All cells in the cortical area of interest (A1 or M2) were counted in sections immunolabelled for PV, and cells within a 5% area through the center of the region of interest were counted in sections immunolabelled for NeuN.

Laminar distributions of cells were estimated using custom MATLAB software designed to calculate cell centroid depth along a line perpendicular to the pial surface and white matter. Laminar distributions were normalized by the pia-to-white-matter distance in each section. Laminar distributions were compared between animal groups using multiple t-tests on cell counts binned by cortical depth; similar results were obtained using 5, 10 or 20 bins in depth. All cell counts and laminar distribution data were gathered blind to genotype and ABR thresholds of the mouse.

2.3 National Institute of Mental Health (NIMH) experiments

2.3.1 Animals

Four male *Df1*/+ mice were transferred from UCL to the National Institute of Mental Health (NIMH). Following health surveillance testing and a two-week quarantine period, male *Df1*/+ mice were paired with both WT C57BL/6J females and PVCre mice. PVCre mice were maintained in standard cages and mouse housing facilities, on a standard 12 h on, 12 h off light/dark cycle. *Df1*/+ crossed with WT C57BL/6J mice were used for the longitudinal hearing loss study. *Df1*/+ crossed with PVCre mice were used for the monosynaptic retrograde tracing study using rabies virus. All NIMH experiments were approved by the Institutional Animal Care and Use Committee (IACUC) at the NIMH, Maryland.

2.3.2 Longitudinal hearing loss experiments

A total of 20 mice (7 WT, 13 *Df1*/+ littermates) were used in longitudinal hearing loss experiments and analyses. Mice were tested at multiple time points between P21 and P102 (postnatal weeks 3-14.6).

2.3.3 Distortion-product otoacoustic emissions (DPOAEs) and ABR recording

Animals were taken to a dedicated Mouse Auditory Testing Core room at NIMH and the experimental animal was weighed and anesthetized by intraperitoneal (I.P.) injection of a fresh mixture of ketamine (100 mg/mL) and

dexmedetomidine (Dexdomitor, 0.5 mg/mL, 5 mg/kg). All ketamine/dexmedetomidine mixtures were made the same day as testing and were discarded if they were greater than 12 hours old. Following the anesthetic, the mouse was placed in a cage on top of a heating pad to maintain normal body temperature (37 degrees Celsius). When adequate sedation was achieved, sterile ophthalmic ointment (e.g., Puralube) was applied to the animal's cornea to prevent damage due to prolonged exposure and dehydration. If additional general anesthesia was necessary, half the original dose of the ketamine/dexmedetomidine cocktail was given via I.P. injection.

For auditory testing, the mouse was placed inside a sound-attenuating chamber (Industrial Acoustics Corporation, Bronx, NY) for the duration of the testing. Body temperature was maintained by placing the animal on an isothermal heating plate connected to an animal temperature controller (World Precision Instruments ATC-1000 or ATC-2000) which uses an integrated rectal probe to provide biofeedback for automatic plate temperature adjustments and indicates body temperature via a digital readout. DPOAE and ABR testing were completed using Tucker-Davis Technologies hardware (RZ6 processor, MF-1 speakers) and software (BioSigRZ) in conjunction with other equipment as indicated below. During DPOAE testing, a small probe microphone (Etymotic ER-10B+, Etymotic Research Inc., Elk Grove Village, IL) was placed at the opening of the ear canal. Two stimulus tones were played to the ear at levels not exceeding 70 dB SPL. Sound levels in the ear canal recorded by the microphone were displayed by the BioSigRZ software. Testing typically required about 5 minutes per ear.

During ABR testing, subdermal needle electrodes were inserted at the vertex and below each ear. Responses to 5 microsecond clicks and/or 3 millisecond tone bursts (4 to 40 kHz) were averaged following 512 (click) or 1024 (tone burst) stimulus presentations. Stimulus levels did not exceed 90 dB SPL. Thresholds were determined by increasing stimulus intensity in 5 dB steps to determine the lowest level at which a reproducible response was measurable.

Testing usually required about 20 to 40 minutes per ear to complete, depending upon the presence and degree of hearing loss, if any.
Following completion of auditory testing, the mouse was placed in a warmed cage and given a subdermal injection of atipamezole (Antisedan, 5mg/ml) to reverse the anesthesia, at a dosage determined by the animal's weight (typically, 0.01-0.05ml). After full recovery from anesthesia the mouse was returned to the cage. After the auditory testing was completed for a group of animals (usually 1-8), the cages were returned to the colony where they were kept for future auditory function analyses and/or breeding.

In between test animals, the subdermal needle electrodes were disinfected with an alcohol wipe. Following the completion of the auditory testing process for a group of animals, electrodes were disposed of in a sharps box. The remaining aliquot of the ketamine/dexmedetomidine cocktail was disposed of in accordance with NIH, EPA and other pertinent government guidelines and established practices regarding disposal of controlled substances. All syringes were disposed of in the proper sharps containers according to NIH guidelines and policies.

In mice that underwent only auditory testing, after full recovery from anesthesia the mice were returned to the colony where they were kept for future auditory function analyses and/or breeding. Mice used for longitudinal analysis of hearing underwent repeated ABR testing at weekly intervals, from approximately 3-14.6 weeks of age. Animals used for viral vector labelling injection and surgery following DPOAE/ABR testing were allowed to fully recover from anesthesia (for at least 24 hours or up to a week) before the viral vector injection procedure.

2.3.4 Monosynaptic retrograde tracing experiments

A total of 8 mice (3 WT, 5 *Df1*/+ littermates) were used in longitudinal hearing loss experiments and analyses. All animals were tested for click ABR thresholds prior to viral vector injection. All *Df1*/+ mice used in these

experiments had hearing loss, and all WT animals had normal ABR thresholds. See Table 2.2 for details of numbers of mice and hearing loss profile.

2.3.5 Viral vector injection and surgery

Mice were first anesthetized with tribromoethanol (Avertin, 1.5% solution given at 0.01 ml/g, I.P.) and then mounted in a stereotaxic frame. Ear bars and a nose cone/tooth mount were used to hold the animal's head securely. The eyes were protected with ophthalmic ointment as described above to prevent irritation and dryness.

The fur between the eyes and ears was trimmed and the skin was disinfected with 3 swabs of 70% ethanol. A ~1.5 cm incision in the scalp above the right hemisphere was made using a sterile surgical blade or scissors. After the skull was dried, the center of the desired injection site relative to Bregma was marked using a stereotaxic instrument. A high-speed microdrill (typically between 7000 and 10,000 rpm) with a 0.5 mm circumference drill bit was used to create a circular craniotomy (approx. 0.5-1mm in diameter) at the desired viral injection location (AP -2.6mm, M-L 4.2mm Bregma or AP -3.16mm, M-L 4.2mm Bregma). Then the craniotomy region was moistened, and the bone island was lifted gently from the brain.

Mice were injected with TVA and left for 2 weeks prior to rabies injection. For both TVA and rabies injections, a glass pipette (tip diameter between 50–100 μm) was attached to a microinjector for viral injection. First, 400 μl adeno-associated virus (AAV, AAV2/9 EF1α-FLEX EGFP-TVA-rabies, 9.279x10^13 g/mL) was drawn into the glass pipette. Using the stereotaxic arm, the glass pipette tip was lowered toward the brain until it was in contact with the intact pia mater. Once in contact with the pia, the pipette was then lowered to the injection coordinate depth and slowly the virus was injected between (0.55-0.95) within 10 minutes. To avoid backflow, an additional 5 minutes was allowed before removing the piepette tip. The scalp was sutured over the injection site and animals were treated with ketoprofen (5 mg/kg) intraperitoneally to reduce pain

and moved to a warm recovery cage until ambulatory. Single housing was adopted post-surgery to protect the surgery site.

For the rabies injection, the same procedure was followed but the injection was of 500 µl rabies virus (EnvA-pseudotyped-rabies delta-G-mcherry, 4.2x10^8 IU/mL, Boston Children's Hospital) two weeks after TVA injections. Animals were single housed in biosafety level 2 after the injection and were sacrificed 1 week after for histology.

2.3.6 Histology, immunohistochemistry and microscopy

Mice were euthanized using an overdose of sodium pentobarbital (0.1-0.2 ml of 20 mg/ml Euthatal; Rhône Mérieux, Essex, UK) and perfused transcardially with 4% paraformaldehyde (PFA) in phosphate-buffered saline (PBS) followed by 4% PFA in PBS postfixation for at least 24 hours. The tissue was cryo-protected with 20% sucrose and processed using cryostat (Leica) (section thickness 50 um). Sections were mounted with DAPI Flouromount-G (Southernbiotech) mounting medium for imaging and analysis. Sections were imaged with a Zeiss Axio Scan 2 Imaging microscope as in the UCL experiments. Images of any cellular staining at the injection site or more anterior/posterior were counted manually and analyzed.

2.3.7 Quantification of viral vector cell counts

Any sections with either PV+ and/or rabies infected cells were included the set of images used for cell counting. Immunohistochemical data from some hemispheres and animals were lost due to problems with perfusion, damage to sections, or aberrant fluorescence in images. In the case of a damaged section, the average number of cells within adjacent images were taken and averaged to calculate that section's projected cell count (i.e. the cell counts of the section immediately before and after were averaged). Counted cells were localized to brain structures with reference to the Franklin and Paxinos mouse atlas (2012).

A1 Injection Site	WT	*Df1/+*	Hearing thresholds (dB SPL)
Anterior A1	2 mice, NHL	2 mice, binaural HL	85dB R & 55dB L (binaural HL) 75dB R & 50dB L (binaural HL)
Posterior A1	1 mouse, NHL	3 mice, monaural HL	55dB R & 40dB L (monaural HL R) 65dB R & 40dB L (monaural HL R) 35dB R & 60dB L (monaural HL L)

Table 2.2 Numbers of mice, hearing loss profile and A1 injection site used in analyses of monosynaptic retrograde tracing experiments

All WT animals had normal ABR thresholds (35dB SPL or less) while all *Df1/+* animals had either monaural or binaural hearing loss.

Chapter 3: Hearing loss promotes schizophrenia-relevant brain and behavioral abnormalities in a mouse model of human 22q11.2 Deletion Syndrome (under review at Journal of Neuroscience)

3.1 Introduction

22q11.2 Deletion Syndrome (22q11DS) is the strongest known cytogenetic risk factor for schizophrenia in humans (McDonald-McGinn et al., 2015). 22q11DS is caused by a 0.7-3Mbp congenital multigene deletion which occurs in approximately 1 out of 3000-6000 live births, making it the most common chromosomal microdeletion syndrome and the second most common chromosomal disorder after Down's Syndrome (McDonald-McGinn et al., 2015; Paylor and Lindsay, 2006). Approximately 25-30% of patients with 22q11DS develop schizophrenia during adolescence or adulthood (Drew et al., 2011; McDonald-McGinn et al., 2015). In addition to increased schizophrenia susceptibility, 22q11DS is also associated with over 100 different malformations and clinical presentations including heart defects, immune dysfunction, hypocalcemia, and craniofacial abnormalities such as cleft palate (Paylor and Lindsay, 2006). Furthermore, patients with 22q11DS have frequent hearing loss, arising primarily from high rates of recurrent or chronic otitis media (middle ear inflammation) (Verheij et al., 2017).

The *Df1*/+ mouse model of 22q11DS has an engineered hemizygous deletion of 1.2Mbp encompassing 18 orthologs of genes deleted in human 22q11DS (Lindsay et al., 1999). Along with other mouse models of 22q11DS, the *Df1*/+ mouse recapitulates many phenotypic features of human 22q11DS (Paylor and Lindsay, 2006), including cardiac defects (Lindsay et al., 1999), craniofacial abnormalities (Aggarwal et al., 2006), and brain and behavioral abnormalities that have been linked to schizophrenia in humans (e.g., Hamm, Peterka, Gogos, & Yuste, 2017; Sigurdsson, Stark, Karayiorgou, Gogos, & Gordon, 2010). Behaviorally, *Df1*/+ mice exhibit reduced prepulse inhibition of the acoustic startle response (Paylor et al., 2001), a robust behavioral marker for schizophrenia-like abnormalities and common feature of 22q11DS in humans

(Drew et al., 2011). Functionally, specific abnormalities in auditory thalamocortical processing have also been reported in *Df1*/+ mice, including abnormal sensitivity of auditory thalamocortical projections to antipsychotic drugs (Chun et al., 2014). Interestingly, like humans with 22q11DS, *Df1*/+ mice have been found to have high rates of hearing loss (Fuchs et al., 2013), due to increased susceptibility to otitis media caused by developmental defects arising from the 22q11DS deletion (Fuchs et al., 2015). However, the potential interaction between hearing loss and auditory brain and behavioral abnormalities in *Df1*/+ mice has not previously been explored.

In humans, hearing loss has been described as the "neglected risk factor for psychosis" (Sommer et al., 2014). Hearing loss is associated with increased risk of psychosis and hallucinations, and hearing impairment in childhood elevates the risk of developing schizophrenia later in life (see Linszen, Brouwer, Heringa, & Sommer, 2016). The mechanisms underlying the association between hearing loss and schizophrenia are unknown, and could include common etiology, top-down influences (e.g., social isolation), and/or bottom-up effects. A role for bottom-up effects is suggested by data from animal studies indicating that loss of peripheral auditory input drives long-lasting changes in central auditory processing which can affect behavior (Chambers et al., 2016; Sanes and Kotak, 2011; Takesian et al., 2009; Yao and Sanes, 2018). Even reversible conductive hearing loss, such as that caused by otitis media, can produce persistent changes in inhibitory synaptic transmission in the auditory cortex (Mowery et al., 2015; Sanes and Kotak, 2011; Takesian et al., 2012, 2009). However, it is not yet known how changes in the auditory brain arising from hearing loss relate to changes in brain circuitry produced by genetic and other risk factors for schizophrenia. Parvalbumin-positive (PV+) interneurons play a key role in maintaining excitation-inhibition balance in the cortex (Moore et al., 2018) and abnormalities in these inhibitory cells are thought to be important to the pathophysiology of schizophrenia (Lewis, 2014). However, reductions in the density of PV+ interneurons have not previously been linked with conductive hearing loss in animal models of either schizophrenia or otitis media.

Here I report a link between hearing loss and schizophrenia-relevant auditory brain and behavioral abnormalities in the *Df1*/+ mouse model of 22q11DS. Putative schizophrenia endophenotypes in *Df1*/+ mice, such as abnormalities in electrophysiological markers of central auditory gain and behavioral measures of auditory sensorimotor gating, were largely explained by hearing loss. Moreover, density of PV+ interneurons was significantly reduced in the auditory cortex of *Df1*/+ mice with hearing loss. Results suggest that peripheral hearing loss arising from the 22q11.2 deletion contributes to the emergence of schizophrenia-relevant auditory brain and behavioral abnormalities in 22q11DS.

3.2 Results

3.2.1 *Df1*/+ mice exhibit hearing loss in 60% of animals (54% of ears)

Both human 22q11DS patients and mouse models of 22q11DS have been reported to have high rates of hearing loss due primarily to middle ear inflammation (Dyce et al., 2002; Fuchs et al., 2015, 2013; Reyes et al., 1999; Verheij et al., 2017). I measured hearing thresholds for each ear in 25 *Df1*/+ mice and 26 WT mice using the auditory brainstem response (ABR). The ABR is an electroencephalographic signal arising from sound-evoked neural activity within the auditory nerve and brainstem (Willott, 2006). The ABR threshold was defined as the lowest sound intensity at which at least one of the characteristic deflections in the ABR waveform could be distinguished upon visualization of the signal across all sound intensity levels (see Materials and Methods). Click-evoked ABR thresholds were estimated for each ear in each mouse by an observer blind to the genotype of the animal. To minimize the influence of age-related sensorineural hearing loss characteristic of the C57BL/6J background strain (Parham, 1997), *Df1*/+ and WT mice tested in each session were littermates between 6 and 12 weeks of age. To reduce the potential for transmission of sound signals to the inner ear via bone or tissue conduction rather than via the middle ear, all sound stimuli were presented free-field rather than through an in-ear coupler.

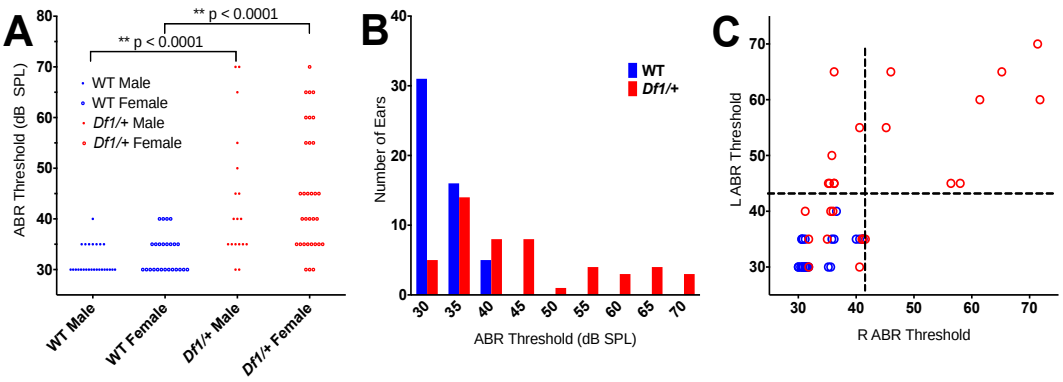

Figure 3.1 Elevated auditory brainstem response (ABR) thresholds in *Df1*/+ mice

(A) Click ABR thresholds recorded from individual ears in male and female WT (blue) and *Df1*/+ (red) mice. Two-way ANOVA with genotype and gender as independent variables reveals a significant effect of genotype ($F(1,97)=44.24$, $p<0.0001$) but not of gender ($F(1,97)=0.63$, $p=0.43$). Data points represent individual ear measurements; each animal contributed two measurements, one for each ear. Number of mice: 13 WT male, 13 WT female, 9 *Df1*/+ male, 16 *Df1*/+ female. (B) Click ABR thresholds pooled across recordings from male and female animals. Note that the *Df1*/+ ABR threshold distribution extends from the minimum to well beyond the maximum of the WT range. (C) Scatter plot showing the relationship between left and right ear ABR thresholds in each mouse. Dashed lines indicate the upper bound of normal hearing, defined as 2.5 SD above the mean ABR threshold for WT ears (see text). 60% (15/25) of *Df1*/+ mice had either monaural or binaural hearing loss, and 54% (27/50) of *Df1*/+ ears exhibited hearing loss. As previously observed (Fuchs et al., 2013), monaural hearing loss in *Df1*/+ mice occurred most commonly in the left ear (cf. Figure 3.2 in Fuchs et al., 2013).

Replicating previous results obtained in a different cohort of *Df1*/+ and WT mice (Fuchs et al. 2013), I found clear evidence for hearing loss in more than half of the *Df1*/+ animals (Figure 3.1). Mean ± SEM values for ABR thresholds were 44.8 ± 1.73 dB SPL in *Df1*/+ ears versus 32.5 ± 0.47 dB SPL in WT ears. Elevation of ABR thresholds in *Df1*/+ relative to WT mice was evident in both male and female animals (Figure 3.1A), and a two-way ANOVA revealed a

significant effect of genotype but not gender (genotype: $F(1,97)=44.24$, $p<0.0001$; gender: $F(1,97)=0.63$, $p=0.43$). The range of ABR thresholds in *Df1*/+ ears extended from the minimum to well beyond the maximum of the WT range (Figure 3.1B); i.e., ABR thresholds were abnormally elevated in some *Df1*/+ ears but not others. Defining the upper bound of normal hearing as 2.5 SD above the mean ABR threshold for WT ears (40.89 dB SPL), I found that 54% (27/50) of *Df1*/+ ears and 0% (0/52) of WT ears displayed hearing loss. Overall, 60% (15/25) of *Df1*/+ mice had either monaural or binaural hearing loss, and monaural hearing loss occurred most commonly in the left ear (Figure 3.1C). These results align both qualitatively and quantitatively with findings previously reported by Fuchs et al. (2013).

3.2.2 ABR Wave I amplitude reductions in *Df1*/+ mice with hearing loss are not maintained in cortical AEPs

Previous studies have reported abnormalities in sound-evoked auditory thalamic and/or cortical activity in mouse models of 22q11DS (Chun et al., 2014; Didriksen et al., 2017). I wondered if auditory brain responses might differ between *Df1*/+ and WT mice, and if so, whether these differences might be related to peripheral hearing loss. To find out, I recorded both ABRs and auditory evoked potentials (AEPs) in 20 WT and 20 *Df1*/+ mice (11 *Df1*/+ with no hearing loss, 9 *Df1*/+ with hearing loss in at least one ear), following presentations of loud (80 dB SPL) clicks at 300 ms inter-click intervals. I then measured latencies and amplitudes of ABR and AEP waves to determine whether the waveforms differed between WT and *Df1*/+ mice, or between WT mice and *Df1*/+ mice with and without hearing loss (Figure 3.2, Figure 3.3, and Figure 3.4). To assess the timing and strength of afferent input to the auditory brain, I measured the peak latency and baseline-to-peak amplitude of ABR wave I (Figure 3.2A), which arises from the auditory nerve (Willott, 2006). Within the AEP, I focused on wave peaks or troughs typically attributed to activity within the auditory thalamus (P1), auditory cortex (N1), and associative cortices (P2), measuring P1, N1, and P2 latency and P1-N1 and N1-P2 amplitudes (Figure 3.2D).

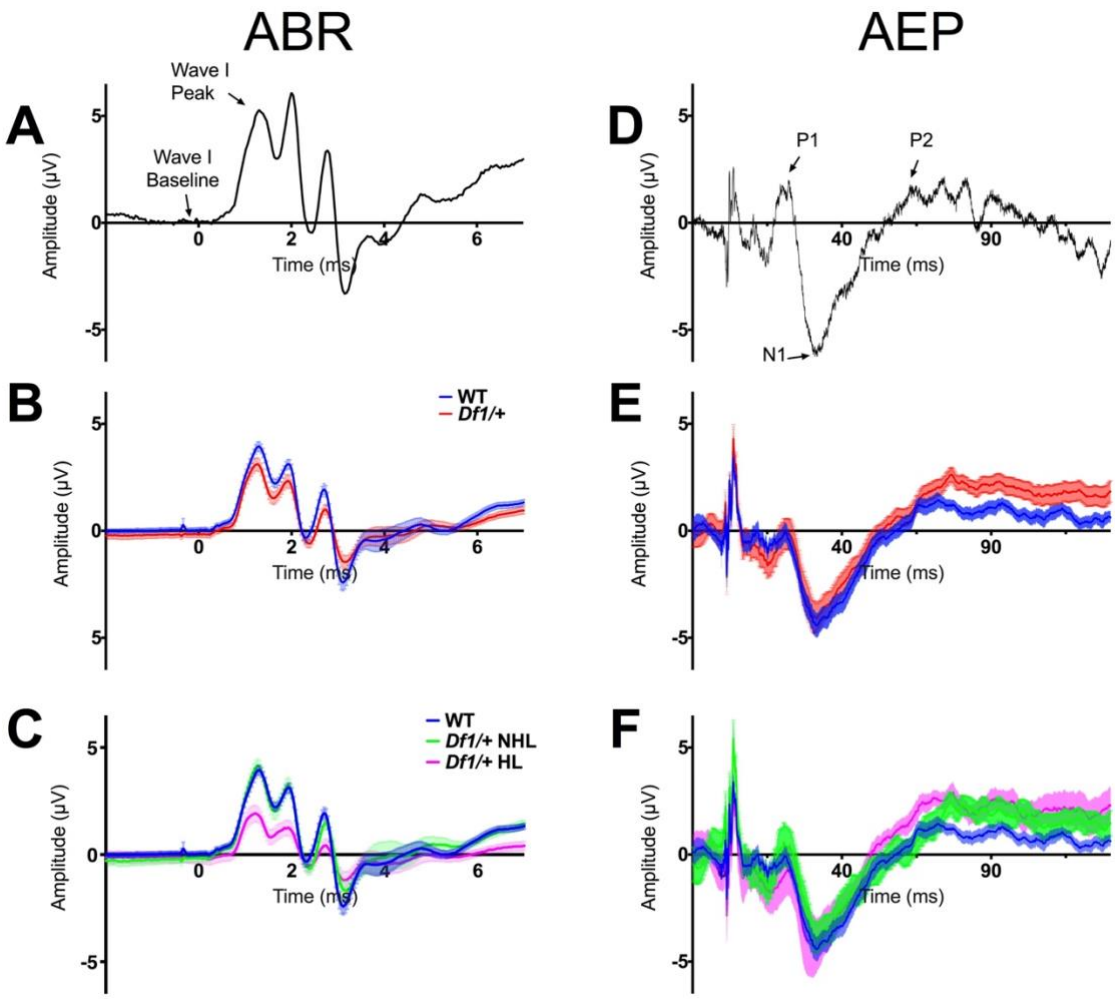

Figure 3.2 Average ABR and auditory evoked potential (AEP) waveforms in WT and *Df1*/+ mice

(A) Example trial-averaged ABR to an 80 dB SPL click, recorded ipsilateral to the stimulated ear in an individual WT animal. Arrows indicate baseline and peak used for measurement of wave I amplitude. (B) Mean ABR waveforms averaged across recordings from WT mice (blue) and *Df1*/+ mice (red). Error bars indicate SEM across all trial-averaged ABR recordings for each group of animals. (C) Same as B, but with *Df1*/+ ABR recordings separated into those from *Df1*/+ mice without hearing loss (green) or *Df1*/+ mice with hearing loss in at least one ear (magenta). (D) Example trial-averaged AEP to an 80 dB SPL click, recorded over auditory cortex contralateral to the stimulated ear in a WT animal. Arrows indicate P1 peak, N1 trough, and P2 peak. (E) Mean AEP waveforms averaged across recordings from different mice; color conventions

as in B. Error bars indicate SEM across all trial-averaged AEP recordings for each group of animals. (F) Same as E, but with *Df1*/+ AEP recordings separated into those from *Df1*/+ mice with or without hearing loss in at least one ear; color conventions as in C. Ipsilateral ABR and contralateral AEP data were obtained from the same recording for each stimulated ear; however, ABR waveforms in A-C represent differential signals while AEP waveforms in D-F are single-ended signals (see Materials and Methods). Number of mice: 20 WT, 20 *Df1*/+ (11 *Df1*/+ without hearing loss, 9 *Df1*/+ with hearing loss). Number of ABR/AEP recordings: 39 WT, 40 *Df1*/+ (22 *Df1*/+ without hearing loss, 18 *Df1*/+ with hearing loss).

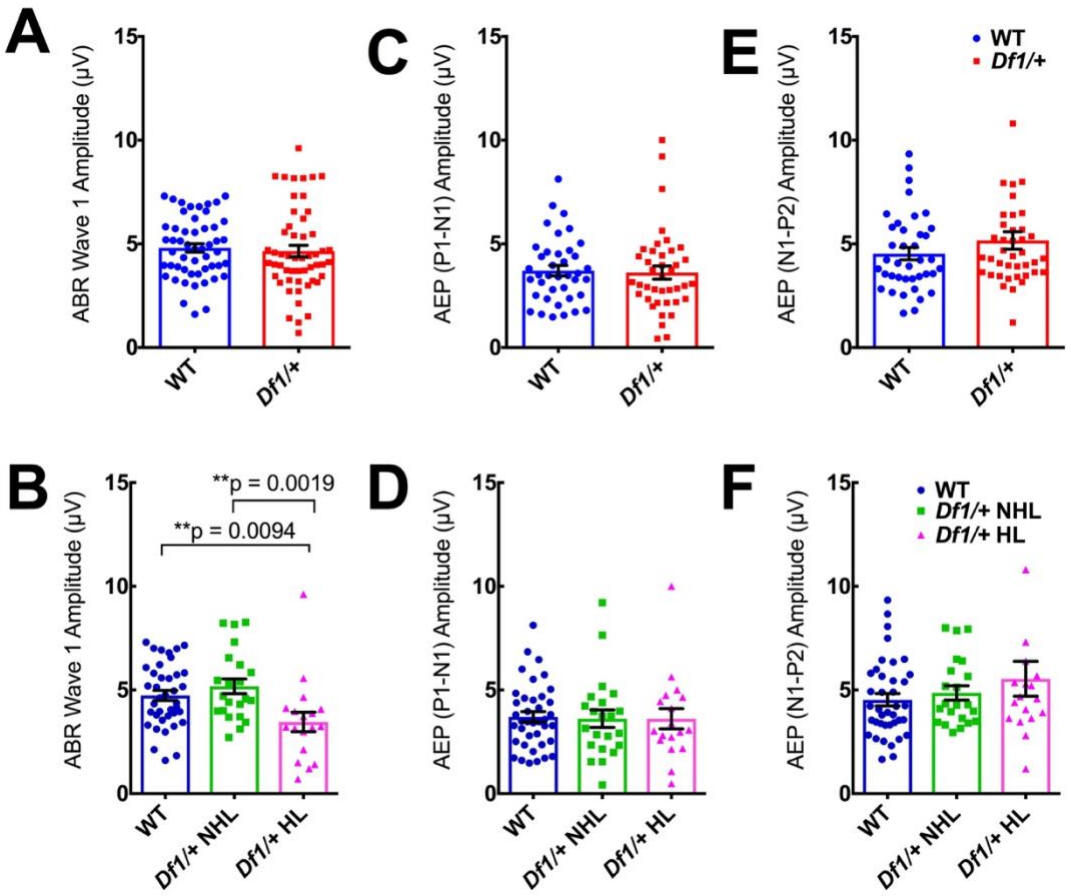

Figure 3.3 Reductions in ABR wave I amplitude in *Df1*/+ mice with hearing loss are not maintained in cortical AEPs

(A) ABR wave I amplitude to an 80 dB SPL click does not differ between WT and *Df1*/+ mice overall (unpaired *t*-test, p=0.66). (B) However, wave I amplitude is reduced in *Df1*/+ mice with hearing loss relative to either WT mice or *Df1*/+ mice without hearing loss (ordinary one-way ANOVA, F(2,76)=5.55, group

difference p=0.0056; Fisher's LSD, *Df1*/+ HL vs. WT p=0.0094, *Df1*/+ HL vs. *Df1*/+ NHL p=0.0019), while there is no significant difference in ABR wave I amplitude between *Df1*/+ mice without hearing loss and WT mice (*Df1*/+ NHL vs. WT p=0.33). (C-D) AEP P1-N1 amplitude does not differ between WT and *Df1*/+ mice, either overall (C; unpaired *t*-test, p=0.82) or when *Df1*/+ mice with and without hearing loss are considered separately (D; ordinary one-way ANOVA, F(2,76)=0.025, group difference p=0.98). (E-F) No significant differences in AEP N1-P2 amplitude between WT and *Df1*/+ mice, either overall (E; unpaired *t*-test, p=0.22), or when *Df1*/+ mice with and without hearing loss are considered separately (F; ordinary one-way ANOVA, F(2,76)=1.20, group difference p=0.31). Number of mice, number of ABR/AEP recordings, and color conventions as in Figure 3.2. Bars and error bars indicate mean ± SEM across recordings.

Hearing loss, defined here as an elevation of the ABR threshold, would be expected to reduce ABR wave I amplitude for a suprathreshold click. As expected, the amplitude of ABR wave I to an 80 dB SPL click was significantly lower in *Df1*/+ mice with hearing loss (HL) than in either *Df1*/+ mice with no hearing loss (NHL) or WT mice (Figure 3.2C and Figure 3.3B; ordinary one-way ANOVA, F(2,76)=5.55, group difference p=0.0056; Fisher's LSD, *Df1*/+ HL vs. NHL p=0.0019; *Df1*/+ HL vs. WT p=0.0094), while there was no significant difference between *Df1*/+ mice without hearing loss and WT animals (*Df1*/+ NHL vs. WT p=0.33), nor between *Df1*/+ and WT mice overall (Figure 3.2B and Figure 3.3A; unpaired t-test, p=0.66). More surprisingly, there were no significant differences in AEP wave amplitudes between *Df1*/+ and WT mice, even when *Df1*/+ mice with and without hearing loss were considered separately (Figure 3.2E,F and Figure 3.3C-F; WT vs. *Df1*/+ overall, unpaired t-tests, P1-N1: p=0.82, N1-P2: p=0.22; WT vs. *Df1*/+ NHL vs. *Df1*/+ HL, ordinary one-way ANOVAs, P1-N1: F(2,76)=0.025, group difference p=0.98, N1-P2: F(2,76)=1.20, group difference p=0.31). There were also no significant differences in latencies of ABR wave I or AEP waves P1, N1 or P2 between WT and *Df1*/+ animals, either overall or when hearing loss in *Df1*/+ mice was taken into account (Figure 3.4; unpaired t-tests and ordinary one-way ANOVAs, all

comparisons p>0.1). Thus, while ABR wave I amplitude was reduced as expected in *Df1*/+ mice with hearing loss, there were no significant differences in the AEP waves between any of the subgroups, suggesting possible central auditory compensation for reduction in auditory nerve input in *Df1*/+ mice with hearing loss.

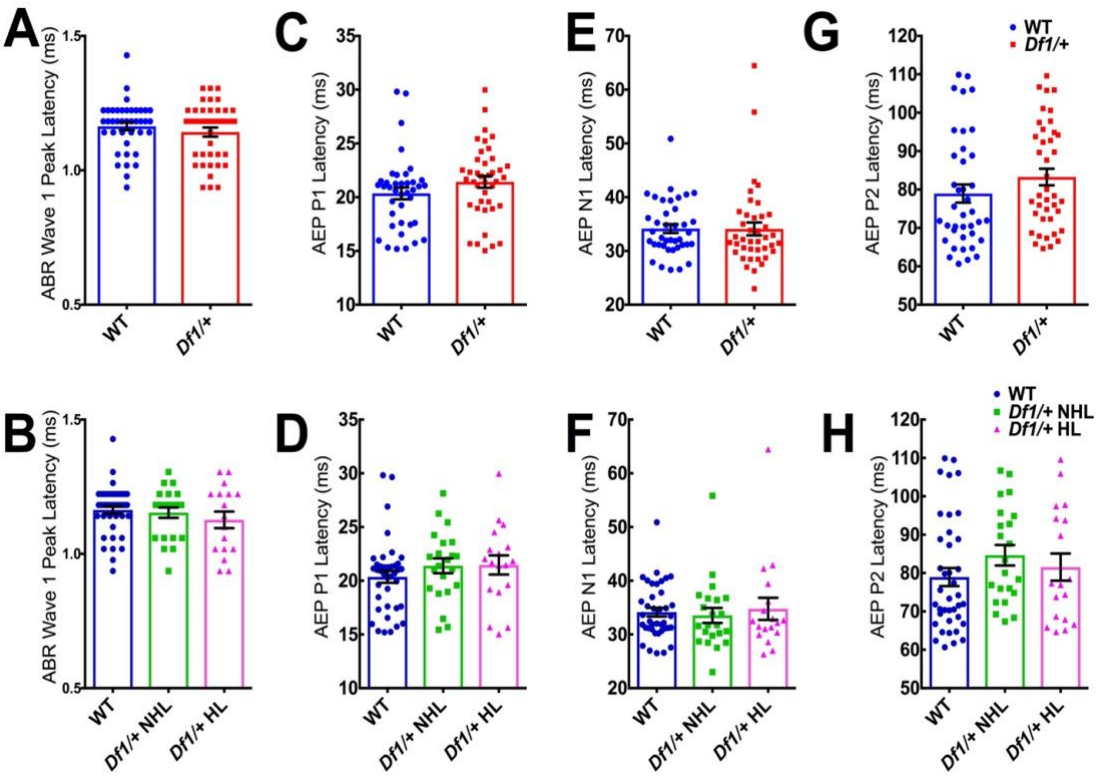

Figure 3.4 No significant differences between *Df1*/+ and WT mice in ABR wave I latency or AEP P1, N1 or P2 latencies

(A-B) There were no significant differences in ABR wave I peak latency between WT and *Df1*/+ mice overall (A; unpaired *t*-test, p=0.34), nor between WT mice, *Df1*/+ mice without hearing loss, and *Df1*/+ mice with hearing loss (B; one-way ANOVA, F(2,76)=0.81, group difference p=0.45). (C-D) Similarly, there were no significant differences in AEP P1 latency between WT and *Df1*/+ mice overall (C; unpaired *t*-test, p=0.17), nor between WT mice, *Df1*/+ mice without hearing loss, and *Df1*/+ mice with hearing loss (D; one-way ANOVA, F(2,76)=0.94, group difference p=0.39). (E-F) No significant differences in AEP N1 latency between WT and *Df1*/+ mice overall (E; unpaired *t*-test, p=0.97), nor between WT mice, *Df1*/+ mice without hearing loss, and *Df1*/+ mice with

hearing loss (F; one-way ANOVA, F(2,76)=0.18, group difference p=0.84). (G-H) No significant differences in AEP P2 latency between WT and *Df1*/+ mice overall (G; unpaired *t*-test, p=0.18), nor between WT mice, *Df1*/+ mice without hearing loss, and *Df1*/+ mice with hearing loss (H; one-way ANOVA, F(2,76)=1.14, group difference p=0.33). Number of mice and number of ABR/AEP recordings as in Figures 2 and 3; plot conventions as in Figure 3.3.

3.2.3 *Df1*/+ mice with hearing loss show elevation of central auditory gain

Given that peripheral hearing loss, including disruption of middle ear function, is known to drive compensatory changes throughout the auditory brain that reduce inhibition and increase "central auditory gain" (Clarkson et al., 2016; Sanes and Kotak, 2011; Takesian et al., 2009; Teichert et al., 2017), I wondered if central auditory gain might differ between *Df1*/+ and WT mice, or between *Df1*/+ mice with and without hearing loss. To determine this, I compared ABR wave I amplitude in each recorded ear to AEP P1-N1 or N1-P2 amplitude recorded over the contralateral cortical hemisphere (number of ear-hemisphere comparisons: 39 WT, 40 *Df1*/+ of which 22 were from *Df1*/+ mice without hearing loss, 18 from *Df1*/+ mice with hearing loss), and I used the ratios of AEP P1-N1 and N1-P2 amplitude to ABR wave I amplitude as measures of central auditory gain in each ABR/AEP recording.

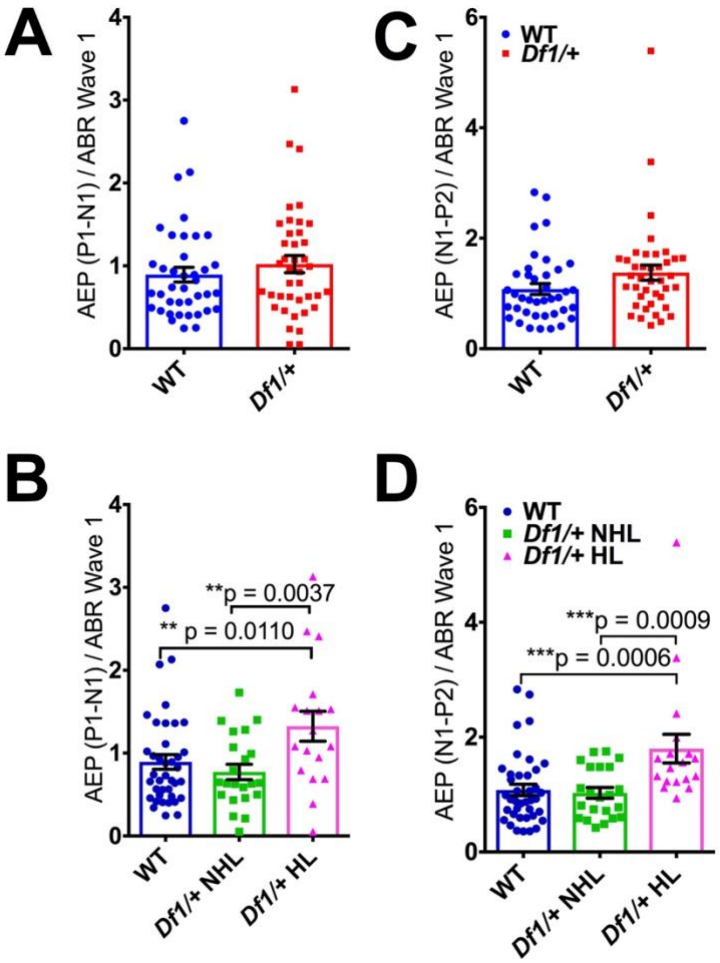

Figure 3.5 Central auditory gain is elevated in *Df1*/+ mice with hearing loss

(A) The ratio of AEP P1-N1 amplitude to ABR wave I amplitude in ABR/AEP recordings does not differ between WT mice and *Df1*/+ mice overall (unpaired *t*-test, p=0.36). (B) However, this measure of central auditory gain for the P1-N1 complex is significantly elevated in *Df1*/+ mice with hearing loss relative to either WT mice or *Df1*/+ mice without hearing loss (ordinary one-way ANOVA, F(2,76)=4.96, group difference p=0.0094; Fisher's LSD, *Df1*/+ HL vs. WT p=0.011, *Df1*/+ HL vs. *Df1*/+ NHL p=0.0037, WT vs. *Df1*/+ NHL p=0.44). (C) The ratio of AEP N1-P2 amplitude to ABR wave I amplitude does not differ between WT mice and *Df1*/+ mice overall (unpaired *t*-test, p=0.084). (D) Central auditory gain for the N1-P2 complex is significantly elevated in *Df1*/+ mice with hearing loss relative to either WT mice or *Df1*/+ mice without hearing loss (ordinary one-way ANOVA, F(2,76)=7.68, group difference p=0.0009; Fisher's LSD, *Df1*/+ HL vs. WT p=0.0006, *Df1*/+ HL vs. *Df1*/+ NHL p=0.0009, WT vs.

Df1/+ NHL p=0.79). Number of mice and number of ABR/AEP recordings as in Figures 2 and 3; plot conventions as in Figure 3.3.

For both the P1-N1 and N1-P2 complexes, central auditory gain was elevated in *Df1*/+ mice with hearing loss (Figure 3.5). There were no significant differences observed in the ratio of either AEP P1-N1 amplitude or N1-P2 amplitude to ABR wave I amplitude when comparing *Df1*/+ mice overall with WT mice (Figure 3.5A,C: unpaired t-tests, P1-N1 p=0.36, N1-P2 p=0.084). However, the P1-N1 / wave I ratio was significantly higher in *Df1*/+ mice with hearing loss than in either WT mice or *Df1*/+ mice without hearing loss (Figure 3.5B; ordinary one-way ANOVA, F(2,76)=4.96, group difference p=0.0094; Fisher's LSD, *Df1*/+ HL vs. WT p=0.011, *Df1*/+ HL vs. *Df1*/+ NHL p=0.0037), while *Df1*/+ mice without hearing loss were not significantly different from WT animals (WT vs. *Df1*/+ NHL p=0.44). Similarly, the N1-P2 / wave I ratio was significantly higher in *Df1*/+ mice with hearing loss than in either WT mice or *Df1*/+ mice without hearing loss (Figure 3.5D; ordinary one-way ANOVA, F(2,76)=7.68, group difference p=0.0009; Fisher's LSD, *Df1*/+ HL vs. WT p=0.0006, *Df1*/+ HL vs. *Df1*/+ NHL p=0.0009), while no significant differences in N1-P2 gain were found between *Df1*/+ mice without hearing loss and WT mice (WT vs. *Df1*/+ NHL p=0.79). These results are consistent with the conclusion that central auditory gain is increased in *Df1*/+ animals with hearing loss.

3.2.4 *Df1*/+ mice exhibit abnormal PPI of ASR for prepulse cues with fixed absolute sound level, but not for cues adjusted relative to startle threshold

I next examined potential behavioral influences of the hearing deficit and altered central auditory gain observed in *Df1*/+ mice. The acoustic startle response (ASR) is a reflexive jump evoked by a loud sound, and prepulse inhibition (PPI) of the ASR is the suppression of this jump that occurs when the loud sound is reliably preceded by a quieter but audible cue (the prepulse). Deficits in PPI of the ASR have been reported in the *Df1*/+ mouse and other mouse models of

22q11DS (Chun et al., 2014; Didriksen et al., 2017; Paylor and Lindsay, 2006), as well as in humans with 22q11DS (Sobin et al., 2004) or schizophrenia (Turetsky et al., 2007). I wondered whether hearing loss and/or central auditory consequences of hearing loss might account for abnormally weak PPI of the ASR in *Df1*/+ mice. To examine this, I measured startle responses and PPI of the ASR in 14 WT mice and 17 *Df1*/+ mice. For testing PPI of the ASR, I chose prepulse sound levels for each mouse that were 5-20 dB below the animal's behaviorally determined startle response threshold (i.e., below the quietest sound that evoked a significant startle response), thereby adjusting the prepulse cue levels for each animal to be as audible as possible without evoking a startle response. The loud startle-eliciting stimulus, in contrast, was always 95 dB SPL (Willott et al., 1984). All mice included in this analysis exhibited a significant startle response to the 95 dB SPL sound, and no significant startle response to the prepulse cues. Behavioral testing was performed blind to the genotype of the animal (and to its ABR thresholds, which were measured only after behavioral testing was completed).

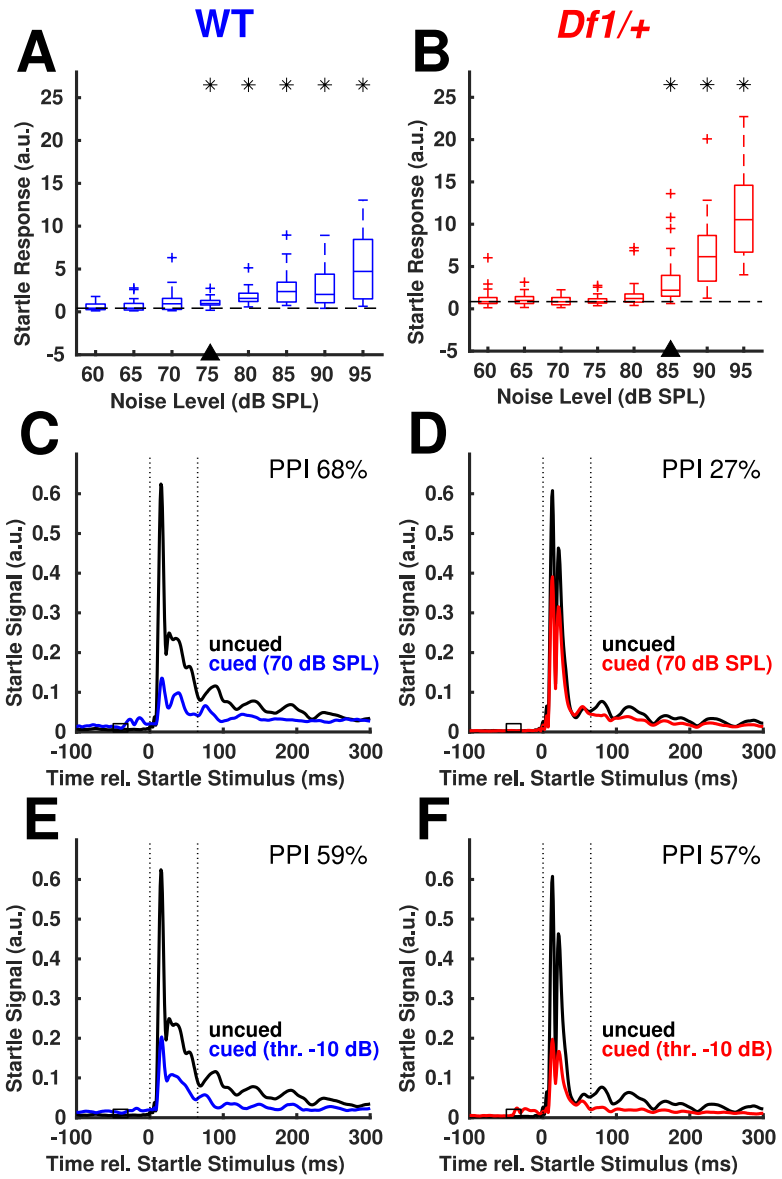

Figure 3.6 Example acoustic startle responses and prepulse inhibition (PPI) of startle in WT and *Df1*/+ mice

(A) Startle response as a function of noise level for an example WT mouse; boxplots indicate median and quartiles for n=25 trials per condition. Startle response (a.u., arbitrary units) is the sum of startle signal amplitudes (sampled at 1000 samples/sec) over the period 0-65 ms relative to noise burst onset. All noise bursts were presented over a 65 dB SPL continuous white noise background sound. Asterisks indicate noise levels for which the startle response is significantly greater than that evoked by a 60 dB SPL noise burst (Wilcoxon rank-sum test, $p<0.01$). Triangle on x-axis indicates the startle response threshold, defined as the lowest noise level for which that level and

all higher noise levels evoked significant startle responses. Startle response threshold was calculated from data pooled across multiple sessions (as shown) for each mouse. (B) Same as A but for a *Df1*/+ mouse; n=30 trials per condition. Note the elevated startle response threshold. (C) Prepulse inhibition of acoustic startle with a 70 dB SPL cue, for the WT mouse. Line plots show startle signal (averaged over n=10 trials per condition) as a function of time relative to startle noise onset. Dotted vertical lines delineate time period used for calculation of startle response. Horizontal open rectangle spanning -50 to -30 ms indicates time of prepulse cue presentation on cued trials. Black trace, uncued trials; colored trace, cued trials. PPI was calculated based on data from a single behavioral session (as shown) and then averaged across repeated sessions for each mouse before population analysis. (D) Same as C but for the *Df1*/+ mouse; n=10 trials per condition. (E) Prepulse inhibition of acoustic startle with cue sound level -10 dB relative to startle threshold, for the WT mouse. (F) Same as E but for the *Df1*/+ mouse. Note that while PPI for a 70 dB SPL prepulse cue is lower for the *Df1*/+ than the WT mouse (C, D), PPI for prepulse cues at -10 dB sound level relative to startle threshold is similar in both mice (E, F).

Startle response functions were determined for each animal by presenting noise bursts of varying sound levels against a 65 dB SPL white noise background. I defined the startle threshold as the lowest sound level that evoked a significant startle response at that sound level and all higher sound levels (Figure 3.6A,B; see Materials and Methods). I also measured the magnitude of the uncued startle response to the fixed 95 dB SPL noise burst used as the startle-eliciting stimulus in all PPI tests. I found that startle thresholds were significantly higher in *Df1*/+ than in WT mice (Figure 3.7A; random permutation test, p=0.023), and uncued startle response magnitudes were significantly lower in *Df1*/+ than WT mice (Figure 3.7C; unpaired t-test, p=0.029). Both of these findings are consistent with the conclusion that hearing loss in *Df1*/+ mice reduces sensitivity to noise bursts used as prepulse cues or startle-eliciting stimuli. I note, however, that the differences between *Df1*/+ and WT mice in startle threshold and uncued startle response magnitude did not reach significance when the *Df1*/+ animals were further subdivided into mice

with and without hearing loss (see Figure 3.7B,D and Figure 3.7 legend for details).

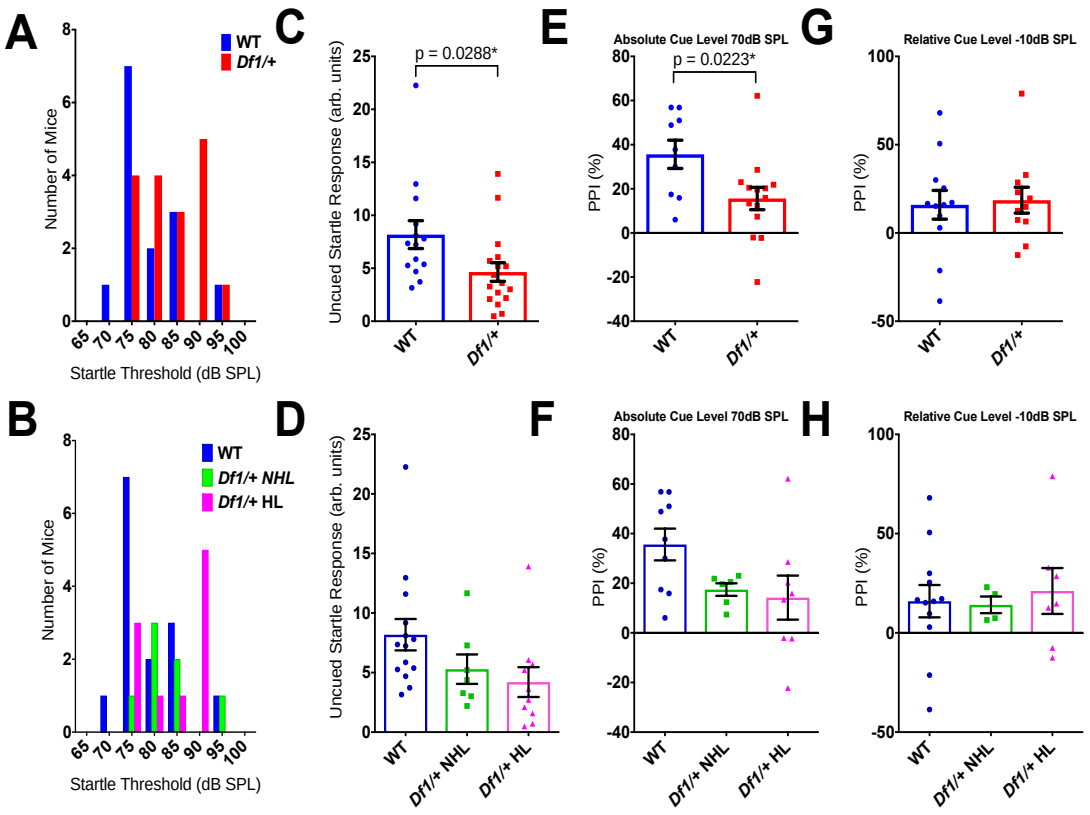

Figure 3.7 Population analysis of acoustic startle response and prepulse inhibition of startle in WT and *Df1*/+ mice

(A-B) Startle response thresholds are significantly higher in *Df1*/+ mice overall than in WT mice (A; random permutation test, p=0.023), while differences between WT mice, *Df1*/+ mice without hearing loss, and *Df1*/+ mice with hearing loss do not reach significance with correction for multiple testing (B; random permutation tests, p-values, WT vs. *Df1*/+ HL p=0.031, WT vs. *Df1*/+ NHL p=0.078, *Df1*/+ NHL vs. *Df1*/+ HL p=0.30). Number of mice: 14 WT, 17 *Df1*/+ (7 NHL, 10 HL). (C-D) Uncued startle responses to a 95 dB SPL noise burst are significantly lower in *Df1*/+ mice overall than in WT mice (C; unpaired *t*-test, p=0.029), although differences are not significant when groups are further subdivided into WT mice, *Df1*/+ mice without hearing loss, and *Df1*/+ mice with hearing loss (D; ordinary one-way ANOVA, F(2,28)=2.71, group difference p=0.084). Number of mice, same as in A and B. (E-F) Prepulse

inhibition with a 70 dB SPL cue, for 9 WT and 14 *Df1*/+ (6 NHL, 8 HL) mice tested at this cue level. PPI is significantly reduced in *Df1*/+ mice overall compared to WT mice (E; unpaired *t*-test, p=0.022). The effect does not reach significance when animal groups are subdivided to compare WT mice and *Df1*/+ mice with and without hearing loss (F; ordinary one-way ANOVA, F(2,20)=2.96, group difference p=0.075). (G-H) PPI for cues with sound level -10 dB relative to startle threshold, for 12 WT and 11 *Df1*/+ (4 NHL, 7 HL) mice tested with this relative cue level. Here, there is no significant difference in PPI either between WT mice and *Df1*/+ mice overall (G; unpaired *t*-test, p=0.82), or between WT mice, *Df1*/+ mice without hearing loss, and *Df1*/+ mice with hearing loss (H; ordinary one-way ANOVA, F(2,20)=0.11, group difference p=0.90).

Several previous studies have reported that PPI of the ASR is reduced in *Df1*/+ mice (Chun et al., 2014; Paylor and Lindsay, 2006). I wondered if PPI of the ASR would still be weaker in *Df1*/+ than WT mice if the sound levels of the prepulse cues were not fixed on an absolute dB SPL scale, but instead adjusted relative to each animal's startle threshold, to match its sensory salience across animals. The examples of Figure 3.6 illustrate our approach. After measuring each animal's startle threshold (Figure 3.6A,B), I tested PPI of the ASR using at least two different prepulse sound levels, chosen to be between 5 and 20 dB SPL below the animal's startle threshold. I then compared PPI for prepulse cues with fixed absolute sound level (Figure 3.6C,D) to PPI when the prepulse cue level was defined relative to startle threshold for each animal (Figure 3.6E,F). As shown for the example mice in Figure 3.6, PPI to a fixed 70 dB SPL prepulse cue was 68% in the WT mouse (Figure 3.6C) but only 27% in the *Df1*/+ mouse (Figure 3.6D). In contrast, PPI to a prepulse cue with sound level of -10 dB relative to startle threshold was very similar in both mice (Figure 3.6E,F; 59% in WT mouse, 57% in *Df1*/+ mouse). This finding held across the population. PPI of the ASR was significantly weaker in *Df1*/+ than WT mice tested with a fixed 70 dB SPL prepulse cue (Figure 3.7E; unpaired t-test, p=0.022; number of mice: 9 WT, 14 *Df1*/+), but there were no significant differences in PPI between *Df1*/+ and WT animals when the cue level was adjusted to be -10 dB

relative to startle threshold (Figure 3.7G; unpaired t-test, p=0.82; number of mice: 11 WT, 12 *Df1*/+). Similar trends but no significant group differences were found when the groups were further subdivided to compare WT mice and *Df1*/+ mice with and without hearing loss (see Figure 3.7F,H and Figure 3.7 legend for details). These results suggest that *Df1*/+ mice do not exhibit reduced PPI of acoustic startle compared to WT mice when the prepulse cue level is adjusted relative to startle threshold for each animal.

3.2.5 *Df1*/+ mice with hearing loss show reduced density of PV+ but not NeuN+ cells in auditory cortex

After examining physiological and behavioral effects of hearing loss in *Df1*/+ mice, I investigated potential neuroanatomical correlates. Abnormalities in parvalbumin-positive (PV+) interneuron networks are a common finding in animal models of schizophrenia (see Lewis, Curley, Glausier, & Volk, 2012 for a review), and alterations in PV+ interneuron activity have previously been linked both to changes in central auditory gain (Resnik and Polley, 2017) and changes in PPI of acoustic startle (Aizenberg et al., 2015). I wondered whether PV+ interneuron density in auditory cortex might be abnormal in *Df1*/+ mice relative to WT mice, and if so, how these abnormalities might relate to hearing loss. To compare PV+ interneuron density to density of neurons overall, I performed immunohistochemical staining for PV and NeuN (a pan-neuronal marker) in coronal brain sections through the auditory cortex (Figure 3.8A and Figure 3.4A) in 26 WT mice and 24 *Df1*/+ mice. The final data set included images from auditory cortex in 66 cortical hemispheres (32 WT, 34 *Df1*/+).

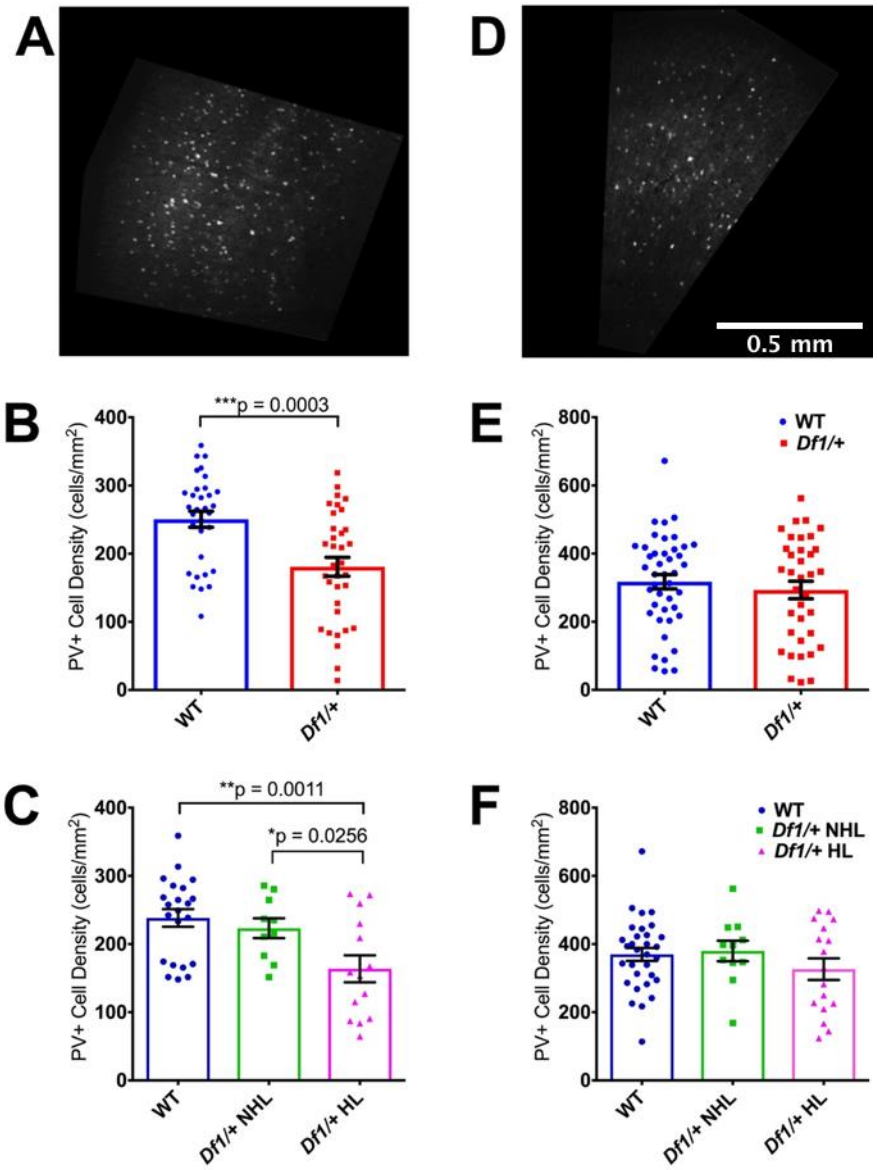

Figure 3.8 PV+ cell density is reduced in the auditory cortex but not the motor cortex of *Df1*/+ mice

(A) Example confocal image of a coronal section through primary auditory cortex (A1) stained with an antibody against the inhibitory interneuron marker parvalbumin (PV). (B) PV+ cell density in A1 was significantly reduced in *Df1*/+ mice compared to WT mice (unpaired *t*-test, p=0.00030). (C) PV+ cell density was also significantly reduced in *Df1*/+ mice with hearing loss compared to either WT mice or *Df1*/+ mice without hearing loss, but there was no significant difference between WT mice and *Df1*/+ mice without hearing loss (ordinary one-way ANOVA, F(2,43)=6.37, group difference p=0.0038; Fisher's LSD, *Df1*/+ HL

vs. WT p=0.0011, *Df1*/+ HL vs. *Df1*/+ NHL p=0.026, WT vs. *Df1*/+ NHL p=0.53). (D) Example PV-immunostained coronal section through secondary motor cortex (M2). (E) In M2, there was no significant difference in PV+ cell density between *Df1*/+ and WT mice (unpaired *t*-test, p=0.46). (F) PV+ cell density in M2 also did not differ between groups when comparing WT mice, *Df1*/+ mice without hearing loss, and *Df1*/+ mice with hearing loss (ordinary one-way ANOVA, F(2,56)=1.04, group difference p=0.36). See Table 2.1 in chapter 2 for numbers of hemispheres (and mice) in each comparison.

PV+ interneuron density in A1 was significantly lower in *Df1*/+ than WT mice (Figure 3.8B; unpaired t-test, p=0.00030). Moreover, PV+ cell density was significantly reduced in *Df1*/+ mice with hearing loss compared to either WT mice or *Df1*/+ mice without hearing loss (Figure 3.8C; ordinary one-way ANOVA, F(2,43)=6.37, group difference p=0.0038; Fisher's LSD, *Df1*/+ HL vs. WT p=0.0011, *Df1*/+ HL vs. *Df1*/+ NHL p=0.026), while *Df1*/+ mice without hearing loss did not differ from WT animals (*Df1*/+ NHL vs. WT p=0.53). In contrast, there were no significant differences in NeuN+ cell density in A1 between WT and *Df1*/+ animals overall (Figure 3.9B; unpaired t-test, p=0.29), nor between WT mice, *Df1*/+ mice without hearing loss, and *Df1*/+ mice with hearing loss (Figure 3.9C; ordinary one-way ANOVA, F(2,22)=0.72, group difference p=0.50). These results indicate that PV+ interneuron density in A1 is reduced in *Df1*/+ mice with hearing loss, suggesting that cortical changes might contribute to central auditory compensation for hearing loss in *Df1*/+ animals.

3.2.6 *Df1*/+ mice do not show abnormalities in PV+ or NeuN+ cell density in M2, nor changes in laminar distributions of PV+ cells in A1

I also wondered if abnormalities in PV+ interneuron density in *Df1*/+ mice might be evident in other cortical areas besides A1. Auditory cortex in mice is reciprocally connected with the secondary motor cortex (M2), and neural activity in M2 is known to modulate auditory cortical processing (Nelson et al., 2013; Schneider et al., 2014). To find out if reductions in PV+ interneuron density observed in A1 of *Df1*/+ mice with hearing loss also occurred in M2, I

analyzed PV and NeuN immunostaining in coronal brain sections through frontal cortex (Figure 3.8D and Figure 3.9D) in 79 hemispheres (43 WT, 36 *Df1*/+).

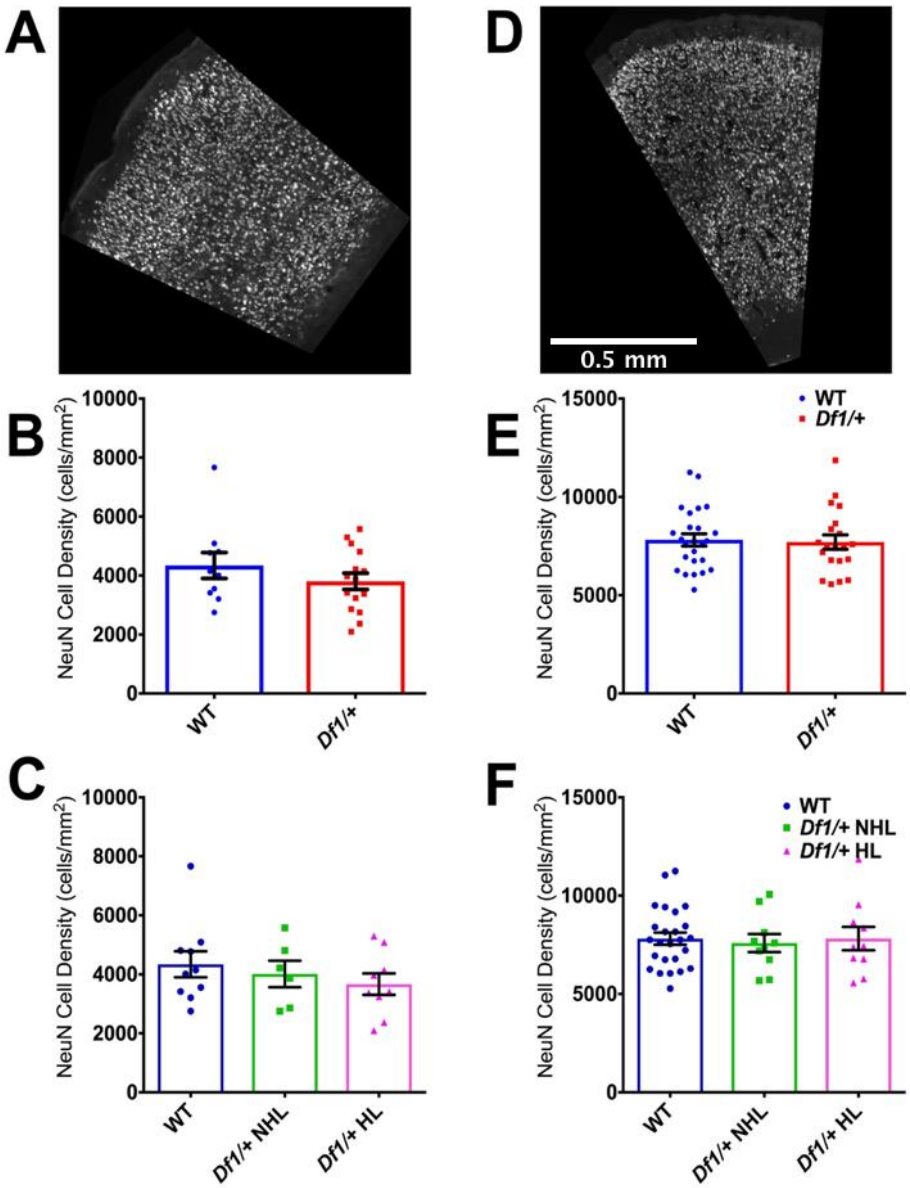

Figure 3.9 NeuN+ cell density is not reduced in the auditory cortex or the motor cortex of *Df1*/+ mice

(A) Example confocal image of a coronal section through primary auditory cortex (A1) stained with an antibody against the pan-neuronal marker NeuN. (B) NeuN+ cell density in A1 was not significantly different in *Df1*/+ mice compared to WT mice (unpaired *t*-test, p=0.29). (C) No significant difference in A1 NeuN+ cell density between WT mice, *Df1*/+ mice without hearing loss, and

Df1/+ mice with hearing loss (ordinary one-way ANOVA, F(2,22)=0.72, group difference p=0.50). (D) Example NeuN-immunostained coronal section through secondary motor cortex (M2). (E) In M2, there was no significant difference in NeuN+ cell density between *Df1*/+ and WT mice (unpaired *t*-test, p=0.82). (F) NeuN+ cell density in M2 also did not differ between groups when comparing WT mice, *Df1*/+ mice without hearing loss, and *Df1*/+ mice with hearing loss (ordinary one-way ANOVA, F(2,42)=0.076, group difference p=0.93). See Table 2.1 in chapter 2 for numbers of hemispheres (and mice) in each comparison.

PV+ interneuron density in M2 did not differ between WT and *Df1*/+ mice (Figure 3.8E; unpaired t-test, p=0.46), nor between WT mice, *Df1*/+ mice without hearing loss, and *Df1*/+ mice with hearing loss (Figure 3.8F; ordinary one-way ANOVA, F(2,56)=1.04, group difference p=0.36). There were also no significant differences between animal groups in NeuN+ cell density in M2, either between WT and *Df1*/+ mice overall or when the Df1/+ animals were further subdivided into those with and without hearing loss (Figure 3.9E,F; WT vs. *Df1*/+, unpaired t-test, p=0.82; WT vs. *Df1*/+ NHL vs. *Df1*/+ HL, ordinary one-way ANOVA, F(2,42)=0.076, group difference p=0.93). These results suggest that reductions in PV+ interneuron density observed in *Df1*/+ mice with hearing loss may be specific to the auditory cortex.

Previous studies have reported aberrant inhibitory interneuron distributions in the frontal cortex in another mouse model of 22q11DS, the LgDel mouse (Meechan et al., 2009). I therefore wondered whether laminar distributions of PV+ interneurons might be altered in A1 or M2 of *Df1*/+ mice. To find out, I quantified the laminar depth of cell centroids along the pia-to-white-matter axis in both areas, normalizing the depth measures by cortical thickness. I then discretized cell counts into 5, 10, or 20 proportional depth bins to analyze effects of genotype or hearing loss on laminar distribution of cells. I found no significant differences in the laminar distribution of PV+ interneurons in *Df1*/+ mice compared to their WT littermates in either A1 or M2 (Figure 3.10A,C; two-way ANOVA, A1 WT vs. *Df1*/+, F(4,164)=0.25, p=0.91, M2 WT vs. *Df1*/+ mice

F(4,212)=1.13, p=0.34). When I compared WT mice and *Df1*/+ mice with and without hearing loss, I again found no significant differences in laminar distribution of PV+ cells in A1, while a weak effect of hearing loss was observed in M2 when using 5 but not 10 or 20 proportional depth bins (Figure 3.10B,D; two-way ANOVA, A1 WT vs. *Df1*/+ NHL vs. *Df1*/+ HL, F(8,160)=0.22, p=0.99, M2 WT vs. *Df1*/+ NHL vs. *Df1*/+ HL mice F(8,208)=2.24, p=0.026). Thus, I found minimal evidence for abnormalities in laminar distributions of PV+ interneurons in either A1 or M2 of *Df1*/+ mice, regardless of hearing loss.

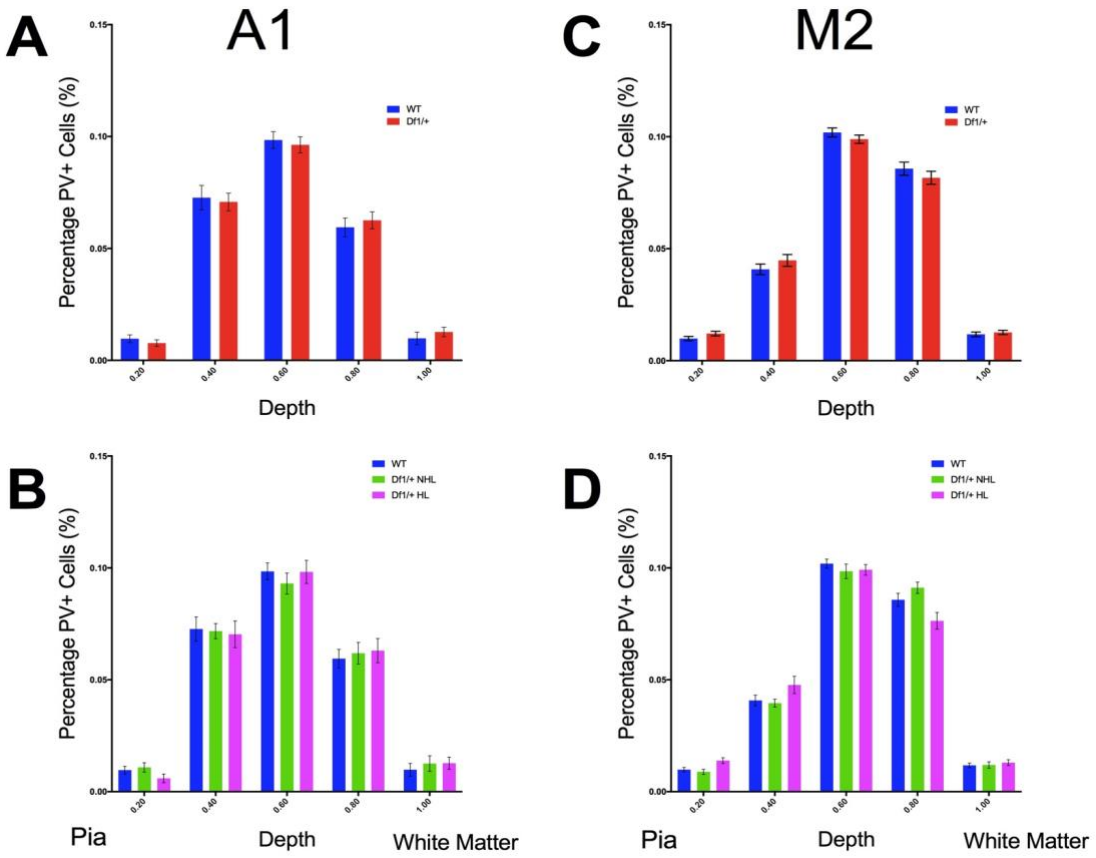

Figure 3.10 *Df1*/+ mice with hearing loss have minimal differences in laminar distribution of PV+ cells in A1 or M2

Laminar distribution of PV+ cells was analyzed in 5 bins representing equal proportional depths in the cortex from pia to white matter. Error bars indicate SEM across hemispheres; see Table 2.1 in chapter 2 for number of hemispheres and mice. (A,B) PV+ cell laminar distribution in A1, compared between WT and *Df1*/+ mice (A) or between WT mice, *Df1*/+ mice without hearing loss, and *Df1*/+ mice with hearing loss (B). A two-way ANOVA revealed

no significant interactions between genotype and bin depth (WT vs. *Df1/+,* F(4,164)=0.25, p=0.91; WT vs. *Df1/+* NHL vs. *Df1/+* HL, F(8,160)=0.22, p=0.99). (C,D) PV+ cell laminar distribution in M2, compared between WT and *Df1/+* mice (C) or between WT mice and *Df1/+* mice with or without hearing loss (D). Two-way ANOVA revealed no significant interaction between genotype and bin depth for WT vs. *Df1/+* mice (F(4,212)=1.13, p=0.34), but a weak interaction for WT vs. *Df1/+* NHL vs. *Df1/+* HL mice (F(8,208)=2.24, p=0.026). Post hoc Tukey's multiple comparisons test identified the significant difference as arising from the 0.8 bin, corresponding to depths 0.6-0.8 of the total distance from pia to white matter (WT vs. *Df1/+* HL p=0.011, *Df1/+* NHL vs. *Df1/+* HL p=0. 0022). However, there was no significant interaction between genotype and bin depth nor any single bin with significant difference between groups when the same analysis was performed with 10 or 20 equal-proportion depth bins (all p>0.05).

3.3 Discussion

3.3.1 Hearing loss in mouse models of 22q11DS

Results reported here confirm that *Df1*/+ mice have high rates of hearing loss, replicating both qualitatively and quantitatively results reported by Fuchs et al. (2013) for a different cohort of animals. Like Fuchs et al. (2013), I found that approximately 60% of *Df1*/+ mice have elevated ABR thresholds in one or both ears; that the incidence of hearing loss is similar in male and female *Df1*/+ mice; and that hearing loss in *Df1*/+ mice can be either monaural or binaural. Fuchs et al. (2013) also showed that hearing loss in *Df1*/+ mice correlates with otitis media (middle ear inflammation). Subsequently, Fuchs et al. (2015) demonstrated that otitis media in *Df1*/+ mice is associated with a bilateral or monolateral defect in the levator veli palatini muscle lining the Eustachian tube, which affects drainage of middle ear effusion. This muscle defect arises early in myogenesis and appears to be caused by haploinsufficiency of the gene *Tbx1* (Fuchs et al., 2015), which has also been linked to other middle and inner ear abnormalities (Liao et al., 2004). Thus, any mouse model of 22q11DS with heterozygous deletion of *Tbx1* may be susceptible to otitis media and hearing

loss. The *Tbx1* gene lies within the minimum human 22q11DS deletion region, and susceptibility to otitis media and hearing loss has been widely reported in human 22q11DS patients (see Verheij et al., 2017 for a review).

There are, however, some discrepant results in the literature on hearing loss in mouse models of 22q11DS. For example, Paylor et al. (2006) tested frequency-dependent distortion-product otoacoustic emissions (DPOAEs) in 6 *Df1*/+ and 6 WT mice, and found no significant differences in DPOAE thresholds between the groups (see their Supplementary Figure 20). DPOAE thresholds reflect outer hair sensitivity, not auditory nerve activity, but conductive hearing loss (e.g. from otitis media) should increase DPOAE as well as ABR thresholds (Qin et al., 2010). A more direct methodological analogy to Fuchs et al. (2013) and the present study comes from a recent characterisation of a new congenic mouse model of the minimum human 22q11DS deletion, the *Df(h22q11)/*+ mouse, which like the *Df1*/+ mouse is heterozygous for deletion of *Tbx1* (Didriksen et al., 2017). Didriksen et al. (2017) found no significant differences in click-evoked ABR thresholds between 13 *Df(h22q11)/*+ and 13 WT animals.

One possible explanation for these discrepancies is differences in methodology. For example, (Paylor et al., 2006) and Didriksen et al. (2017) used in-ear speakers or couplers for sound delivery, rather than free-field speakers as in Fuchs et al. (2013) and the present work. While in-ear and free-field sound delivery techniques should produce similar results, hearing loss arising from middle ear dysfunction might not be detected if physical coupling of a sound delivery device to the ear canal enables transmission of sound signals directly to the inner ear via bone or tissue conduction (Steel et al., 1987).

Age differences and genetic differences in the mice might also help to explain the discrepant results. The *Df(h22q11)1/*+ mice that underwent ABR testing in Didriksen et al. (2017) were indicated to be approximately 5 months old (see their Supplementary Figure A2), while the mice used here and in Paylor et al. (2006) were somewhat younger (here, 1.5-4.5 months old, mean 3 months; 2-4 months old in Paylor et al. 2006). It is possible that the accelerated age-

related hearing loss characteristic of the C57BL/6 background strain (Hequembourg and Liberman, 2001) might have obscured hearing loss due to middle ear problems in the Didriksen et al. (2017) study. Alternatively (or additionally), genetic differences between *Df(h22q11)1/*+ and *Df1/*+ mice might have affected results of hearing tests, since the *Df(h22q11)1/*+ mice used by Didriksen et al. (2017) have a slightly larger chromosomal deletion affecting an extra 5 genes (*Dgcr2, Tssk2, Tssk1, Mrpl40,* and *Hira*). However, both *Df1/*+ mice and *Df(h22q11)1/*+ mice exhibit the haploinsufficiency for *Tbx1* that is thought to underlie vulnerability to otitis media and hearing loss (Didriksen et al., 2017; Fuchs et al., 2015), and genetically, the *Df1/*+ mice used by Paylor et al. (2006) should have been essentially identical to the *Df1/*+ mice used here.

Microbiological status of the mice might also be a factor, but is rarely discussed in published reports. Opportunistic pathogens that are common in laboratory mouse facilities can increase risk of otitis media in susceptible animals (Bleich et al., 2008). Mice used in the present study were maintained in standard mouse housing facilities; it is possible that the incidence of otitis media and hearing loss in *Df1*/+ mice might be reduced if animals were housed in a super-clean facility. Importantly, however, hearing loss and otitis media have been estimated to affect a majority of human 22q11DS patients (Verheij et al., 2017). Therefore, even if it were possible to reduce the incidence of otitis media in *Df1*/+ mice by restricting their microbiological exposure, the resulting animals would be poorer models of the human syndrome. Similar concerns about the translational value of "squeaky-clean" mouse models have recently been raised by many immunologists (Willyard, 2018).

3.3.2 Central auditory abnormalities in mouse models of 22q11DS

I found that the magnitude of the cortical auditory evoked potential to a loud sound was similar in *Df1*/+ and WT mice, even for *Df1*/+ mice with abnormally elevated ABR thresholds. Measures of central auditory gain (e.g., ratios between AEP P1-N1 or N1-P2 amplitude and ABR wave I amplitude) were significantly higher in *Df1*/+ mice with hearing loss than in WT mice or in *Df1*/+

mice without hearing loss. These results suggest a compensatory increase in central auditory gain in *Df1*/+ mice with hearing loss. Interestingly, although Didriksen et al. (2017) did not observe differences in ABR thresholds between *Df(h22q11)/*+ and WT mice, they did find evidence for increased central auditory gain: AEP amplitude increased more steeply with sound loudness in *Df(h22q11)/*+ than WT animals.

Increased central auditory gain in *Df1*/+ mice with hearing loss could arise at multiple stages of the central auditory pathway. Loss of peripheral auditory input drives homeostatic changes throughout the auditory brainstem, midbrain, thalamus and cortex, which typically manifest as reductions in inhibitory synaptic transmission, increased spontaneous activity, and increased gain of sound-evoked responses (Chambers et al., 2016; Eggermont, 2017; Takesian et al., 2012, 2009). Conductive hearing loss – the form of hearing loss caused by otitis media – has been shown to be sufficient to evoke plastic changes throughout the central auditory system (Clarkson et al., 2016; Sinclair et al., 2017; Teichert et al., 2017; Xu et al., 2007), even when it affects only one ear (Keating et al., 2015; Popescu and Polley, 2010). Moreover, conductive hearing loss that occurs transiently during development can produce a reduction in inhibitory synaptic currents in the auditory cortex that persists in adulthood (Mowery et al., 2015; Sanes and Kotak, 2011; Takesian et al., 2012). Thus, otitis media and hearing loss in mouse models of 22q11DS would be expected to produce abnormalities throughout the central auditory system, even if the hearing loss occurred only transiently during development.

Our results are consistent with this literature, and suggest a possible re-interpretation of auditory thalamocortical deficits previously reported in mouse models of 22q11DS (Chun et al., 2014). Using in vitro electrophysiology and calcium imaging, Chun et al. (2014) observed a reduction in auditory thalamocortical synaptic transmission in the *Df(16)1/*+ mouse (which has the same deletion as the *Df1*/+ mouse). No such abnormality was detected in visual or somatosensory thalamocortical slices, indicating that the deficit was specific to the auditory system. Chun et al. (2014) linked the disruption of auditory

thalamocortical synaptic transmission to aberrant elevation of D2 dopamine receptor (*Drd2*) expression in the auditory thalamus, apparently caused by haploinsufficiency of the microRNA-processing gene *Dgcr8*. They argued that *Drd2*-dependent disruption of thalamic inputs to the auditory cortex could be a key pathogenic mechanism underlying auditory hallucinations in schizophrenia.

A different interpretation is that hearing loss could be the proximal cause of the auditory thalamic and thalamocortical abnormalities reported by Chun et al. (2014). The possibility of hearing loss in *Df(16)1/+* (or *Dgcr8/+*) animals was not explicitly examined in that study. Furthermore, some of the conclusions were based on analysis of small numbers of in vitro recordings, taken from only a few animals (or an unspecified number of animals). Given that 60% of *Df1*/+ mice have hearing loss in one or both ears (Fuchs et al., 2013 and present work), it is possible that results in Chun et al. (2014) could have been affected by the chance inclusion of differing numbers of animals with or without hearing loss in different analyses. In the absence of animal-by-animal controls for hearing loss, it remains unclear whether elevation of *Drd2* expression in auditory thalamus and disruption of auditory thalamocortical transmission are abnormalities specific to 22q11DS models, or more general consequences of hearing loss. Notably, hearing loss has been shown to affect dopaminergic function in the central auditory system (Fyk-Kolodziej et al., 2015; Tong et al., 2005).

3.3.3 Auditory sensorimotor gating in mouse models of 22q11DS

Consistent with findings of previous reports (Didriksen et al., 2017; Paylor et al., 2001; Paylor and Lindsay, 2006; Stark et al., 2008), prepulse inhibition of the acoustic startle response was reduced in *Df1*/+ mice relative to WT mice, for prepulse cues with 70 dB SPL absolute sound level. However, there was no significant difference in PPI between *Df1*/+ and WT mice when the prepulse cue sound level was adjusted to be 10 dB below the startle threshold to match its sensory salience across animals. I also found that uncued startle responses to the startle-eliciting stimulus (a fixed 95 dB SPL noise) were weaker in *Df1*/+ than WT mice.

Acoustic startle thresholds and/or PPI can be affected by abnormalities in either auditory or motor circuitry, or both (Swerdlow et al., 2001). While I cannot rule out the possibility that motor control deficits in *Df1*/+ mice (Sumitomo et al., 2018) might also have contributed to the results, these findings are clearly consistent with known effects of hearing loss. Hearing loss reduces auditory nerve input to the cochlear nucleus, which is the first stage of the acoustic startle circuit, and also alters neural activity in the inferior colliculus, which is involved in PPI (Swerdlow et al., 2001; Takesian et al., 2009).

Central auditory compensation for loss of peripheral input might counteract some effects of hearing loss, but such compensation is likely to be less complete for the subcortical auditory structures providing input to the startle and PPI circuits than for cortical responses (Chambers et al., 2016). Therefore, the fact that cortical AEPs appeared normal in *Df1*/+ mice with hearing loss does not mean that subcortical auditory inputs to the startle and PPI circuits were unimpaired. Similarly, a low threshold for acoustic startle did not necessarily imply normal hearing (cf. Paylor et al., 2001; Scott et al., 2018). While the median startle response threshold was higher in *Df1*/+ than WT animals, the range of thresholds (75-95 dB SPL) largely overlapped in WT mice and *Df1*/+ mice with and without hearing loss.

3.3.4 Parvalbumin-positive cortical interneurons and hearing loss

In immunohistochemical studies, I found that the density of PV+ inhibitory interneurons was significantly reduced in the auditory cortex of *Df1*/+ relative to WT mice. The reductions in PV+ cell density did not arise from an overall change in neuronal density, and were not observed in the frontal region M2 which is interconnected with the auditory cortex (Nelson et al., 2013; Tomescu et al., 2014). Moreover, the auditory cortex abnormality in PV+ cell density arose primarily in *Df1*/+ mice with hearing loss, again suggesting central auditory compensation for loss of peripheral input.

To my knowledge, this is not only the first report of a link between hearing loss and reduced PV+ interneuron density in an animal model of schizophrenia, but also the first indication that hearing loss due to middle ear inflammation may influence PV+ interneurons in the auditory cortex. Previous studies in mice have demonstrated that PV+ interneurons in the auditory cortex can be affected by age-related (sensorineural) hearing loss (Martin del Campo et al., 2012), or by mutations that disrupt both auditory hair cell function and cortical interneuron migration (Libé-Philippot et al., 2017). It has also been shown that conductive hearing loss during development decreases inhibitory synaptic strength in the auditory cortex (Takesian et al., 2012). Current findings raise the additional possibility that conductive hearing loss, either alone or in combination with genetic risk factors for schizophrenia, may lead to reductions in PV+ interneuron density. Further experiments are required to test this hypothesis in other mouse models with conductive hearing loss, and to identify the reasons for the change in PV+ cell labelling (e.g., disruption of PV+ cell migration, increased PV+ cell death, or decreased PV expression).

3.3.5 Parvalbumin-positive cortical interneurons in mouse models of 22q11DS

Previous studies of mouse models of 22q11DS have reported abnormalities in PV+ cortical interneurons in other brain areas and at other developmental stages (Meechan et al., 2015, 2009; Piskorowski et al., 2016). In the *Lgdel*/+ mouse (with deletion of 5 more genes than in the *Df1*/+ mouse), Meechan et al. (2009) found that corticogenesis and subsequent differentiation of the cerebral cortex was disrupted. Laminar distribution of PV+ interneurons was altered in the medial prefrontal cortex at P21, but there was no apparent reduction in the density of PV+ interneurons (although the density of layer 2/3 pyramidal neurons was reduced). In adult *Df1*/+ and WT mice, I found no significant differences in the laminar distribution of PV+ interneurons in A1 and minimal differences in M2, despite a larger sample size (WT n=30, *Df1*/+ n=25 hemispheres) than that used in the Meechan et al. (2009) study. Therefore, while abnormalities in PV+ interneurons appear to be a reliable finding in mouse

models of 22q11DS, the form of these abnormalities may differ between mouse models, between brain areas, or between developmental time points. Further work is needed to understand these differences, and also to determine their origins.

Decreased PV+ interneuron density in *Df1*/+ mice might produce abnormalities in cortical dynamics that also occur in schizophrenia. Abnormalities in PV+ interneurons, including reductions in PV+ interneuron density, are a common finding in human schizophrenia (Beasley et al., 2002; Hamburg et al., 2016; Hashimoto et al., 2003; Uhlhaas and Singer, 2010) and are thought to contribute to cognitive dysfunction (Lewis, 2014). Optogenetic reductions in PV+ interneuron activity in animal models significantly attenuate the power of cortical gamma oscillations (Cardin et al., 2009; Sohal et al., 2009). Gamma oscillations are associated with active information processing, and are attenuated in power or synchrony both in animal models of schizophrenia and in human schizophrenia patients (Haenschel et al., 2009; Hamm et al., 2017; Uhlhaas and Singer, 2010).

While changes in PV+ immunostaining in cortex do not necessarily imply changes in interneuron activity or cortical gamma oscillations, results reported here and those of Meechan et al. (2009, 2015) suggest that mouse models of 22q11DS might have chronic abnormalities in PV+ interneuron function. My results further indicate that hearing loss either drives or contributes to the emergence of auditory cortical abnormalities in mouse models of 22q11DS. Further studies are required to disentangle the impact of schizophrenia associated genetic risk factors from the effects of hearing loss on auditory cortical function.

3.3.6 Implications for schizophrenia research

Disruption of auditory brain function in *Df1*/+ mice has previously been described as a key schizophrenia-relevant pathology (Chun et al., 2014), but the possible contribution of hearing loss was not considered. My results point

to a significant role for hearing loss in promoting auditory brain and behavioral abnormalities in *Df1*/+ mice. Increased central auditory gain and reduced auditory cortical PV+ interneuron density were most pronounced in *Df1*/+ mice with hearing loss, and there were no significant differences between WT mice and *Df1*/+ mice without hearing loss. Moreover, abnormalities in prepulse inhibition of acoustic startle in *Df1*/+ mice were reduced when prepulse cue level was adjusted relative to each animal's acoustic startle threshold. Further experiments in other mouse models, including WT mice with induced hearing loss, will be required to determine whether these and other central auditory abnormalities in *Df1*/+ mice arise from hearing loss alone or from an interaction between hearing loss and genetic risk factors for schizophrenia.

There is compelling evidence that hearing loss in adulthood increases the risk of psychosis and hallucinations (see Linszen et al., 2016 for a recent review). Moreover, hearing impairment in childhood elevates the risk of developing schizophrenia in adulthood. The mechanisms underlying the association between hearing loss and psychosis remain unknown, but could include not only common etiology but also bottom-up changes in neuronal networks driven by loss of sensory input, and top-down changes in cognition driven by difficulty with social communication (Linszen et al., 2016). In individuals with genetic or other risk factors for schizophrenia – such as 22q11DS patients – these consequences of hearing loss might be a critical “second hit” promoting development of hallucinations and other psychotic symptoms. Thus, the *Df1*/+ mouse and other mouse models of 22q11DS may help to reveal how hearing loss interacts with other schizophrenia risk factors to produce brain and behavioral abnormalities underlying psychiatric disease.

Chapter 4: Characterization of hearing loss in *Df1*/+ mice

4.1 Introduction

Chronic otitis media reduces afferent signal transmission during childhood and can lead to lasting central auditory impairments (Whitton and Polley, 2011). Unilateral conductive hearing loss can alter central encoding of spatial location and perceptual abilities (Thornton et al., 2014). The consequences of hearing loss on auditory perception are even greater when they appear during developmental sensitive periods than in adulthood (Buran et al., 2014). Takesian and colleagues (2012) found that conductive hearing loss at a very early developmental timepoint, at the time of ear canal opening, caused significant disruptions in synapse function (Takesian et al., 2012). However, other studies highlight that hearing loss at any age can have lasting effects. An ABR study in adults indicated that whether or not there was current otitis media or hearing loss, there were still lasting ABR latency changes. This was true regardless of whether hearing loss first occurred during an early developmental critical period or during adulthood (Ferguson et al., 1998). Taken together, these studies indicate that fluctuation of hearing levels at any point can result in changes to auditory function and structure.

Although hearing loss can have lasting effects upon the auditory system, it is important to know when hearing loss first appears in this mouse model. *Df1*/+ animals, like 22q11DS patients, consistently display elevated hearing thresholds. However, no study to date has characterized the hearing loss present in these animals. To address this, I tested how hearing loss progresses in these mice. I investigated whether hearing loss is persistent or whether mice recover normal hearing, and when in development hearing loss first appears. Previously only click ABRs had been studied within the Linden Lab so I also tested additional stimuli to assess frequency-specific hearing loss in *Df1*/+ mice.

4.2 Results

Auditory function was assayed in *Df1*/+ mice and WT littermates through measurement of distortion-product otoacoustic emissions (DPOAEs) and auditory brainstem response (ABR) at multiple time points between P21 and P102 (postnatal weeks 3-14.6). I used ABR measurements at 8k, 16k, 32k and 40k tones as well as click ABRs and DPOAEs to track the duration of hearing loss. DPOAEs are soft sounds that are produced by the inner ear in response to input sound. DPOAEs can be recorded by a small microphone temporarily inserted non-invasively in the ear canal. The presence of measurable DPOAEs is an objective measure of cochlear (inner ear) outer hair cell function, specifically electromotility (Abdala and Visser-Dumont, 2001). ABR tests are measurements of evoked potentials. After a sound stimulus is presented, electrical potentials are measured as they ascend the auditory pathway using scalp electrodes and displayed as a time waveform (microvolts over milliseconds). These neural potentials are used to estimate hearing sensitivity.

Mice were between the ages of post natal day (PND)21 and PND102 with at least 7 days between recording sessions. The average age at first recording was 31.8 days (4.54 weeks) and the median was 31 days (4.43 weeks). The average age at final recording was 68.4 days (9.77 weeks) and the median was 79 days (11.29 weeks). There was a total of 20 mice with two or more recording sessions, five mice had two recording sessions, two mice had three recording sessions, 12 mice had four recording sessions and one mouse had seven recording sessions. An additional 16 *Df1*/+ animals were tested only once (32 ears) and were included in the *Df1*/+ ABR averages.

4.2.1 ABR click thresholds indicate that 76% of Df1/+ animals have hearing loss at any given point

Using a different cohort of animals and a different testing facility, I replicated previous results obtained at UCL which showed that *Df1*/+ mice exhibit high rates of hearing loss. Over the course of at least 2 DPOAE and ABR click and tone testing sessions we found clear evidence of hearing loss during at least

one ABR click session in 10 of 13 *Df1*/+ mice (76%). Three of the 13 *Df1*/+ mice (23%) showed no evidence of hearing loss in any session. Mean ± SEM values for ABR click thresholds were 32.05 ± 0.41 dB SPL in WT ears versus 39.19 ± 0.98 dB SPL in *Df1*/+ ears. We defined the upper bound of normal hearing as 3 SD above the mean ABR threshold for WT ears (40.18 dB SPL). Hearing loss was monaural and occurred more commonly in the left ear, but in this data set there were at least three animals that had an elevated ABR click threshold in the right ear. Again, 0% (0/7) WT animals displayed hearing loss to ABR click stimuli.

The click ABR threshold of WT animals was 32.05 dB SPL, and the cutoff for normal hearing (3 SD from the mean) was 40.18 dB SPL (n=7, 14 ears). The average *Df1*/+ ABR click threshold was 37.48 dB SPL (n=29, 58 ears). Animals with only one ABR session were used in creating average thresholds, but when characterizing the types of hearing loss only animals with at least two sessions were included. *Df1*/+ animals without hearing loss had an average ABR click threshold of 34.29 dB SPL (n=17, 34 ears) while *Df1*/+ mice with hearing loss averaged 42.20 dB SPL (n= 12, 24 ears).

Three of ten animals with hearing loss at any given point (30%) were adult onset and the hearing loss appeared after eight weeks with an average ABR click threshold of 41.67 dB SPL (n=3). Seven of ten animals with hearing loss (70%) were categorized as developmental hearing loss that appeared before eight weeks. These animals had an average ABR click threshold of 42.00 dB SPL (n= 7).

Two of these ten animals with hearing loss didn’t have another ABR session after hearing loss was observed and were thus not included in the transient/persistent analysis. Of the *Df1*/+ mice with hearing loss, three of eight animals (37.5%) displayed transient hearing loss that eventually recovered with an average click threshold of 38.13 dB SPL (n=3). Five of eight animals with hearing loss (62.5%) displayed persistent hearing loss which was defined as elevated for two or more sessions.

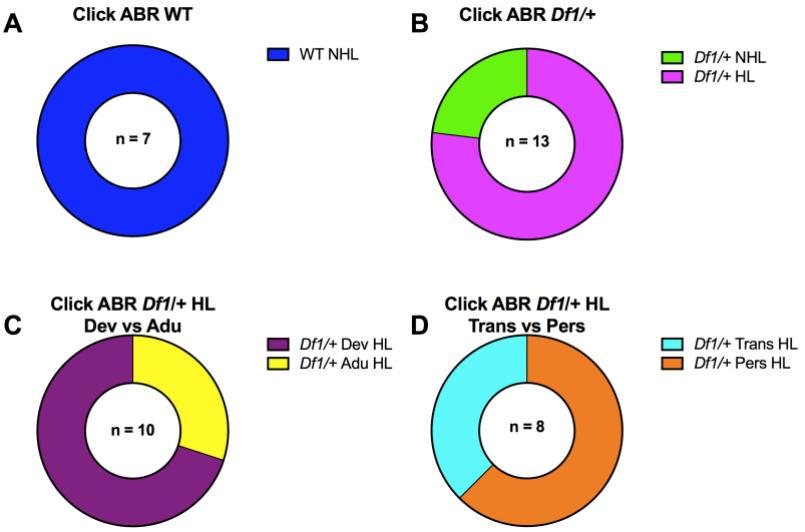

Figure 4.1 No WT mice and 76% of *Df1*/+ mice show hearing loss to click ABR stimuli that first appears more often during development and is persistent

(A) WT animals had an average ABR threshold of 32.05 dB SPL and the threshold for normal hearing was set to 3 standard deviations above the average WT threshold (40.18 dB SPL, n = 7). (B) *Df1*/+ mice had an average ABR click threshold of 39.19 dB SPL. Normal hearing thresholds were present in 23% of mice while ten animals (76%) had elevated thresholds consistent with hearing loss (n = 13). (C) Elevated click ABR thresholds in *Df1*/+ animals first appeared during development (prior to 8 weeks of age) in 70% of mice, while adult-onset hearing loss was present in the remaining 30% (n = 10). (D) When hearing loss occurred it was more likely persistent and elevated for two or more sessions (62.5%) and 37.5% of animals displayed transient hearing loss (n = 8). Two of the *Df1*/+ animals with hearing loss did not have an additional recording session after elevated thresholds were discovered.

4.2.2 No WT animals display elevated thresholds to ABR 8k tone stimuli, while approximately 62% of *Df1*/+ have hearing loss

The 8k tone ABR threshold of WT animals was 32.88 ± 0.69 dB SPL and the cutoff for normal hearing was 45.98 dB SPL. No WT animals displayed 8k tone thresholds above 45dB SPL (0%, 0/7). The average 8k tone ABR threshold of

Df1/+ animals was 39.61 ± 1.21 dB SPL (n=13). Of the *Df1*/+ animals, the average 8k tone threshold of animals without hearing loss was 34.17 dB SPL (n=5) and mice with hearing loss had an average threshold of 43.01 dB SPL (n=8). Five of the 13 *Df1*/+ animals (38.46%) showed no sign of hearing loss while eight showed hearing loss (61.54%).

There were six animals (75% of animals with hearing loss) that displayed developmental hearing loss, while two animals (25% of animals with hearing loss) displayed adult onset hearing loss (after 8 weeks of age).

Hearing loss could be transient or persistent with two animals displaying transient hearing loss (28.57%) and five animals (71.43%) displaying persistent hearing loss. One animal didn't have an additional ABR session after an elevated 8k tone threshold and was not included in the persistent versus transient comparison.

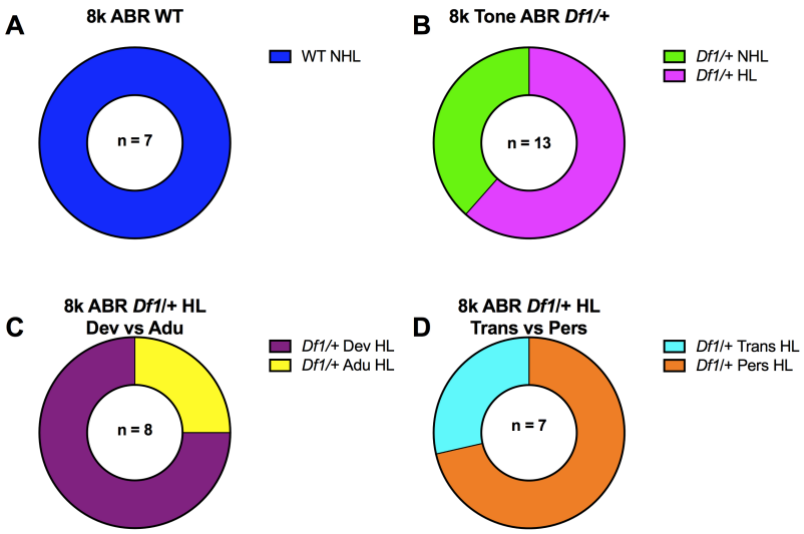

Figure 4.2 Approximately 62% of *Df1*/+ mice have elevated 8k tone ABR thresholds that first appear during development and are persistent, WT animals show no hearing loss

(A) WT mice had an average 8k ABR threshold of 32.88 dB SPL and the threshold for normal hearing was 45.98 dB SPL (3 standard deviations above WT average thresholds, n = 7). (B) *Df1*/+ mice had an average ABR tone

threshold of 39.61 dB SPL (n = 13). Normal hearing thresholds were present in 38.46% of mice while eight animals (61.54%) had elevated thresholds consistent with hearing loss. (C) Elevated tone ABR thresholds in *Df1*/+ animals first appeared during development (prior to 8 weeks of age) in 75% of mice, while adult-onset hearing loss was present in the remaining 25% (n = 8). (D) When hearing loss occurred it was more likely persistent and elevated for two or more sessions (71.43%) and 28.57% of animals displayed transient hearing loss (n = 7). One of the eight *Df1*/+ animals with hearing loss did not have a test session after hearing loss was observed and was not included.

4.2.3 16k ABR tone thresholds are elevated in approximately 54% of *Df1*/+ mice, WT display no hearing loss

Mean ± SEM values for 16k ABR tone thresholds were 36.75 ± 1.14 dB SPL in WT ears versus 44.49 ± 1.15 dB SPL in *Df1*/+ ears. The cutoff for normal hearing was 58.38 dB SPL based upon WT thresholds and no WT animals had a threshold higher than 55 dB SPL (0/7, 0%). Six of the 13 *Df1*/+ animals (46.15 %) showed no sign of hearing loss while seven (53.85%) had elevated ABR thresholds.

Of the *Df1*/+ mice with hearing loss, five (71.43%) displayed developmental hearing loss. In two animals (28.57%) hearing loss presented itself during adulthood.

Two animals displayed hearing loss that was transient and eventually recovered (33.33%) while four animals (66.67%) displayed persistent hearing loss. One animal had a final ABR test session with an elevated threshold and was not included in the persistent versus transient comparison.

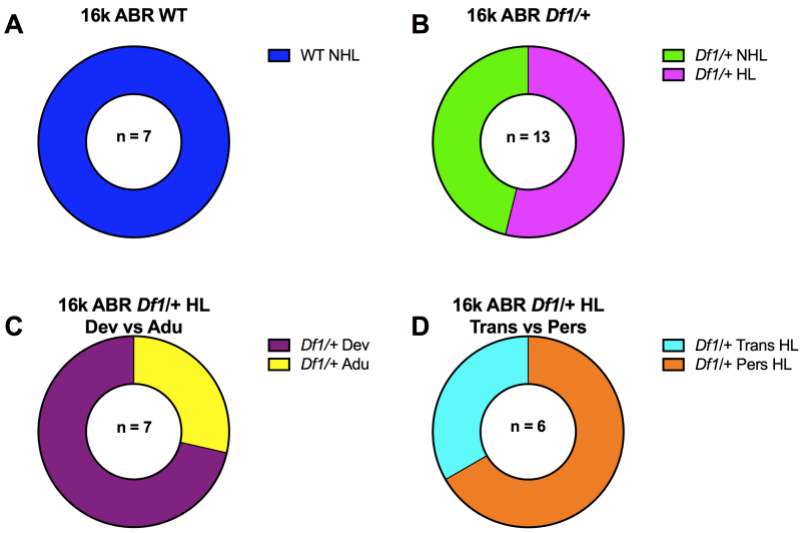

Figure 4.3 No WT mice and approximately 54% of *Df1*/+ mice show hearing loss to 16k tone ABR stimuli that first appears more often during development and is persistent

(A) WT animals had an average ABR threshold of 36.75 dB SPL and the threshold for normal hearing was set to 3 standard deviations above the average WT threshold (58.38 dB SPL, n = 7). (B) *Df1*/+ mice had an average ABR tone threshold of 44.49 dB SPL. Normal hearing thresholds were present in 46.15 % of mice while seven animals (53.85%) had elevated thresholds consistent with hearing loss (n = 13). (C) Elevated tone ABR thresholds in *Df1*/+ animals first appeared during development (prior to 8 weeks of age) in 71.43% of mice, while adult-onset hearing loss was present in the remaining 28.57% (n = 7). (D) When hearing loss occurred it was more likely persistent and elevated for two or more sessions (66.67%) and 33.33% of animals displayed transient hearing loss (n = 6). One of the seven *Df1*/+ animals did not have an ABR session after hearing loss was last observed.

4.2.4 ABR 32k tone thresholds indicate hearing loss in 14% of WT mice and 23% of *Df1*/+ mice

The 32k tone ABR threshold of WT animals was 50.13 ± 2.73 dB SPL and the average ABR threshold of *Df1*/+ animals was 68.75 dB SPL. In *Df1*/+ animals the average 32k tone threshold was 50.46 ± 1.76 dB SPL. The cutoff for normal hearing was 101.92 dB SPL. Since ABR stimuli only went up to 90dB SPL to

protect the animals' ears, any ABR threshold not visible at 90 dB SPL was recorded as 100 dB SPL. One WT animal (1/7, 14.29%) had a 32k tone threshold of 100 dB SPL while three of 13 *Df1/+* animals (23.08%) had thresholds of 100 dB SPL.

Of the *Df1/+* animals with significantly elevated thresholds, two animals displayed elevated thresholds before 8 weeks of age and were classified as developmental (66.67%), and one (33.33%) displayed elevated thresholds in adulthood.

One animal didn't have an ABR session after displaying an elevated threshold and wasn't included in the persistent versus transient comparison and the two remaining animals (100%) both displayed persistent hearing loss with an average of 70.63 dB SPL.

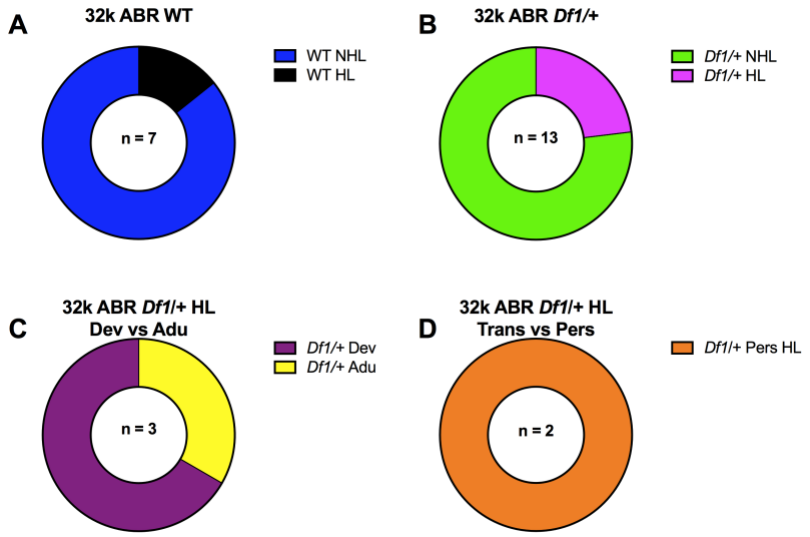

Figure 4.4 ABR responses to 32k tones revealed approximately 14% of WT mice and 23% of *Df1/+* mice show hearing loss

(A) WT animals had an average ABR threshold of 50.13 dB SPL and the threshold for normal hearing was set to 3 standard deviations above the average WT threshold (101.92 dB SPL, n = 7). Test stimuli only reached 90 dB SPL but all thresholds not visible at 90 dB were recorded as 100 dB SPL. One WT animal (14.29%) had an ABR threshold not visible at 90 dB SPL. (B) *Df1/+*

mice had an average ABR tone threshold of 68.75 dB SPL. Normal hearing thresholds were present in 76.92% of mice while 3 animals (23.08%) had elevated thresholds consistent with hearing loss (n = 13). (C) Elevated tone ABR thresholds in *Df1*/+ animals first appeared during development (prior to 8 weeks of age) in 66.67% of mice, while adult-onset hearing loss was present in the remaining 33.33% (n = 3). (D) When hearing loss occurred it was more likely persistent and elevated for two or more sessions in both animals (100%, n = 2). One of the three *Df1*/+ animals did not have an ABR session after hearing loss was last observed.

4.2.5 At 40k, ABR tone thresholds both WT mice (~43%) and *Df1*/+ mice (23%) display hearing loss

The 40k tone mean ± SEM values were 65.50 ± 3.45 dB SPL in WT ears versus 55.46 ± 2.18 dB SPL in *Df1*/+ ears. The cutoff for normal hearing was 131.00 dB SPL. Again, ABR stimuli only went as high as 90 dB SPL and any threshold not apparent at 90dB was recorded as 100 dB SPL. With such a high hearing loss threshold, ten of the 13 *Df1*/+ animals (76.92%) showed no sign of hearing loss. Three WT animals (3/7, 42.86%) had thresholds of 100 dB SPL and three *Df1*/+ animals (23.08%) also had elevated thresholds.

Two *Df1*/+ animals (66.67%) displayed hearing loss prior to 8 weeks of age with, while one animal (33.33%) elevated thresholds in adulthood.

Again, one animal didn't have an ABR session after displaying an elevated threshold and wasn't included in the persistent versus transient comparison, but the two remaining animals both displayed persistent hearing loss.

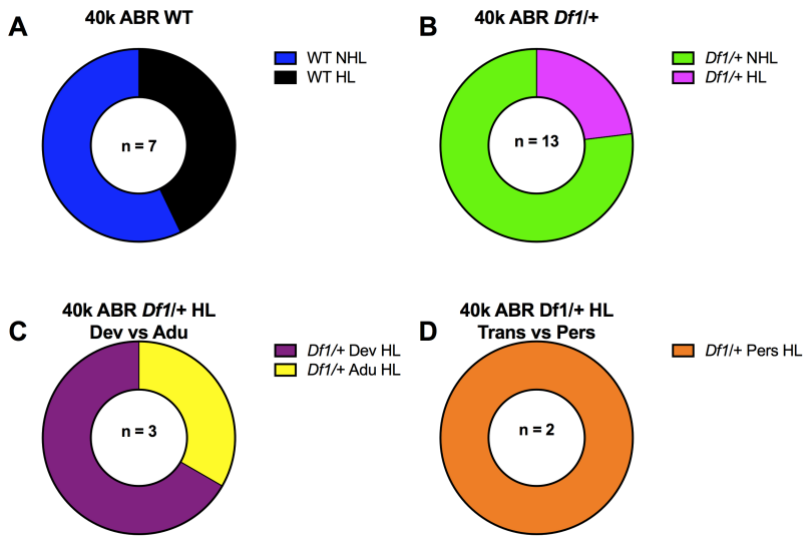

Figure 4.5 ABR responses to 40k frequency tones show that approximately 43% of WT mice and 23% of *Df1*/+ mice show hearing loss (A) WT animals had an average ABR threshold of 65.50 dB SPL and the threshold for normal hearing was set to 3 standard deviations above the average WT threshold (131 dB SPL, n = 7). 42.86% of animals had thresholds above 90 dB SPL and were recorded as 100 dB SPL. (B) The average ABR tone threshold in *Df1*/+ mice was 55.46 dB SPL. Normal hearing thresholds were present in 76.92% of mice while 23.08% had elevated thresholds consistent with hearing loss (n = 13). (C) Elevated tone ABR thresholds in *Df1*/+ animals first appeared during development (prior to 8 weeks of age) in 66.67% of mice, while adult-onset hearing loss was present in the remaining 33.33% (n = 3). (D) When hearing loss occurred it was more likely persistent and elevated for two or more sessions both *Df1*/+ animals displayed transient hearing loss (100%, n = 2). One of the three *Df1*/+ animals did not have an ABR session after hearing loss was last observed.

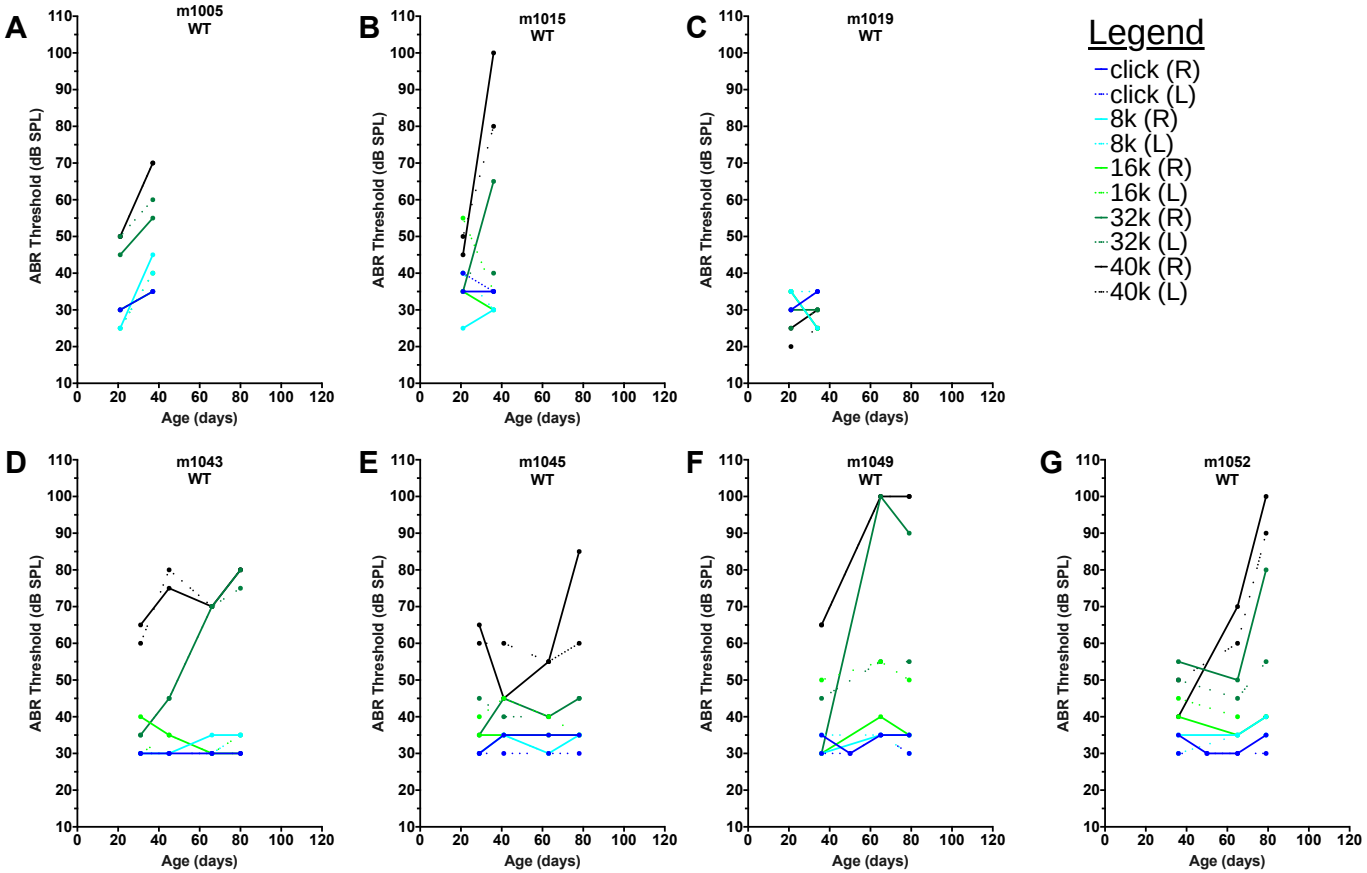

Figure 4.6 Even WT thresholds are increased at higher tone frequencies

(A-G) WT animals' thresholds across stimuli throughout development indicate that hearing loss appears only at higher frequencies (32k and 40k).

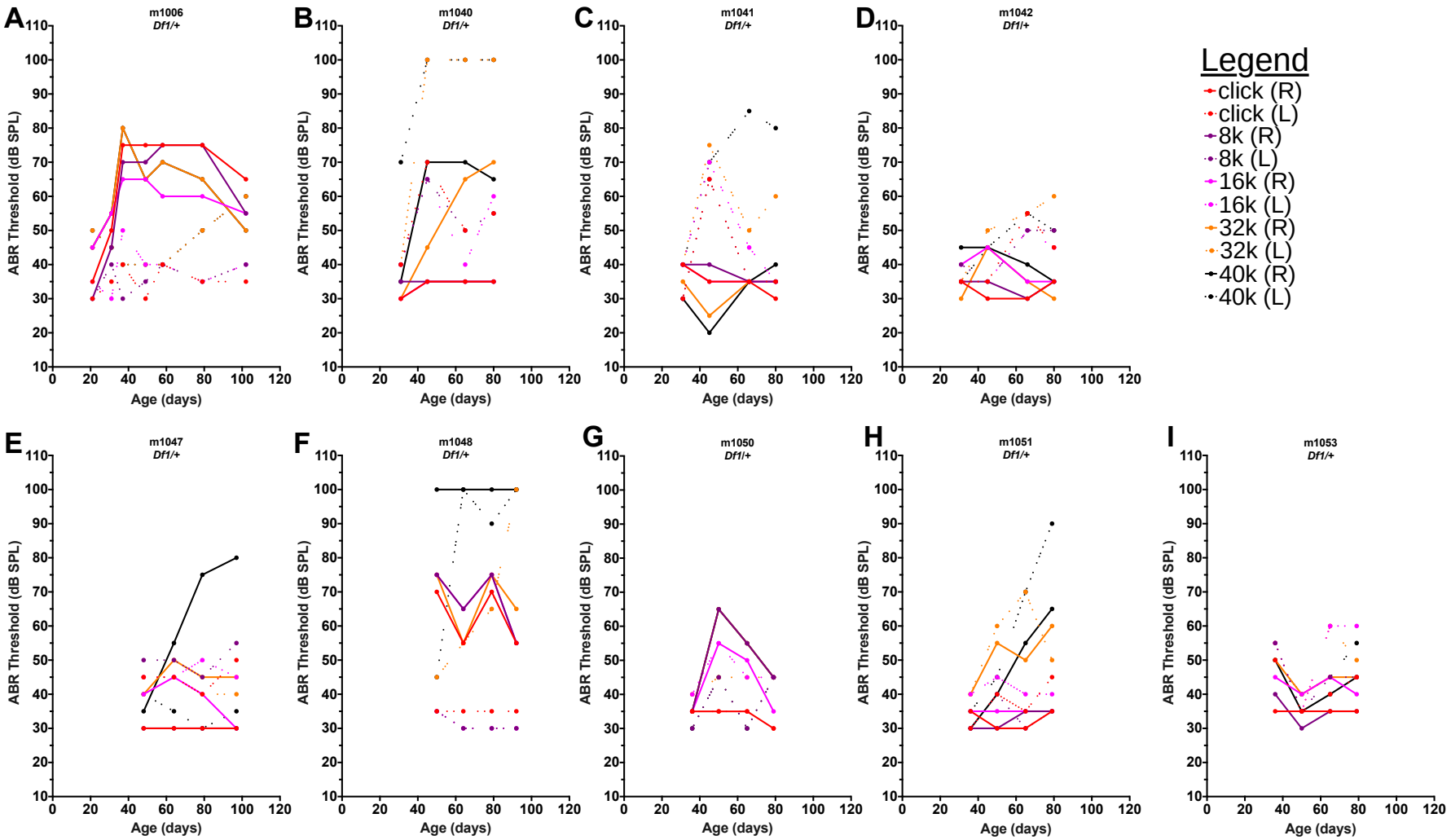

Figure 4.7 *Df1*/+ testing sessions indicate animals have hearing loss at all frequencies (continued on the next page)

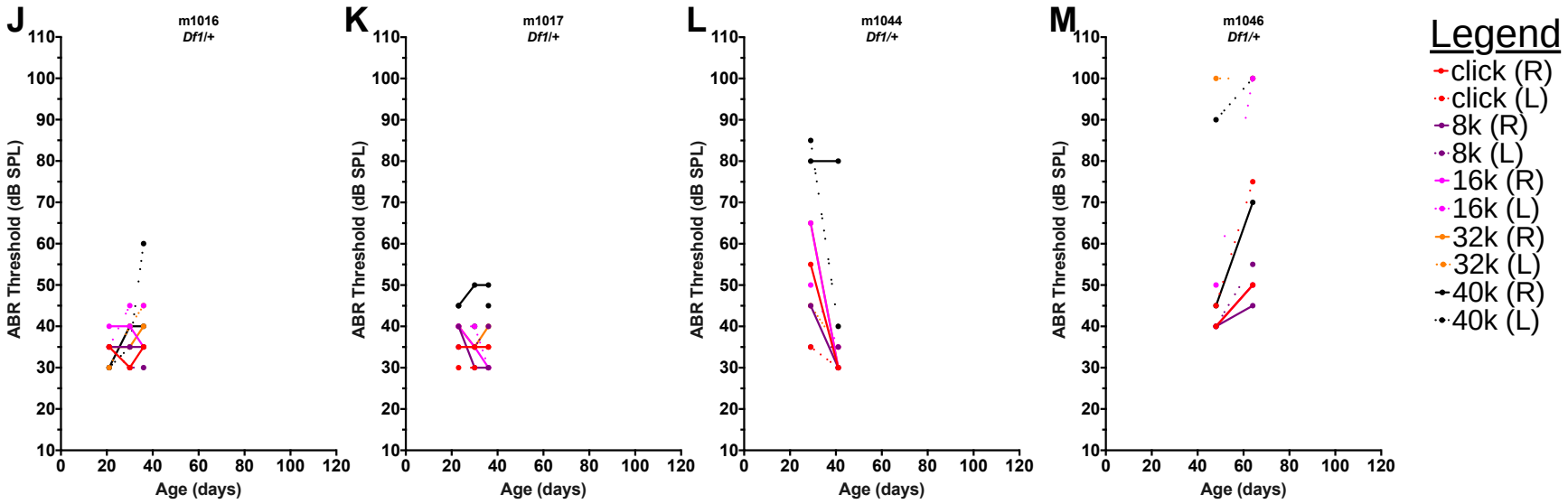

Figure 4.7 cont. *Df1/+* testing sessions indicate animals have hearing loss at all frequencies

(A-M) *Df1/+* animals' thresholds across stimuli throughout development indicate that hearing loss can appear at any developmental timepoint and can be persistent or transient. (A-I presented on the previous page, J-M on this page.)

ABR stimulus	WT average (n = 7)	% WT w/HL	*Df1/+* average (n = 13)	*% Df1/+* w/HL
Click	32.05 dB SPL	0%	39.19 dB SPL	76%
8k Tone	32.88 dB SPL	0%	39.61 dB SPL	61.54%
16k Tone	36.75 dB SPL	0%	44.49 dB SPL	53.85%
32k Tone	50.13 dB SPL	14.29%	68.75 dB SPL	23.08%
40k Tone	65.50 dB SPL	42.86%	55.46 dB SPL	23.08%

Table 4.1 ABR thresholds increase with frequency tested

At higher frequencies (32k and 40k) WT animals began to display elevations in average ABR thresholds indicating potential high frequency hearing loss. *Df1/+* animals displayed hearing loss at all frequencies.

4.2.6 DPOAEs

Results of the DPOAE tests were inconclusive. Animals that had completely normal ABR click and tone thresholds displayed reduced frequencies or totally absent DPOAEs and other animals with elevated ABRs had DPOAEs present at almost all frequencies. We chose a single frequency tone, 16k, that was well within the mice's normal frequency range to assess the consistency of results in mice with and without hearing loss as indicated by click ABRs. There were three animals with normal or borderline ABR click thresholds (ABR visible at 45dB SPL or less) yet had completely absent DPOAE measurements.

4.3 Discussion

Results replicate previous findings and 76% of *Df1/+* animals have hearing loss at any given point during development. This percentage is larger than our previous study (Fuchs et al., 2013) which saw an elevation in only 48% of animals and in the previous chapter (chapter 3) where I saw elevations in 60% of animals. Since I tested over multiple time points, hearing loss was more likely to be noticed before it had a chance to recover. ABR click hearing loss in *Df1/+* mice can be either transient (37.5%) or persistent (62.5%) in nature and can first occur in earlier developmental time points (70%) or in adulthood (30%).

This study added frequency specific hearing assessments at 8k, 16k, 32k and 40kHz to previous studies. The average mouse can hear from about 1 to 100kHz, but has a very narrow range of exceptionally good hearing (audible as low as 10dB SPL), which is around 16kHz (Heffner and Heffner, 2007). At 8k and 16kHz no WT animals displayed hearing loss, but at higher frequencies mice display elevated thresholds. At 32kHz one animal displayed an elevated threshold (14.29%) and at 40kHz three animals (42.86%) showed signs of hearing loss. Hearing loss in *Df1*/+ mice appeared at all frequencies. At 8kHz 61.54% of *Df1*/+ animals had hearing loss, at 16kHz 53.85%, at 32kHz 23.08%, and at 40kHz 23.08%. The decreasing percentage of mice with elevated thresholds is due to the fact that at higher frequencies even WT mice showed reduced sensitivity to tone stimuli, which in turn increased the threshold for normal hearing. Across frequencies, hearing loss tended to occur prior to 8 weeks of age and to be persistent (lasting longer than two sessions which were on average two weeks apart).

Current results indicate that *Df1*/+ mice are more likely to first experience hearing loss during development. Combined with previous study (chapter 3) which indicate increased central auditory gain in *Df1*/+ mice with hearing loss, these changes seem to occur before 8 weeks of age and are more likely to be persistent. Previous studies have shown that even transient conductive hearing loss can reduce inhibitory synaptic currents in the auditory cortex that persists in adulthood (Mowery et al., 2015; Sanes and Kotak, 2011; Takesian et al., 2012).

4.3.1 Otitis media in *Df1*/+ mice

Our previous studies have demonstrated that increases in ABR threshold are not attributed to age-related hearing loss (Fuchs et al., 2013), but instead due to otitis media (Fuchs et al., 2015). Otitis media can occur with or without effusion. Otitis media without effusion, also referred to as acute otitis media, occurs when fluid that is normally within the middle ear (which usually drains through the eustachian tube) becomes infected (Atkinson et al., 2015a). In otitis

media with effusion fluid becomes trapped in the middle ear, usually due to a blocked eustachian tube (Atkinson et al., 2015b). In humans, both usually occur following a cold or viral upper respiratory infection. Both can impede the movement of the middle ear bones (ossicles) and consequently reduce the multiplication of force onto the oval window and tympanic membrane. Using micro trichrome staining we established *Df1/+* ears that had elevated ABR thresholds had concurrent otitis media and the air-filled space within the middle ear was reduced. This reduction can lead to otitis media with effusion.

The onset and resolution of otitis media depends upon a variety of factors including pathogen exposure and genetics (Tyrer et al., 2013). In our previous study, bacteriology revealed that the only pathogens present were opportunistic and normally do not cause infections in healthy ears and there was no unusual susceptibility to a specific pathogen (Fuchs et al., 2013). In theory, since otitis media normally occurs as a consequence of bacteria that are normally present, the *Df1/+* mouse could represent a particularly useful model of opportunistic middle ear infection (Tyrer et al., 2013). However, this vulnerability to otitis media arises from abnormalities of middle ear physiology, particularly a reduction of the levator veli palatini muscles that control eustation tube function (Fuchs et al., 2015). This limits the ability to adequately clear middle ear effusions and thus the *Df1/+* mouse is more accurately a model of syndromic otitis media.

4.3.2 DPOAEs vs ABRs

This study highlighted that DPOAE results were not as reliable as ABR recordings in characterizing hearing loss. We found multiple occasions when ABR thresholds were quite low (at or below 45dB SPL), yet DPOAEs were completely absent. It is possible that DPOAEs and ABRs yielded different results because the middle ear contributes to ABR and ear canal DPOAE production differently. DPOAEs require sound energy to pass through the middle ear twice, whereas ABRs need only traverse the middle ear once. During DPOAE measurement a microphone and speaker are inserted into the

ear and tones are presented from low to high frequencies. The sounds need to make their way through the outer, middle and inner ear and the microphone will then record small sounds emitted from the inner ear (Abdala and Visser-Dumont, 2001). In ABR measurement, the stimulus only needs to pass through the middle ear and the electrodes measure the signals of the ascending auditory pathway. Since the middle ear must contribute and conduct sound twice within DPOAE measurement, any middle-ear conductive impairments could produce larger effects within DPOAEs vs ABRs.

It is possible that elevated high frequency thresholds within WT animals are a result of the fact that mice were bred with a C57BL/6J background strain. These mice have well characterized progressive hearing loss starting at higher frequencies and are commonly used as a model of age related hearing loss (Ison et al., 2007). An ABR study of 80 inbred strains of mice, C57BL/6J mice had normal thresholds at 33 weeks, but by 100 weeks thresholds were 60dB above average (Zheng et al., 1999). Another study also found that C57BL/6J mice have elevated high-frequency ABR thresholds at 14-36 weeks of age when compared with 7-week-old mice (Ison and Allen, 2003). Mice in this study were between the ages of postnatal weeks 3-14.6, however, only one animal was tested at 14.6 weeks of age (PND 102). The average age at final test sessions was 9.77 weeks (PND 68.4), yet high frequency hearing loss was apparent. It seems that within this cohort of animals, high frequency hearing loss appears even earlier than previously reported. This is consistent with a recent report indicating that mice between 9 and 12 weeks of age showed reduced thalamocortical bouton best frequencies in C57BL/6J mice, potentially highlighting the start of high-frequency hearing loss (Vasquez-Lopez et al., 2017).

4.3.3 Duration of hearing loss in *Df1*/+ mice

On average mice were tested fortnightly, which makes it difficult to accurately assess the onset and resolution of otitis media in these mice. In the one animal with persistent hearing loss that had the longest testing duration (from post

natal day (PND) 31 until PND 102), hearing loss was observed from the second session until the end of experiments, a total of 71 days. Other animals with transient hearing loss, the shortest duration was 14 days, but again this was simply how often these mice were tested. It is entirely possible that hearing loss resolved more quickly. In pilot experiments we observed that testing weekly led to anesthesia tolerance, which is why we tested every two weeks. Future studies are needed to determine exactly how long hearing loss lasts on average in *Df1*/+ mice.

Chapter 5: Viral-based neuronal tracing of PV+ neurons within the auditory cortex

5.1 Introduction

As demonstrated in chapter 3, *Df1/+* mice with hearing loss had an abnormally low density of PV+ inhibitory interneurons in the auditory cortex. I wondered if neuronal projections to auditory cortical PV+ interneurons might also be abnormal in *Df1/+* mice, with or without hearing loss. To investigate this question, I conducted a pilot study to test monosynaptic viral vector retrograde labelling in PV-Cre/*Df1/+* mice. In this pilot study, I validated this technique in WT mice and in *Df1/+* mice with and without hearing loss, and also obtained preliminary data on brain areas providing input to PV+ interneurons in different parts of A1.

To trace where PV+ cells within A1 receive input from, I first derived a PV-Cre/*Df1/+* mouse line. I then targeted PV+ cells in these animals by injecting Cre recombinase-dependent adeno-associated virus (AAV, AAV2/9 EF1α-FLEX-EGFP-TVA-G) into A1 (see methods in chapter 2 for detailed description). I allowed two weeks for PV+ cells to express TVA and glycoprotein G from injected AAV. These cells are selected on the basis of Cre expression and will express green fluorescent protein (GFP) and fluoresce green. I then performed another injection within the same A1 site to deliver the rabies virus (EnvA+ RV-dG-mCherry).

The envelope protein (EnvA) of subgroup A avian sarcoma and leukosis virus (ASLV-A) directs pseudotyped rabies virus (RV) to specifically infect cells that express its receptor TVA. A key structural component of RV is glycoprotein G, which allows for trans-synaptic propagation of rabies virus. The RV used in this study is a modified RV, a glycoprotein (G)-deleted rabies virus (RVdG). Without G the virus would not be able to propagate between cells. The only G protein to be found in injected mice is in PV+ cells that have been infected with the AAV virus expressing protein G and TVA, thus restricting the spread of the RV. The

rabies virus is unable to spread beyond directly connected neurons because those cells are missing the viral G (which has been deleted).

Our RVdG selectively infects neurons that express TVA and tags cells with mCherry which fluoresces red. These are called starter cells (which are PV+ cells that express Cre, originally tagged with GFP that fluoresces green), and they express rabies G so the virus can propagate. The RV exclusively infects cells in the retrograde direction so after infection, cells connected with the PV+ starter cells (which fluoresce in green) will fluoresce in red. Those starter cells will now fluoresce in both red and green, so they appear as yellow during imaging (see Figure 5.1). A week after RV*dG* injection, mice are sacrificed for imaging.

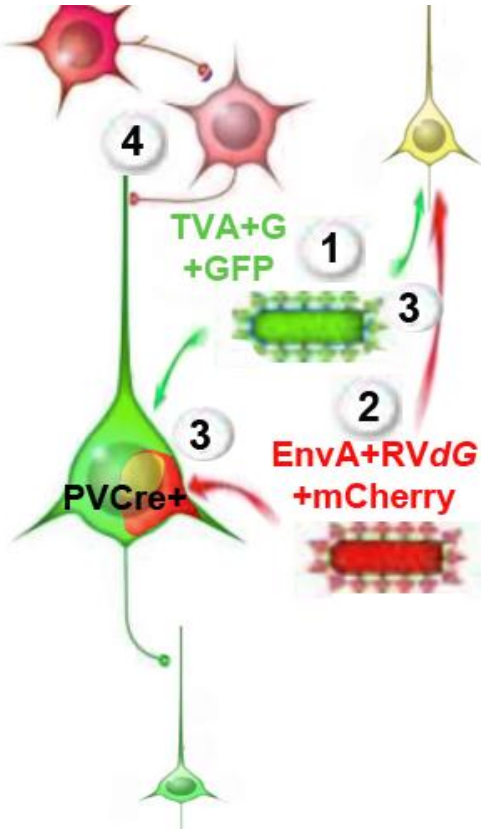

Figure 5.1 Diagram of TVA and RV*dG* viral injections and infection

(1) The helper virus that expresses TVA, G, and our tag/marker green fluorescent protein (GFP) in cells that are PV+ (and Cre dependent) is injected in A1. This makes the PV+ cells within A1 green since they express GFP along

with TVA and G. (2) After allowing two weeks for TVA and G to be accumulated within the cells, EnvA +RVdG is injected into A1. EnvA +RVdG contains the coding sequence for mCherry resulting in red fluorescence in the starter cells. (3) EnvA +RVdG selectively infects the TVA+ starter cells and then fluoresces both green (from the Cre dependent PV+ cells initially injected with TVA) and red (from the EnvA +RVdG mCherry) and are visible as yellow cells. (4) The RVdG then replicates in the starter cells and through trans-complementation with G produces G +RVdG that spreads trans-synaptically to input cells. These cells express mCherry from the RV genome (red). The result is that starter cells are yellow from having been injected with both TVA (green) and RVdG (red) while input cells express only red. (Modified from Wickersham et al., 2007)

To see what areas project to varied sections of A1, I injected PV-Cre/*Df1*/+ animals in two different locations within A1. One location was more anterior within A1 (AP -2.6mm, M-L 4.2mm Bregma) and one more posterior (AP -3.16mm, M-L 4.2mm Bregma). Our previous studies (chapter 3 and Fuchs et al., 2013) have shown a tendency for hearing loss to occur most often in the left ear of *Df1*/+ mice. Since the pathway from each ear to the contralateral auditory cortex is comprised of more nerve fibers (Baars and Gage, 2013; Wolpaw and Penry, 1977), all viral injections were done in the right hemisphere. Results indicate our injection methodology (adopted from Nelson and Mooney, 2016) was successfully replicated in PV-Cre/*Df1*/+ animals. PV+ neurons within both the anterior and posterior injection sites received input from the basal forebrain (BF) and auditory thalamus. In both the anterior and posterior A1 injection sites there were similar numbers of cells labeled by both viral injections and indistinguishable amounts of rabies infected cells in both the basal forebrain and auditory thalamus.

5.2 Results

5.2.1 Monosynaptic input tracing using PV-Cre/*Df1*/+ mice demonstrates basal forebrain and auditory thalamus projections to A1

Previous studies have used monosynaptic input tracing to visualize connections from both the auditory thalamus (Ji et al., 2016) and the basal forebrain (BF) (Nelson and Mooney, 2016) to PV+ interneurons within the primary auditory cortex. However, no study to date has examined these connections within a mouse model with hearing loss or elevated risk for schizophrenia such as the Df1/+ mouse. Given these mice have reduced PV+ cell density in A1 (Martin del Campo et al., 2012), I traced PV+ inputs to A1 in *Df1/*+ and WT mice. Following ABR click screening for hearing loss, injections indicated successful viral tracing.

Replicating previous studies, I found staining in both the BF and auditory thalamus when monosynaptic inputs were traced from PV+ cells within varying A1 injection sites (Figure 5.2). This pilot study included four animals with the anterior A1 injection site (2 WT, 2 *Df1*/+) and four with the more posterior injection site (1 WT, 3 *Df1*/+).

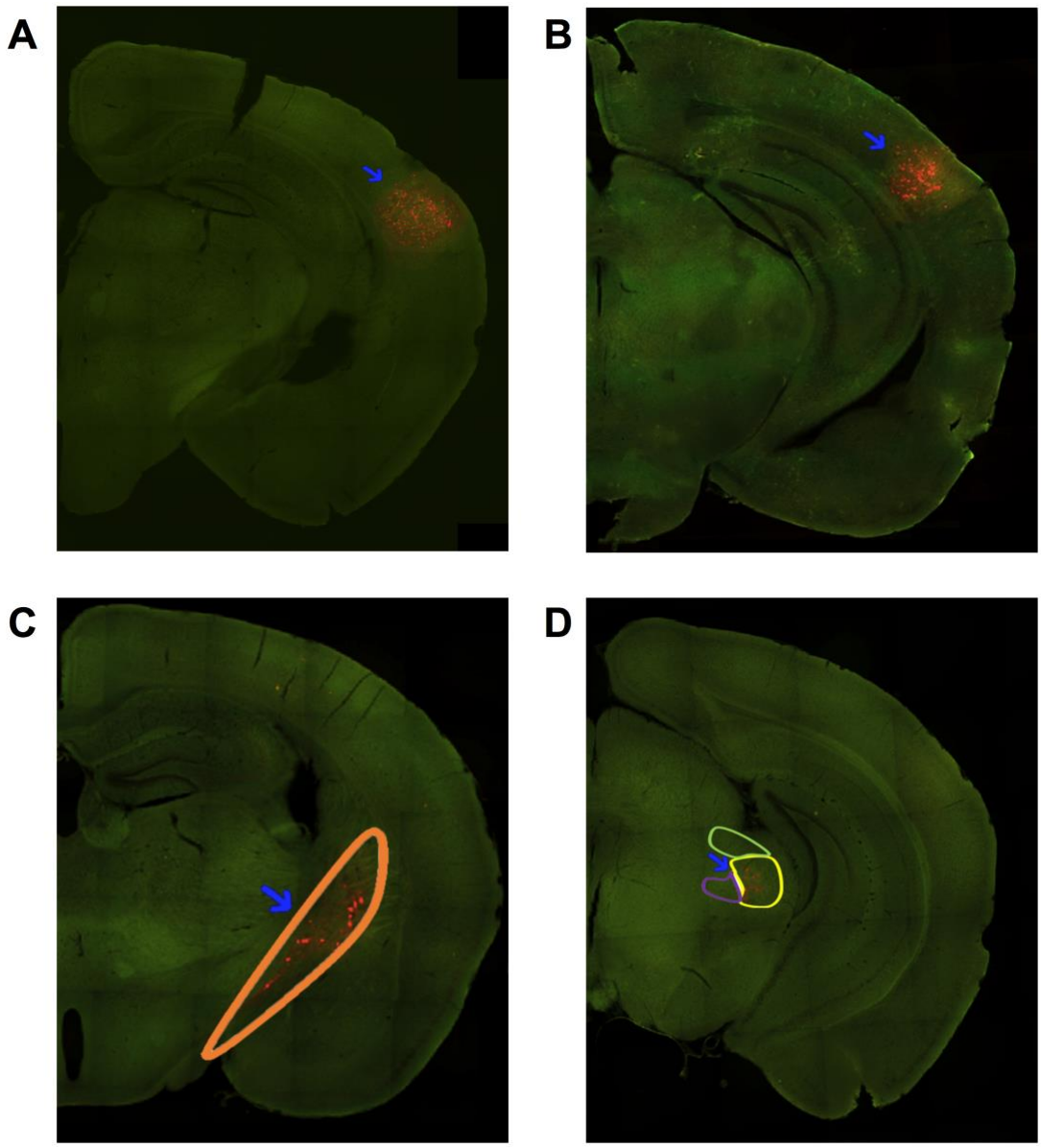

Figure 5.2 BF and auditory thalamic neurons target both anterior and posterior A1 locations

(A-B) Example images of a coronal section through both trialed injection sites. The more anterior (A) and posterior (B) injection sites within the primary auditory cortex (A1) of PV-Cre/*Df1*/+ mice both display viral labelling. (C) Example image of retrograde monosynaptic tracing visible in the basal forebrain (BF) within the orange highlighted area. An example image of retrograde monosynaptic tracing visible in the auditory thalamus, the yellow highlights the , ventral part of the medial geniculate nucleus, the dorsal part is in green and the medial part in purple. Regions of interest are indicated with a blue arrow.

5.2.2 Both A1 injection sites revealed a similar number of AAV stained PV+ cells

To find out the efficiency of both viral injections I calculated the total number of cells infected in the TVA and RV injections for the anterior and posterior injection sites (see Figure 5.3 for example of TVA, RV infected, and starter cells). Monosynaptic labeling resulted in TVA-infected PV+ cells (GFP, green), RV-labelled cells (mCherry, red cells which are presynaptic to TVA-infected green, PV+ cells) and starter cells (double labelled GFP and mCherry cells). Results indicated there were no significant differences between anterior and posterior injection sites in the number of GFP-labelled cells after the initial TVA injection (Figure 5.4A; unpaired t-test, p=0.61). There were also no differences in the number of RV-infected cells (Figure 5.4B**;** unpaired t-test, p=0.68), double-stained starter cells (Figure 5.4C; unpaired t-test, p=0.32) or the convergence index (the ratio of rabies cells to starter cells (Figure 5.4D; unpaired t-test, p=0.97).

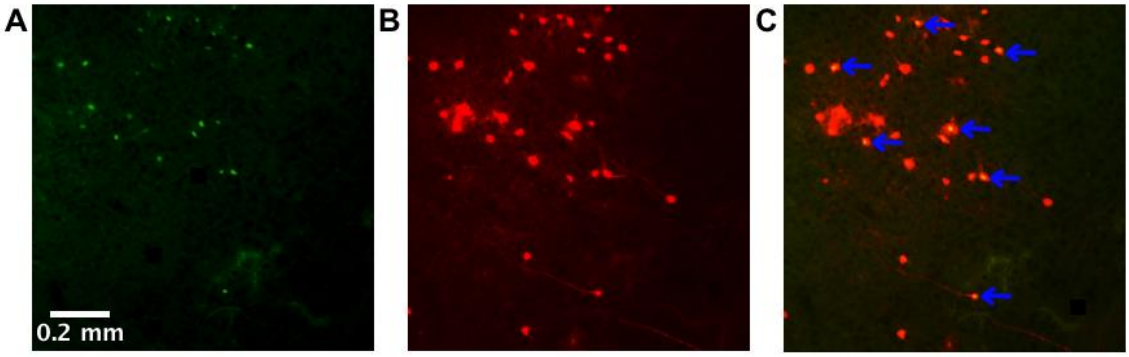

Figure 5.3 TVA, RV infected and starter cell identification

(A-C) Example confocal images of coronal sections through A1 of PV-Cre/*Df1/*+ mice illustrating TVA-labelled (A, GFP), RV-infected (B, mCherry) and starter cells (C, yellow cells indicated with blue arrows).

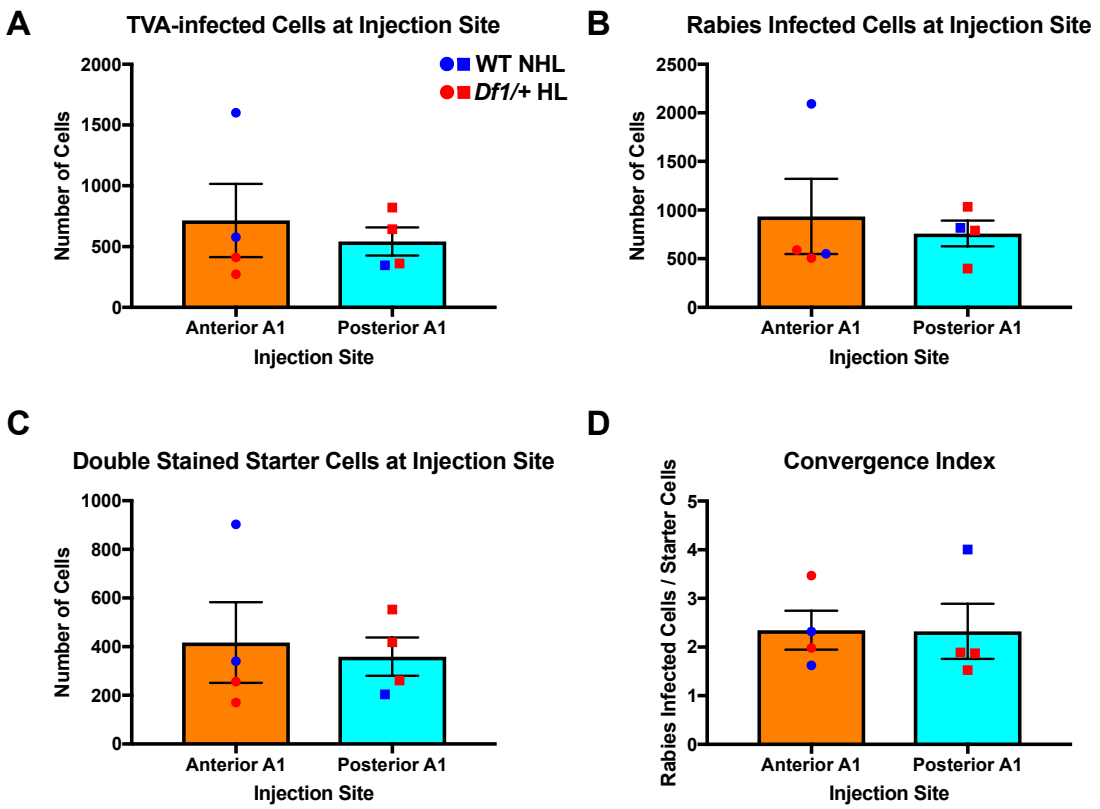

Figure 5.4 No difference in numbers of TVA+, RV-infected or starter cells in anterior vs posterior injection site

(A) The number of PV+ TVA-infected cells in the anterior A1 injection is not significantly different than within the posterior A1 (unpaired *t*-test, p=0.61). No differences were found in the number of RV-infected cells (B, unpaired *t*-test, p=0.68), starter cells (C, unpaired *t*-test, p=0.32), or the convergence index (D, unpaired *t*-test, p=0.97).

5.2.3 No difference was found in the amount of connections traced from the auditory thalamus in the anterior A1 injection site

Finally, I analyzed the number of fluorescent cells within the BF and auditory thalamus for both A1 injection sites. No difference was found in the number of RV-labelled cells arising from anterior versus posterior A1 injection sites in the BF (Figure 5.5A**,** unpaired t-test, p=0.14) or the auditory thalamus (Figure 5.5B, unpaired t-test, p=0.74).

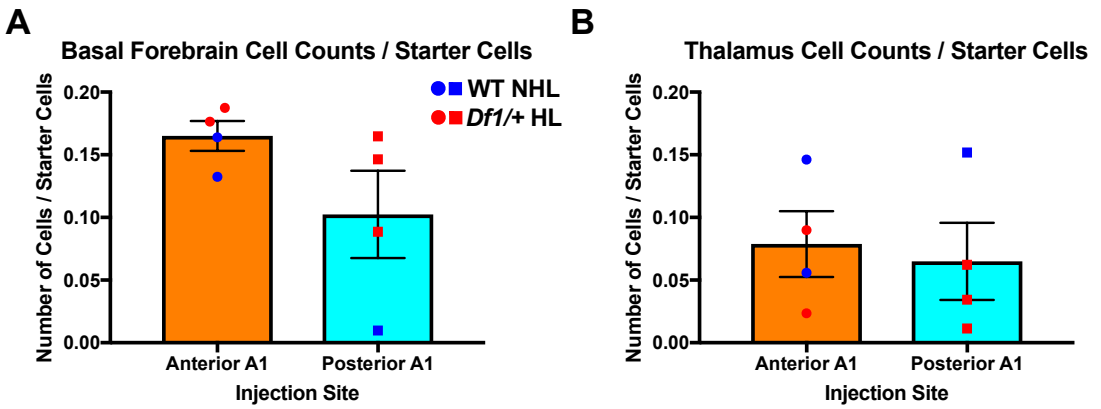

Figure 5.5 No differences in the number of RV-labelled cells from the auditory thalamus or BF regardless of injection site

(A) In the BF, anterior and posterior A1 injection sites showed no difference in RV labelled cells (unpaired *t*-test, p=0.14). (B) In the auditory thalamus, no significant differences in the amount of RV- labelled cells were found (unpaired *t*-test, p=0.74).

5.3 Discussion

Monosynaptic rabies tracing is a powerful tool with the potential to identify neurons that make direct presynaptic connections onto neurons of interest across the entire nervous system. Our results complement previous work examining projections to PV+ interneurons within A1 (Ji et al., 2016; Nelson and Mooney, 2016). I have extended these studies by varying injection sites within A1 and using the PV-Cre/*Df1*/+ mouse. These pilot studies have set the groundwork to later analyze differences between *Df1*/+ and WT littermates in projections to PV+ interneurons within A1, including how hearing loss contributes to any differences.

Results indicate that viral injections were successful in both the more anterior and posterior A1 locations. Both areas demonstrated clear signaling within both the BF and the auditory thalamus (Figure 5.5). Current observations indicate that either injection location can reveal A1 projections originating in either area. There were no differences in the TVA-infected PV+ cells (Figure 5.4A), the number of RV infected cells (Figure 5.4B), starter cells (Figure 5.4C) or the

convergence index (the ratio between RV-infected and starter, Figure 5.4D). This indicates that both viral infections seem stable despite differences in genotype and hearing loss. However, these results should be interpreted with caution considering the relatively small sample size.

Over the past decade rabies-based monosynaptic tracing has led to novel insights into the organization and function of neural circuits. This technology could be particularly useful to trace abnormalities across entire neural networks in mutant mouse lines. However, important limitations exist, one of which is that rabies experiments only label a fraction of the inputs to starter cells. Another limitation is the time of infection. The structural integrity of neurons and efficiency of viral transfer doesn't change significantly between four and eight days after rabies infection (Miyamichi et al., 2013), but RV kills neurons after approximately 14 days (Wickersham et al., 2007). However, newer versions of the modified RV have been developed. The RV has been improved to increase synaptic labelling and efficiency (Kim et al., 2016). Also new "self-inactivating" RV stops replicating once it infects a cell, which will allow the virus to perpetuate without harming the cell (Ciabatti et al., 2017). These improvements will allow for long term, longitudinal studies of neuronal connections in health and disease.

In these experiments I successfully replicated monosynaptic viral tracing in PV-Cre/*Df1*/+ mice with and without hearing loss. Another question that remains is whether hearing loss in *Df1*/+ mice has any effect upon the connections between A1, the BF and the auditory thalamus. Numbers of animals in this study were not sufficient to allow effective statistical comparison of mice with and without hearing loss. However, with additional data, the same technique piloted here could be used to determine whether acute hearing loss in *Df1*/+ mice correlates with abnormalities in thalamic or BF projections to PV+ interneurons. Moreover, with the substitution of a newer modified RV that would be able to trace neurons over longer periods of time, future studies in *Df1*/+ mice have the potential to parse out how developmental hearing loss affects projections to PV+ interneurons in A1.

Chapter 6: Summary, limitations and future directions

6.1 Summary

22q11.2 Deletion Syndrome (22q11DS, aka DiGeorge syndrome or Velocardiofacial syndrome) is a 1.5-3 Megabase pair deletion which causes a wide array of variable symptoms including neuro-behavioral abnormalities. 22q11DS is the strongest known risk factor for schizophrenia, conferring a 25-30% chance of developing schizophrenia. Patients with 22q11DS also exhibit high rates of hearing loss. This hearing loss is commonly conductive and arises from increased risk of middle ear inflammation (otitis media). Hearing loss has been identified as a risk factor for schizophrenia in humans, but the reasons for this association---and its possible relevance to the development of neuro-behavioral abnormalities in 22q11DS---are unknown.

In this thesis, I used the *Df1*/+ mouse model of 22q11DS to investigate interactions between genetic risk for schizophrenia, hearing loss, and brain and behavioral abnormalities. *Df1*/+ mice have a multi-gene deletion analogous to the chromosomal microdeletion that causes human 22q11DS and approximately 60% of animals display hearing loss related to otitis media. The main objective of the work covered in this thesis was to study the nature and resulting electrophysiological, behavioral and cellular consequences of hearing loss in *Df1*/+ mice.

I report results of three main experiments. First, I asked whether genotype, hearing loss or a combination of the two affected sensorimotor gating, cortical auditory evoked potentials, or parvalbumin-positive (PV+) inhibitory interneuron cell counts in the primary auditory cortex (A1) (Chapter 3). Next, I characterized the development of hearing loss in *Df1*/+ mice over postnatal weeks 3-14.6 (Chapter 4). Lastly, I investigated the origins of synaptic projections to PV+ interneurons in the auditory cortex (Chapter 5).

In experiments described in Chapter 3, hearing loss in *Df1*/+ mice and their wildtype littermates was assessed using measurement of auditory brainstem

responses (ABRs) to click stimuli. Auditory sensorimotor gating was tested using prepulse inhibition of the acoustic startle response, and cortical abnormalities were measured using auditory evoked potentials and immunohistochemical analysis of PV+ interneuron density. In experiments for Chapter 4, development of hearing loss in *Df1*/+ mice was characterized by obtaining repeated ABRs to both click and pure tone stimuli along with distortion product otoacoustic emissions in the same mice through development into adulthood. Finally, in experiments for Chapter 5, a modified retrograde rabies virus was injected into A1 of *Df1*/+ animals and their wildtype littermates to trace monosynaptic projections to PV+ interneurons. Two A1 injection sites were trialed, one more anterior and one more posterior within A1.

Results from chapter 3 indicate that hearing loss in *Df1*/+ mice was associated with schizophrenia-relevant endophenotypes, including altered electrophysiological measures of central auditory gain and behavioral measures of auditory sensorimotor gating. Moreover, PV+ inhibitory interneurons, another marker for schizophrenia pathology, were significantly reduced in density in A1 but not in the secondary motor cortex of *Df1*/+ mice with hearing loss. Laminar distribution of PV+ interneurons also remained unaltered in both areas.

Results from chapter 4 showed that hearing loss onset and duration in *Df1/*+ animals were highly variable. Elevated hearing thresholds could be either transient or persistent, and first appeared during postnatal development in some animals and during adulthood in others. Thus, the data revealed diverse developmental profiles for hearing loss in *Df1/*+ animals. However, in the majority of cases, hearing loss onset occurred relatively early, and persisted across at least two timepoints spaced two weeks apart.

Results from chapter 5 highlighted similar projection patterns to PV+ interneurons regardless of the A1 injection location. Both the more anterior and posterior A1 injection sites showed projections originating within the auditory thalamus and basal forebrain. Although small n-values limit the scope of

conclusions from this study, overall projection patterns were consistent in multiple animals with similar A1 injection location, and in *Df1/+* as well as wildtype animals regardless of hearing loss. This monosynaptic retrograde tracing approach therefore holds promise for future experiments comparing projection patterns between wildtype and *Df1/+* mice with and without hearing loss.

This work has examined the relationship between hearing loss and susceptibility to schizophrenia-relevant brain and behavioral abnormalities within 22q11DS using a combination of behavioral, electrophysiological, immunohistochemical and viral tracing techniques. Overall, this thesis provides evidence for bottom-up neurobiological mechanisms through which peripheral hearing loss arising from the 22q11.2 deletion may promote the emergence of schizophrenia-relevant auditory brain and behavioral abnormalities. It also sets the stage for future experiments to combine these works to potentially explore how the trajectory, duration and onset of hearing loss affects these abnormalities within A1 and areas that project to it.

6.2 Limitations of this PhD study

The main limitation of this PhD study is that it is still uncertain whether the abnormalities seen in *Df1/+* animals are a result of an interaction between hearing loss and genetic risk for schizophrenia or hearing loss alone. None of the WT animals tested in any study displayed elevated thresholds to click or tonal stimuli below 16kHz (which is within the very narrow range of exceptionally good sensitivity in mice, Heffner and Heffner, 2007). To begin to answer this question there would need to be WT animals with hearing loss. This could be done by earplugging WT animals to recreate temporary hearing loss or surgically (e.g. by removing the ossicles) to study more permanent and persistent threshold elevations. It would be interesting to confirm whether the same changes and abnormalities exist in WT animals, or whether hearing loss acts as a “second hit” to systems that are already altered with elevated genetic risk for schizophrenia.

Another limitation is that the question still remains whether hearing loss during a developmental critical period or adulthood led to the observed abnormalities within A1 and PV+ interneuron networks in *Df1*/+ mice. The answer to this question would essentially lie in combining the studies in chapter 3 and chapter 4. In chapter 3, we only had ABR measurements at the moment of ASR and AEP testing. It is possible that the changes seen in these animals arose from either acute hearing loss in adulthood or previous hearing loss during development which persisted into adulthood. By longitudinally testing animals and tracking hearing thresholds along with any behavioral and electrophysiological abnormalities, it could be possible to determine whether the effects of hearing loss in *Df1*/+ mice arose in development or adulthood (or both).

6.3 Future directions

This study provided strong evidence that hearing loss is associated with schizophrenia-relevant abnormalities within a mouse model of 22q11DS. Although this study failed to clearly delineate whether hearing loss or an interaction between hearing loss and the 22q11.2 deletion is responsible for the abnormalities seen in *Df1*/+ mice, it did identify assays for further investigation.

Further investigation could combine the experiments within chapter 3 and chapter 4 to assess hearing loss over a longer period of time to track its onset and resolution. This experiment would allow us to examine when hearing loss matters most and how it affects behavioral and electrophysiological assays in these animals. The addition of WT animals with induced hearing loss during different critical periods to this experiment would then be able to expose whether hearing loss, genetic risk for schizophrenia or a combination of the two are responsible for the abnormalities reported in this thesis.

While this thesis presented immuohistochemical and monosynaptic viral tracing of PV+ interneurons post mortem in *Df1*/+ mice, it would be interesting to see

how these neurons respond in vivo. One way to do so would be to use in vivo two-photon calcium imaging. Many recent investigations have analyzed activity of PV+ interneurons in vivo in the mouse auditory cortex using this technique (Kato et al., 2017; Kuchibhotla et al., 2017). Another recent study has successfully used in vivo two-photon microscopy to trace and monitor thalamocortical neurons within the auditory cortex as they respond to pure tones (Vasquez-Lopez et al., 2017). By combining *in vivo* two-photon calcium imaging with the results from an additional monosynaptic rabies tracing study, it would be possible not only to assess how hearing loss affects basal forebrain and thalamic projections to PV+ neurons in A1, but also to track how hearing loss affects the density and response properties of PV+ interneurons.

Given that the prefrontal cortex has been heavily linked to many cortical deficits seen in schizophrenia and 22q11DS (Karayiorgou et al., 2010; Shad et al., 2006), another interesting avenue would be to look at PV+ cell counts within the frontal cortices of *Df1/+* animals. Varying mouse models have shown abnormalities in PV+ interneurons, but do not show the same alterations. Polymorphisms of platelet-derived growth factor receptor β (PDGFR-β) have been associated with schizophrenia, and mice with an engineered knockout of the PDGFR-β gene show schizotypical behavior such as reduced PPI. These PDGFR-β knockout mice also show reductions in PV+ interneurons in the medial prefrontal cortex (Nguyen et al., 2011). Studies in mouse models more similar to the *Df1/+* mouse have also focused on PV+ interneurons within the frontal cortex. *Df(16)A+/−* mice show a modest reduction in layer 5 PV+ interneurons within the medial prefrontal cortex (Fenelon et al., 2013), while *Lgdel+/-* mice show no reduction, but display altered laminar distribution in PV+ interneurons in the same area (Meechan et al., 2009). The pursuit of these frontal changes, and potentially how they interact with the reductions in PV+ interneurons within A1 would be of interest.

However, the frontal areas I analyzed showed no difference in PV+ cell number or density. In chapter 3 I looked at PV+ interneuron density in M2 and in pilot studies (appendix 1) I also counted PV+ cell numbers in a more anterior M2

region and the cingulate cortex area A24b. However, I found no significant differences in *Df1/+* mice versus their WT littermates. It is possible that there are other abnormalities that weren't detected in PV+ interneuron density counts. Previous studies have shown that long-range cortical-hippocampal synchrony is decreased and synaptic transmission in thalamocortical glutamatergic projections to the auditory cortex are disrupted in *Df(16)A+/-* mice (Sigurdsson et al., 2010). This study highlights that the normal flow of auditory information is altered in a very similar mouse model of 22q11DS. Further investigations exploring physiological responses (eg *in vivo* electrophysiological or two-photon calcium imaging) in M2 and other areas receiving A1 input may be a more sensitive index of possible abnormalities in *Df1/+* mice.

A study found that neurons of the agranular motor cortex project directly to the auditory cortex, with aberrances between these connections speculated to underlie auditory hallucinations in schizophrenia (Nelson et al., 2013). However, these predictions have never been tested at the level of single cortical neurons and small networks of neurons in an animal model of 22q11DS or schizophrenia. An interesting possibility would be to use *in vivo* electrophysiology and/or two-photon calcium imaging during an auditory temporal discrimination task that uses auditory information to guide a motor decision. This experimental setup would be well suited to engaging interactions between the auditory cortex and the frontal cortex and could be further stratified based on hearing loss profile as in the current thesis. As an example, mice could be trained to perform a two-alternative forced-choice auditory temporal discrimination task where a sound stimulus with a high or low rate of temporal modulation is presented. The ultimate goal of the task would be for the mouse to increase or decrease the click rate to bring it to an intermediate value through a motor guided behavior (e.g. pushing a lever or turning a wheel). This temporal task would allow us to focus on temporal precision, as the proposed role of cortical inhibitory networks is to refine the temporal precision of firing (Cardin, 2018). It is possible that given the reduction of PV+ interneurons in A1

described in this work, the sound-evoked responses of auditory cortical neurons in *Df1*/+ mice could be less reliable in their temporal response patterns. This test of temporal reliability has yet to be assessed in a mouse model of schizophrenia. Depending upon the results of these experiments, perhaps Cre-dependent optogenetic manipulation of interneuron activity could be a next step. These sets of studies could further improve our understanding of how increased genetic susceptibility to schizophrenia alters systems-level neuronal networks.

Given that both hearing loss (Linszen et al., 2016) and PV+ interneuron dysfunction (Marín, 2012) have been implicated as contributing etiologies within schizophrenia, the *Df1*/+ mouse model of 22q11DS and elevated genetic risk for schizophrenia allows unparalleled insight into hearing loss and how it affects the physiology, function, and projections to PV+ interneurons in A1. Findings from this thesis will hopefully contribute towards knowledge that can lead to the early detection and correction of cortical circuit deficits in neuropsychiatric disorders.

Appendix 1: Pilot studies of hearing loss assessment and PV+ cortical interneuron density in *Df1*/+ mice

The main aims of this pilot study were to evaluate tympanic membrane scoring as an alternative method for quantifying hearing loss in *Df1*/+ mice, and to compare PV+ cell counts in the frontal and auditory cortices of *Df1*/+ mice and their WT littermates. Tympanic membrane scores were found to be a relatively unreliable indicator of auditory function, which did not correlate with ABR thresholds. Analysis of PV+ cell counts revealed significantly lower PV+ cell numbers in A1 of *Df1*/+ mice relative to WT littermates, but no differences in the frontal cortices. Following this pilot study, I developed an improved strategy for selecting frontal cortex sections for analysis based on the density of the A1-to-M2 projection (see Chapter 2), and refined the experimental design for the larger subsequent study described in Chapter 3 of this thesis. As a result of this data collection, a more in-depth study was planned which formed the basis of the work presented in chapter 3 of this thesis.

Pilot experiments discussed here included data collection partially collected by another member of the Linden Lab.

Introduction

PV+ cortical interneuron abnormalities are strongly associated with schizophrenia (Gonzalez-Burgos et al., 2015; Lewis, 2014; Lewis et al., 2005; Lodge et al., 2009), and previous studies of mouse models of 22q11DS have identified PV+ cortical interneuron abnormalities in the frontal cortex (Meechan et al., 2012, 2009). Based on previous findings that conductive hearing loss can have profound impact on inhibitory synaptic strength in auditory cortex (Kotak et al., 2005; Mowery et al., 2015; Takesian et al., 2009; Xu et al., 2007), we wondered whether cortical PV+ interneuron density might be reduced in the *Df1*/+ mouse model of schizophrenia, especially in the auditory cortex of animals with hearing loss. However, it was not previously known whether PV+ cortical interneuron abnormalities occur in A1 of *Df1*/+ mice, nor whether conductive hearing loss in *Df1*/+ mice might influence PV+ interneurons in

auditory and/or motor cortex. Therefore, we decided to count PV+ cells in auditory and frontal/motor cortices of *Df1/+* mice and their wildtype littermates. Additionally, we investigated secondary motor cortex (M2), since previous studies had found that M2 sends projections to the auditory cortex and motor-related changes in A1 are driven by PV+ interneurons in M2 (Nelson et al., 2013; Schneider et al., 2014).

Results

Tympanic membrane scoring and ABR measurements

Tympanic membrane scores were determined *post-mortem*, after the completion of *in vivo* ABR testing, so that the outer ear could be removed for visual inspection of the eardrum (see Chapter 2 and Figure 2.2 for photo and details). A score of 0 indicated a normal tympanic membrane appearance; 1 indicated presence of bubbles and fluid behind the tympanic membrane; and 2 indicated an opaque tympanic membrane suggesting an entirely fluid-filled middle ear. Previous tympanic membrane scoring performed in the lab had indicated that 9 of 10 wildtype mice (90%) showed no signs of otitis media using this method while 3 of 7 *Df1/+* mice (43%) showed elevated tympanic membrane scores (see Chapter 2 for details) in at least one ear. One mouse showed elevated scores in both ears.

Of the 7 wildtype mice and 5 *Df1/+* mice that had ABRs recorded in each ear, wildtype mice had ABR thresholds between 35 and 75 dB SPL while their *Df1/+* littermates had ABR thresholds between 35 and 65 dB SPL (mean = 47.50 dB SPL). It should be noted that one wildtype mouse had ABR thresholds of 75 dB SPL and 60 dB SPL, while all other mice had ABR thresholds between 35 dB SPL and 40 dB SPL (mean without outlier = 37.08 dB SPL). Age-related hearing loss is common in the background strain of mice used (C57BL6) and these mice were between 17 and 19.3 weeks old, so it is possible that these elevated thresholds arose from age-related sensorineural hearing loss (Hequembourg and Liberman, 2001) rather than conductive hearing loss from otitis media (Fuchs et al., 2015, 2013).

We found that although the tympanic membrane scores were performed immediately *post-mortem,* the results did not correlate consistently with elevated *in vivo* ABR thresholds as we had expected (See Table A.1 below). Only 6 animals had both tympanic membrane scoring as well as ABR thresholds.

Mouse ID	Genotype	TM score L	ABR Threshold L	TM score R	ABR Threshold R
m10089	WT	0	35	0	40
m10090	WT	0	35	0	40
m10091	WT	0	35	0	40
m10088	*Df1*/+	1	35	1	40
m10092	*Df1*/+	2	55	0	40
m10093	*Df1*/+	0	65	1	65

Table A.1 ABR thresholds were not correlated with tympanic membrane scores

Animals with elevated ABR thresholds could have normal tympanic membrane (TM) scores and vice versa, indicating reduced reliability of TM scores as an sign of hearing loss.

PV+ cell counts in A1

Comparing results between *Df1*/+ and WT mice, we found significant reductions in PV+ interneuron density in A1 of *Df1*/+ mice (Figure A.1). There was also a possible trend toward correlation between increased ABR threshold and reduction in PV+ interneuron density (Figure A2) but the relatively small numbers of mice with elevated ABR thresholds made this analysis inconclusive. Correlation between A1 cell counts and contralateral ABR threshold was p=0.04 for WT mice and p=0.11 for *Df1*/+ mice; correlation with the ipsilateral ABR threshold was p=0.74 for WT mice and p=0.03 for *Df1*/+ mice. These data suggested a possible relationship between A1 cell counts and ABR thresholds in both contralateral and ipsilateral ears.

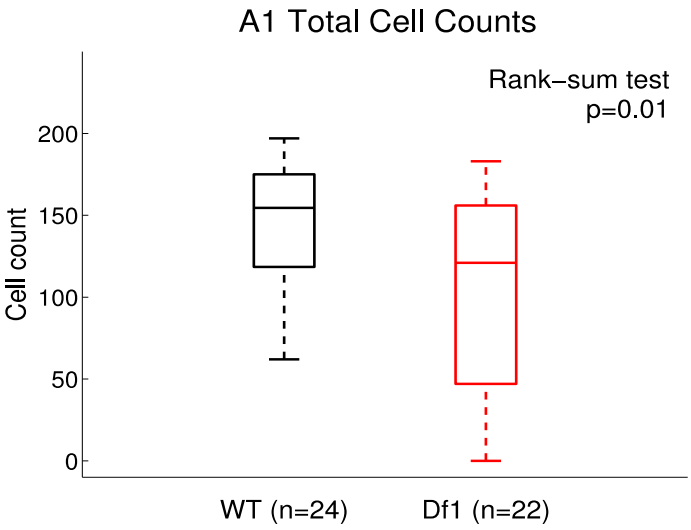

Figure A.1 Results indicated a significant reduction in PV+ cell counts in A1 of Df1/+ mice relative to WT mice

There were significantly fewer PV+ cell counts within A1 of *Df1/+* animals versus WT littermates.

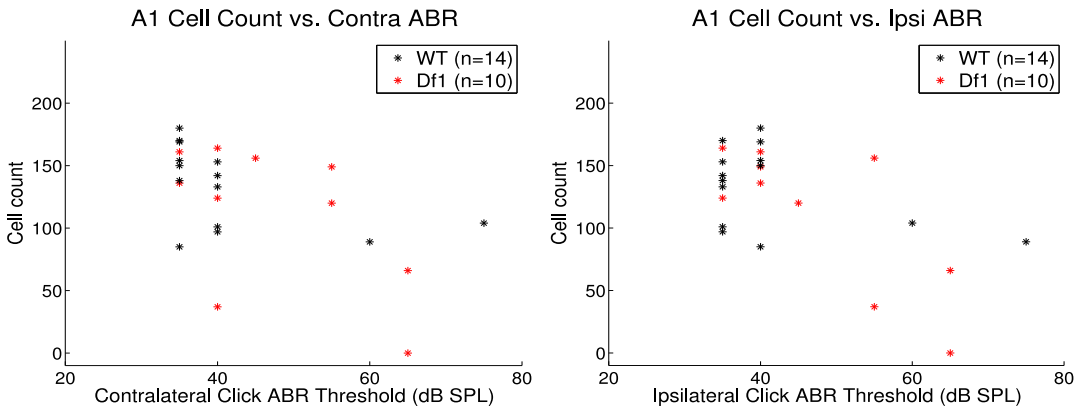

Figure A.2 The reduction in A1 PV+ cell counts showed some correlation with increased ABR thresholds in the contralateral ear (in WT mice) and the ipsilateral ear (for *Df1/+* mice)

The correlation between PV+ cell count in A1 and contralateral ABR was significant, but that between the A1 cell count and the ipsilateral ABR was significant for *Df1/+* mice. A1 Cell Count vs. Contra ABR Spearman rank corr: WT rho=−0.55, p=0.04; Df1 rho=−0.54, p=0.11. A1 Cell Count vs. Ipsi ABR Spearman rank corr: WT rho=−0.10, p=0.74; Df1 rho=−0.68, p=0.03.

PV+ cell counts in M2

No significant difference was found in PV+ cell density within the motor cortex (Figure A.3). Hearing loss was not related to PV+ cell density in M2 (Figure A.4).

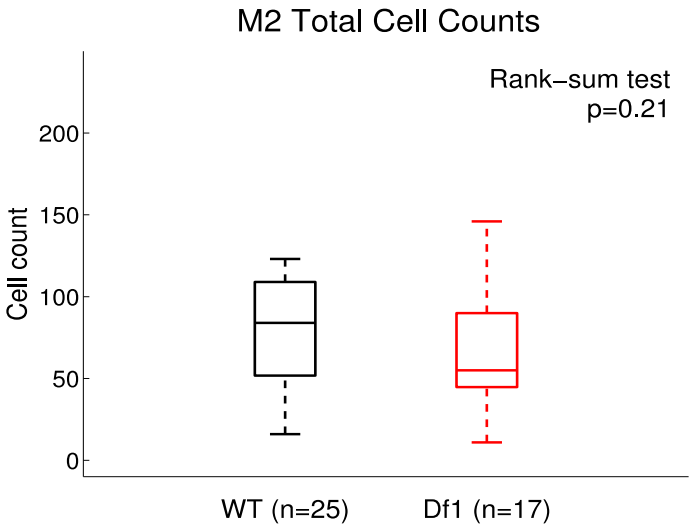

Figure A.3 No significant difference between *Df1*/+ and WT mice was found for PV+ cell counts within the motor cortex

The median PV+ cell count was lower in *Df1*/+ than WT animals, but not significantly so.

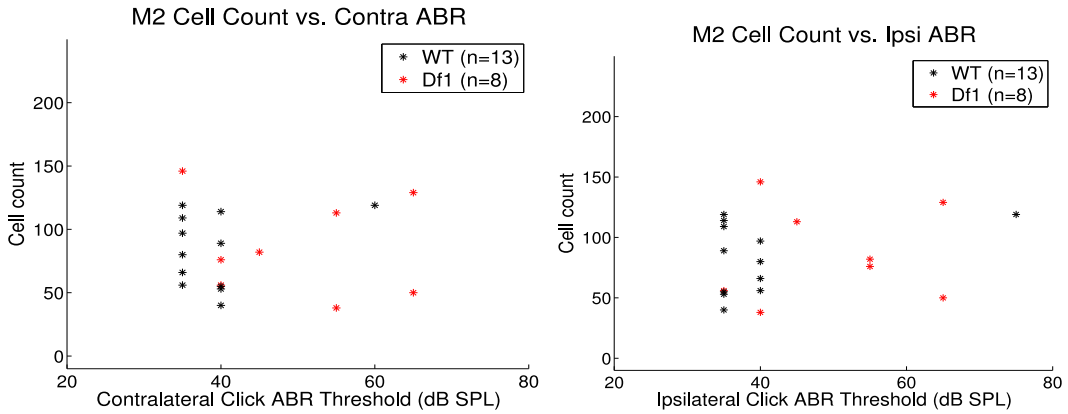

Figure A.4 Reductions in PV+ cell counts in M2 were not correlated with increased ABR thresholds in either the contralateral or ipsilateral ear

There was no correlation between PV+ cell count in A1 and ipsilateral or contralateral ABR for *Df1*/+ or WT mice within M2. M2 Cell Count vs. Contra ABR Spearman rank corr: WT rho=−0.10, p=0.74; Df1 rho=−0.25, p=0.54. M2

Cell Count vs. Ipsi ABR Spearman rank corr: WT rho=0.20, p=0.52; Df1 rho=0.11, p=0.80.

PV+ cell counts in A24b

No significant difference was found in PV+ cell counts within the cingulate cortex A24b (Figure A.5), and hearing loss was not related to PV+ cell density in A24b (Figure A.6).

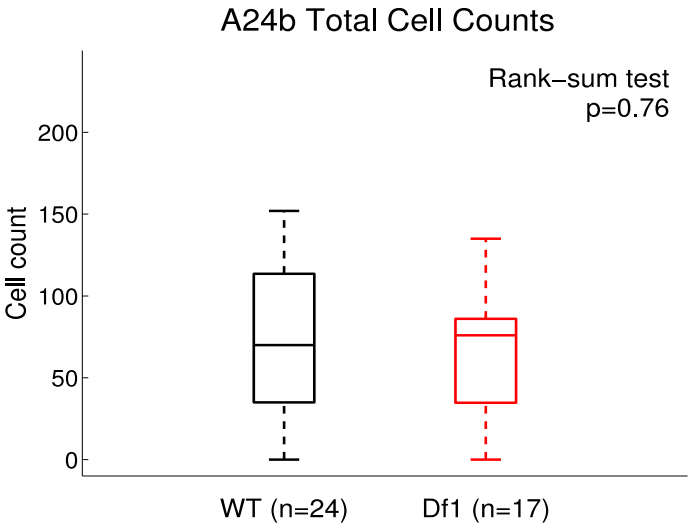

Figure A.5 No significant difference between *Df1*/+ and WT mice was found in PV+ cell counts within the cingulate cortex

There were no significant differences in cell counts in A24b between *Df1*/+ and WT animals.

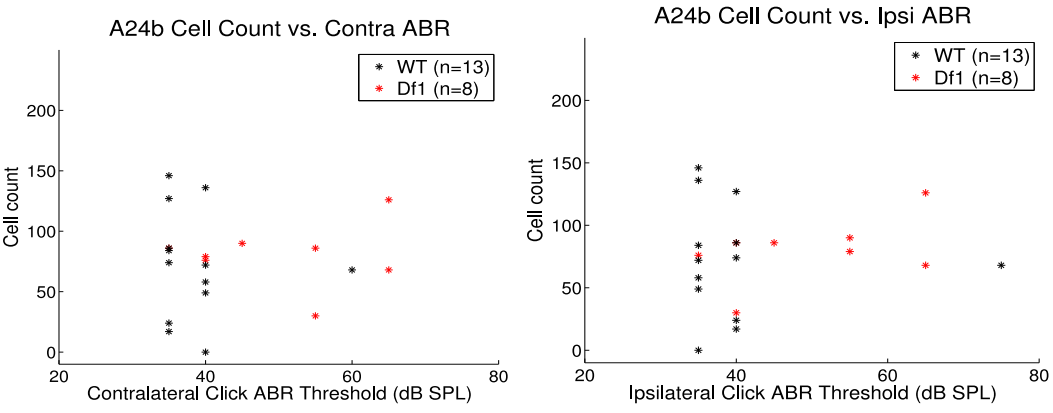

Figure A.6 No significant correlation between PV+ cell counts in A24b and ABR thresholds in either the contralateral or ipsilateral ear

There was no correlation between PV+ cell count in A1 and ipsilateral or contralateral ABR for *Df1*/+ or WT mice in A24b. A24b Cell Count vs. Contra

ABR Spearman rank corr: WT rho=−0.28, p=0.36; Df1 rho=−0.01, p=0.99. A24b Cell Count vs. Ipsi ABR Spearman rank corr: WT rho=−0.09, p=0.76; Df1 rho=0.36, p=0.37.

Implications for future study (Chapter 3)

Results of this pilot study motivated refinements of the experimental design for the much larger study reported in Chapter 3. In particular, we showed that tympanic membrane scores estimated immediately following euthanasia did not correlate with ABR thresholds measured *in vivo*, suggesting that the quick process of tympanic membrane scoring could not be used as a substitute for the more time-intensive process of ABR threshold measurement.

My experiments aimed to determine whether the density of PV+ interneurons is reduced in the auditory and/or frontal cortex of *Df1*/+ mice. Comparing cell counts between similar counting areas *Df1*/+ and WT mice, we found significant reductions in PV+ interneuron density in A1 of *Df1*/+ mice. These PV+ interneuron density reductions showed some correlation with increased ABR thresholds in both the contralateral and ipsilateral ear, although this finding was inconclusive due to the relatively low numbers of mice with elevated ABR thresholds in the pilot data set. In future cell count and ABR analyses I stratified mice based on hearing loss profile (see Chapter 3).

Pilot studies revealed reduced PV+ cell counts in A1 of *Df1*/+ mice relative to their WT littermates, but no abnormalities in PV+ cell counts in A24b or M2. This result was somewhat surprising, given that a previous study in a similar mouse models of 22q11DS found PV+ interneuron abnormalities in frontal cortex (Meechan et al., 2009). I therefore sought to optimize the choice of frontal cortex location for analysis in future studies, by identifying a target M2 location corresponding the region with the highest density of projections from A1 to M2 (Nelson et al., 2013; Schneider et al., 2014). I reasoned that since PV+ cell counts were significantly lower in A1 of *Df1*/+ than WT mice, any PV+

cell count abnormalities in M2 might be most prominent in the M2 region receiving the strongest projections from A1.

I used two approaches to define this optimal M2 location. First, I analyzed anterograde tracing data for C57Bl6 mice using data available online in the Allen Brain Atlas. Second, I performed my own anterograde tracing experiments to confirm the findings from the Allen Brain Atlas. These two approaches produced broadly consistent results (see methods in Chapter 2), allowing me to define the optimal M2 location for the larger study described in Chapter 3.

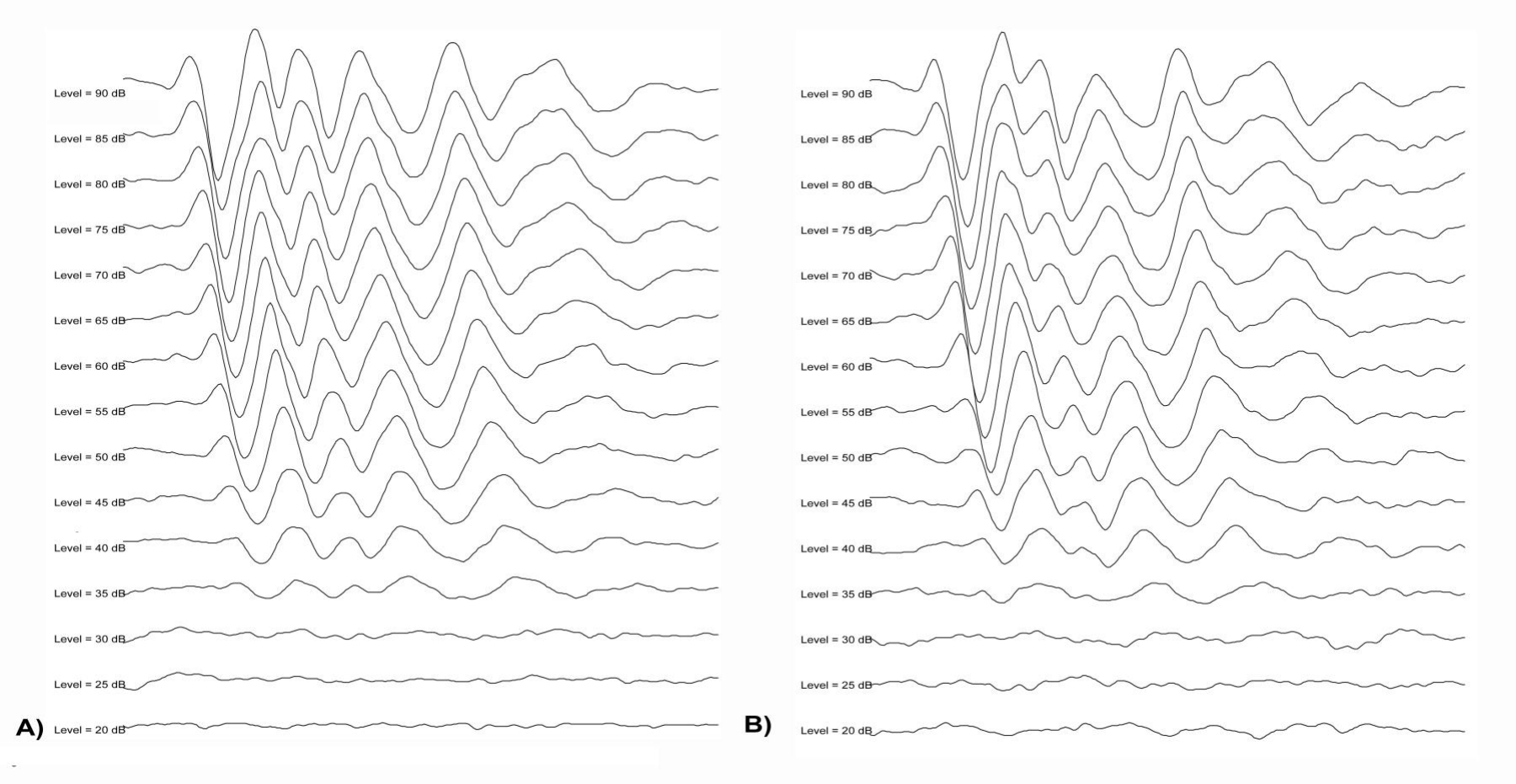

Figure A.7 ABRs were repeatable

ABR recordings were recorded consecutively in the same animal to assess reproducibility. Both ABR waveforms (A, B) were similar with a threshold of 35dB.

References

Abdala C, Visser-Dumont L. 2001. Distortion Product Otoacoustic Emissions: A Tool for Hearing Assessment and Scientific Study. *Volta Rev* **103**:281–302. doi:10.1038/nature13314.A

Aggarwal VS, Liao J, Bondarev A, Schimmang T, Lewandoski M, Locker J, Shanske A, Campione M, Morrow BE. 2006. Dissection of Tbx1 and Fgf interactions in mouse models of 22q11DS suggests functional redundancy. *Hum Mol Genet* **15**:3219–3228. doi:10.1093/hmg/ddl399

Aizenberg M, Mwilambwe-Tshilobo L, Briguglio JJ, Natan RG, Geffen MN. 2015. Bidirectional Regulation of Innate and Learned Behaviors That Rely on Frequency Discrimination by Cortical Inhibitory Neurons. *PLOS Biol* **13**:e1002308. doi:10.1371/journal.pbio.1002308

Arinami T. 2006. Analyses of the associations between the genes of 22q11 deletion syndrome and schizophrenia. *J Hum Genet* **51**:1037–1045. doi:10.1007/s10038-006-0058-5

Atkinson H, Wallis S, Coatesworth AP. 2015a. Acute otitis media. *Postgrad Med* **127**:386–390. doi:10.1080/00325481.2015.1028872

Atkinson H, Wallis S, Coatesworth AP. 2015b. Otitis media with effusion. *Postgrad Med* **127**:381–385. doi:10.1080/00325481.2015.1028317

Baars BJ, Gage NM. 2013. Fundamentals of cognitive neuroscience : a beginner's guide. Academic Press.

Barnett JH, Scoriels L, Munafò MR. 2008. Meta-analysis of the cognitive effects of the catechol-O-methyltransferase gene Val158/108Met polymorphism. *Biol Psychiatry* **64**:137–44. doi:10.1016/j.biopsych.2008.01.005

Bassett AS, Chow EWC. 1999. 22q11 deletion syndrome: a genetic subtype of schizophrenia. *Biol Psychiatry* **46**:882–91.

Bassett AS, Chow EWC, AbdelMalik P, Gheorghiu M, Husted J, Weksberg R. 2003. The schizophrenia phenotype in 22q11 deletion syndrome. *Am J Psychiatry* **160**:1580–6. doi:10.1176/appi.ajp.160.9.1580

Beasley CL, Zhang ZJ, Patten I, Reynolds GP. 2002. Selective deficits in prefrontal cortical GABAergic neurons in schizophrenia defined by the presence of calcium-binding proteins. *Biol Psychiatry* **52**:708–715. doi:10.1016/s0006-3223(02)01360-4

Bleich A, Kirsch P, Sahly H, Fahey J, Smoczek A, Hedrich HJ, Sundberg JP. 2008. Klebsiella oxytoca: opportunistic infections in laboratory rodents. *Lab Anim* **42**:369–375. doi:10.1258/la.2007.06026e

Breedlove SM, Watson N V., Rosenzweig MR. 2010. Biological Psychology: An Introduction to Behavioral, Cognitive, and Clinical Neuroscience, Sixth Edition. *Biol Psychol An Introd to Behav Cogn Clin Neurosci (6th ed)*. http://www.amazon.com/Biological-Psychology-Introduction-Behavioral-Neuroscience/dp/0878933247

Buran BN, Sarro EC, Manno FAM, Kang R, Caras ML, Sanes DH. 2014. A Sensitive Period for the Impact of Hearing Loss on Auditory Perception. *J Neurosci* **34**:2276–2284. doi:10.1523/JNEUROSCI.0647-13.2014

Buzsáki G, Draguhn A. 2004. Neuronal oscillations in cortical networks. *Science* **304**:1926–9. doi:10.1126/science.1099745

Cardin JA. 2018. Inhibitory Interneurons Regulate Temporal Precision and Correlations in Cortical Circuits. *Trends Neurosci* **41**:689–700. doi:10.1016/J.TINS.2018.07.015

Cardin JA, Carlen M, Meletis K, Knoblich U, Zhang F, Deisseroth K, Tsai LH, Moore CI. 2009. Driving fast-spiking cells induces gamma rhythm and controls sensory responses. *Nature* **459**:663–667. doi:10.1038/nature08002

Chambers AR, Resnik J, Yuan YS, Whitton JP, Edge AS, Liberman MC, Polley DB. 2016. Central Gain Restores Auditory Processing following Near-Complete Cochlear Denervation. *Neuron* **89**:867–879. doi:10.1016/j.neuron.2015.12.041

Chavez C, Zaborszky L. 2017. Basal Forebrain Cholinergic-Auditory Cortical Network: Primary Versus Nonprimary Auditory Cortical Areas. *Cereb Cortex* **27**:2335–2347. doi:10.1093/cercor/bhw091

Cho RY, Konecky RO, Carter CS. 2006. Impairments in frontal cortical gamma synchrony and cognitive control in schizophrenia. *Proc Natl Acad Sci U S A* **103**:19878–83. doi:10.1073/pnas.0609440103

Chun S, Westmoreland JJ, Bayazitov IT, Eddins D, Pani AK, Smeyne RJ, Yu J, Blundon JA, Zakharenko SS. 2014. Specific disruption of thalamic inputs to the auditory cortex in schizophrenia models. *Science (80-)* **344**:1178–1182. doi:10.1126/science.1253895

Ciabatti E, González-Rueda A, Mariotti L, Morgese F, Tripodi M. 2017. Life-Long Genetic and Functional Access to Neural Circuits Using Self-Inactivating Rabies Virus. *Cell* **170**:382–392.e14. doi:10.1016/j.cell.2017.06.014

Clarkson C, Antunes FM, Rubio ME. 2016. Conductive Hearing Loss Has Long-Lasting Structural and Molecular Effects on Presynaptic and Postsynaptic Structures of Auditory Nerve Synapses in the Cochlear Nucleus. *J Neurosci* **36**:10214–10227. doi:10.1523/jneurosci.0226-16.2016

Consortium SWG of the PG, Ripke S, Neale BM, Corvin A, Walters JTR, Farh K-H, Holmans PA, Lee P, Bulik-Sullivan B, Collier DA, Huang H, Pers TH, Agartz I, Agerbo E, Albus M, Alexander M, Amin F, Bacanu SA, Begemann M, Belliveau Jr RA, Bene J, Bergen SE, Bevilacqua E, Bigdeli TB, Black DW, Bruggeman R, Buccola NG, Buckner RL, Byerley W, Cahn W, Cai G, Campion D, Cantor RM, Carr VJ, Carrera N, Catts S V, Chambert KD, Chan RCK, Chen RYL, Chen EYH, Cheng W, Cheung EFC, Ann Chong S, Robert Cloninger C, Cohen D, Cohen N, Cormican P, Craddock N, Crowley JJ, Curtis D, Davidson M, Davis KL, Degenhardt F, Del Favero J, Demontis D, Dikeos D, Dinan T, Djurovic S, Donohoe G, Drapeau E, Duan J, Dudbridge F, Durmishi N, Eichhammer P, Eriksson J, Escott-Price V, Essioux L, Fanous AH, Farrell MS, Frank J, Franke L, Freedman R, Freimer NB, Friedl M, Friedman JI, Fromer M, Genovese G, Georgieva L, Giegling I, Giusti-Rodríguez P, Godard S, Goldstein JI, Golimbet V, Gopal S, Gratten J, de Haan L, Hammer C, Hamshere ML, Hansen M, Hansen T, Haroutunian V, Hartmann AM, Henskens FA, Herms S, Hirschhorn JN, Hoffmann P, Hofman A, Hollegaard M V, Hougaard DM, Ikeda M, Joa I, Julià A, Kahn RS, Kalaydjieva L, Karachanak-Yankova S, Karjalainen J, Kavanagh D, Keller MC, Kennedy

JL, Khrunin A, Kim Y, Klovins J, Knowles JA, Konte B, Kucinskas V, Ausrele Kucinskiene Z, Kuzelova-Ptackova H, Kähler AK, Laurent C, Lee Chee Keong J, Hong Lee S, Legge SE, Lerer B, Li M, Li T, Liang K-Y, Lieberman J, Limborska S, Loughland CM, Lubinski J, Lönnqvist J, Macek Jr M, Magnusson PKE, Maher BS, Maier W, Mallet J, Marsal S, Mattheisen M, Mattingsdal M, McCarley RW, McDonald C, McIntosh AM, Meier S, Meijer CJ, Melegh B, Melle I, Mesholam-Gately RI, Metspalu A, Michie PT, Milani L, Milanova V, Mokrab Y, Morris DW, Mors O, Murphy KC, Murray RM, Myin-Germeys I, Müller-Myhsok B, Nelis M, Nenadic I, Nertney DA, Nestadt G, Nicodemus KK, Nikitina-Zake L, Nisenbaum L, Nordin A, O'Callaghan E, O'Dushlaine C, O'Neill FA, Oh S-Y, Olincy A, Olsen L, Van Os J, Pantelis C, Papadimitriou GN, Papiol S, Parkhomenko E, Pato MT, Paunio T, Pejovic-Milovancevic M, Perkins DO, Pietiläinen O, Pimm J, Pocklington AJ, Powell J, Price A, Pulver AE, Purcell SM, Quested D, Rasmussen HB, Reichenberg A, Reimers MA, Richards AL, Roffman JL, Roussos P, Ruderfer DM, Salomaa V, Sanders AR, Schall U, Schubert CR, Schulze TG, Schwab SG, Scolnick EM, Scott RJ, Seidman LJ, Shi J, Sigurdsson E, Silagadze T, Silverman JM, Sim K, Slominsky P, Smoller JW, So H-C, Spencer CA, Stahl EA, Stefansson H, Steinberg S, Stogmann E, Straub RE, Strengman E, Strohmaier J, Scott Stroup T, Subramaniam M, Suvisaari J, Svrakic DM, Szatkiewicz JP, Söderman E, Thirumalai S, Toncheva D, Tosato S, Veijola J, Waddington J, Walsh D, Wang D, Wang Q, Webb BT, Weiser M, Wildenauer DB, Williams NM, Williams S, Witt SH, Wolen AR, Wong EHM, Wormley BK, Simon Xi H, Zai CC, Zheng X, Zimprich F, Wray NR, Stefansson K, Visscher PM, Trust Case-Control Consortium W, Adolfsson R, Andreassen OA, Blackwood DHR, Bramon E, Buxbaum JD, Børglum AD, Cichon S, Darvasi A, Domenici E, Ehrenreich H, Esko T, Gejman P V, Gill M, Gurling H, Hultman CM, Iwata N, Jablensky A V, Jönsson EG, Kendler KS, Kirov G, Knight J, Lencz T, Levinson DF, Li QS, Liu J, Malhotra AK, McCarroll SA, McQuillin A, Moran JL, Mortensen PB, Mowry BJ, Nöthen MM, Ophoff RA, Owen MJ, Palotie A, Pato CN, Petryshen TL, Posthuma D, Rietschel M, Riley BP, Rujescu D, Sham PC, Sklar P, St Clair D, Weinberger DR, Wendland JR, Werge T, Daly MJ, Sullivan PF, O'Donovan MC. 2014. Biological insights from 108 schizophrenia-associated genetic loci. *Nature* **511**:421.

David A. 1995. Are there neurological and sensory risk factors for schizophrenia? *Schizophr Res* **14**:247–251. doi:10.1016/0920-9964(94)00068-J

de Koning MB, Boot E, Bloemen OJN, van Duin EDA, Abel KM, de Haan L, Linszen DH, van Amelsvoort TAMJ. 2012. Startle reactivity and prepulse inhibition of the acoustic startle response are modulated by catechol-O-methyl-transferase Val(158) Met polymorphism in adults with 22q11 deletion syndrome. *J Psychopharmacol* **26**:1548–60. doi:10.1177/0269881112456610

Didriksen M, Fejgin K, Nilsson SRO, Birknow MR, Grayton HM, Larsen PH, Lauridsen JB, Nielsen V, Celada P, Santana N, Kallunki P, Christensen K V., Werge TM, Stensbøl TB, Egebjerg J, Gastambide F, Artigas F, Bastlund JF, Nielsen J, Stensbol TB, Egebjerg J, Gastambide F, Artigas

F, Bastlund JF, Nielsen J. 2017. Persistent gating deficit and increased sensitivity to NMDA receptor antagonism after puberty in a new mouse model of the human 22q11.2 microdeletion syndrome: a study in male mice. *J Psychiatry Neurosci* **42**:48–58. doi:10.1503/jpn.150381

Digilio MC, Pacifico C, Tieri L, Marino B, Giannotti A, Dallapiccola B. 1999. Audiological Findings in Patients with Microdeletion 22Qll (Di George/Velocardiofacial Syndrome). *Br J Audiol*.

Douglas NC, Washkowitz AJ, Naiche LA, Papaioannou VE. 2015. Principles of Developmental Genetics, Principles of Developmental Genetics. Elsevier. doi:10.1016/B978-0-12-405945-0.00034-X

Drew LJ, Crabtree GW, Markx S, Stark KL, Chaverneff F, Xu B, Mukai J, Fenelon K, Hsu P-KK, Gogos JA, Karayiorgou M. 2011. The 22q11.2 microdeletion: fifteen years of insights into the genetic and neural complexity of psychiatric disorders. *Int J Dev Neurosci* **29**:259–281. doi:10.1016/j.ijdevneu.2010.09.007

Dyce O, McDonald-McGinn D, Kirschner RE, Zackai E, Young K, Jacobs IN. 2002. Otolaryngologic manifestations of the 22q11.2 deletion syndrome. *Arch Otolaryngol Neck Surg* **128**:1408–1412. doi:10.1001/archotol.128.12.1408

Earls LR, Zakharenko SS. 2014. A Synaptic Function Approach to Investigating Complex Psychiatric Diseases. *Neuroscientist* **20**:257–271. doi:10.1177/1073858413498307

Egan MF, Goldberg TE, Kolachana BS, Callicott JH, Mazzanti CM, Straub RE, Goldman D, Weinberger DR. 2001. Effect of COMT Val108/158 Met genotype on frontal lobe function and risk for schizophrenia. *Proc Natl Acad Sci U S A* **98**:6917–22. doi:10.1073/pnas.111134598

Eggermont JJ. 2017. Acquired hearing loss and brain plasticity. *Hear Res* **343**:176–190. doi:10.1016/j.heares.2016.05.008

Fénelon K, Mukai J, Xu B, Hsu P-KK, Drew LJ, Karayiorgou M, Fischbach GD, Macdermott AB, Gogos JA, Fenelon K, Mukai J, Xu B, Hsu P-KK, Drew LJ, Karayiorgou M, Fischbach GD, Macdermott AB, Gogos JA. 2011. Deficiency of Dgcr8, a gene disrupted by the 22q11.2 microdeletion, results in altered short-term plasticity in the prefrontal cortex. *Proc Natl Acad Sci U S A* **108**:4447–4452. doi:10.1073/pnas.1101219108

Fenelon K, Xu B, Lai CS, Mukai J, Markx S, Stark KL, Hsu P-K, Gan W-B, Fischbach GD, MacDermott AB, Karayiorgou M, Gogos JA. 2013. The Pattern of Cortical Dysfunction in a Mouse Model of a Schizophrenia-Related Microdeletion. *J Neurosci* **33**:14825–14839. doi:10.1523/JNEUROSCI.1611-13.2013

Ferguson MO, Cook RD, Iii JWH, Grose JH, Iii HCP. 1998. Chronic Conductive Hearing Loss in Adults. *Head Neck* **124**:678–685.

Fernandez A, Meechan D, Baker JL, Karpinski BA, LaMantia A-S, Maynard TM. 2015. Principles of Developmental Genetics, Principles of Developmental Genetics. Elsevier. doi:10.1016/B978-0-12-405945-0.00036-3

Flore G, Cioffi S, Bilio M, Illingworth E. 2017. Cortical Development Requires Mesodermal Expression of Tbx1, a Gene Haploinsufficient in 22q11.2 Deletion Syndrome. *Cereb Cortex* **27**:2210–2225.

doi:10.1093/cercor/bhw076
Ford LC, Sulprizio SL, Rasgon BM. 2000. Otolaryngological manifestations of velocardiofacial syndrome- a retrospective review of 35 patients. *Laryngoscope* **110**:362–7. doi:10.1097/00005537-200003000-00006
Foxe JJ, Yeap S, Snyder AC, Kelly SP, Thakore JH, Molholm S. 2011. The N1 auditory evoked potential component as an endophenotype for schizophrenia: High-density electrical mapping in clinically unaffected first-degree relatives, first-episode, and chronic schizophrenia patients. *Eur Arch Psychiatry Clin Neurosci* **261**:331–339. doi:10.1007/s00406-010-0176-0
Fuchs JC, Linden JF, Baldini A, Tucker AS. 2015. A defect in early myogenesis causes Otitis media in two mouse models of 22q11.2 Deletion Syndrome. *Hum Mol Genet* **24**:1869–82. doi:10.1093/hmg/ddu604
Fuchs JC, Zinnamon FA, Taylor RR, Ivins S, Scambler PJ, Forge A, Tucker AS, Linden JF. 2013. Hearing loss in a mouse model of 22q11.2 Deletion Syndrome. *PLoS One* **8**:e80104. doi:10.1371/journal.pone.0080104
Funke BH, Lencz T, Finn CT, DeRosse P, Poznik GD, Plocik AM, Kane J, Rogus J, Malhotra AK, Kucherlapati R. 2007. Analysis of TBX1 variation in patients with psychotic and affective disorders. *Mol Med* **13**:407–414. doi:10.2119/2006-00119.Funke
Fyk-Kolodziej BE, Shimano T, Gafoor D, Mirza N, Griffith RD, Gong T-W, Holt AG. 2015. Dopamine in the auditory brainstem and midbrain: co-localization with amino acid neurotransmitters and gene expression following cochlear trauma. *Front Neuroanat* **9**:1–17. doi:10.3389/fnana.2015.00088
Gogos JA, Morgan M, Luine V, Santha M, Ogawa S, Pfaff D, Karayiorgou M. 1998. Catechol-O-methyltransferase-deficient mice exhibit sexually dimorphic changes in catecholamine levels and behavior. *Proc Natl Acad Sci U S A* **95**:9991–6.
Gogos JA, Santha M, Takacs Z, Beck KD, Luine V, Lucas LR, Nadler J V, Karayiorgou M. 1999. The gene encoding proline dehydrogenase modulates sensorimotor gating in mice. *Nat Genet* **21**:434–9. doi:10.1038/7777
Gonzalez-Burgos G, Cho RY, Lewis DA. 2015. Alterations in cortical network oscillations and parvalbumin neurons in schizophrenia. *Biol Psychiatry* **77**:1031–1040. doi:10.1016/j.biopsych.2015.03.010
Gothelf D, Presburger G, Levy D, Nahmani A, Burg M, Berant M, Blieden LC, Finkelstein Y, Frisch A, Apter A, Weizman A. 2004. Genetic, developmental, and physical factors associated with attention deficit hyperactivity disorder in patients with velocardiofacial syndrome. *Am J Med Genet B Neuropsychiatr Genet* **126B**:116–121. doi:10.1002/ajmg.b.20144
Gottesman II, Wolfgram DL. 1991. Schizophrenia genesis : the origins of madness. Freeman.
Green MF, Kern RS, Braff DL, Mintz J. 2000. Neurocognitive Deficits and Functional Outcome in Schizophrenia: Are We Measuring the “Right Stuff”? *Schizophr Bull* **26**:119–136. doi:10.1093/oxfordjournals.schbul.a033430

Guillin O, Abi-Dargham A, Laruelle M, Abi-Dargham A, Laruelle M. 2007. Neurobiology of Dopamine in Schizophrenia. *Int Rev Neurobiol* **78**:1–39. doi:10.1016/s0074-7742(06)78001-1

Guna A, Butcher NJ, Bassett AS. 2015. Comparative mapping of the 22q11.2 deletion region and the potential of simple model organisms. *J Neurodev Disord* **7**:18. doi:10.1186/s11689-015-9113-x

Haenschel C, Bittner RA, Waltz J, Haertling F, Wibral M, Singer W, Linden DEJ, Rodriguez E. 2009. Cortical Oscillatory Activity Is Critical for Working Memory as Revealed by Deficits in Early-Onset Schizophrenia. *J Neurosci* **29**:9481–9489. doi:10.1523/jneurosci.1428-09.2009

Hamburg H, Trossbach S V., Bader V, Chwiesko C, Kipar A, Sauvage M, Crum WR, Vernon AC, Bidmon HJ, Korth C. 2016. Simultaneous effects on parvalbumin-positive interneuron and dopaminergic system development in a transgenic rat model for sporadic schizophrenia. *Sci Rep* **6**:1–14. doi:10.1038/srep34946

Hamm JP, Peterka DS, Gogos JA, Yuste R. 2017. Altered Cortical Ensembles in Mouse Models of Schizophrenia. *Neuron* **94**:153–+. doi:10.1016/j.neuron.2017.03.019

Hangya B, Ranade SP, Lorenc M, Kepecs A. 2015. Central Cholinergic Neurons Are Rapidly Recruited by Reinforcement Feedback. *Cell* **162**:1155–68. doi:10.1016/j.cell.2015.07.057

Hashimoto T, Volk DW, Eggan SM, Mirnics K, Pierri JN, Sun ZX, Sampson AR, Lewis DA. 2003. Gene expression deficits in a subclass of GABA neurons in the prefrontal cortex of subjects with schizophrenia. *J Neurosci* **23**:6315–6326.

Hayashida Y, Mitani Y, Hosomi H, Amemiya M, Mifune K, Tomita S. 1986. Auditory brain stem responses in relation to the clinical symptoms of schizophrenia. *Biol Psychiatry* **21**:177–188. doi:10.1016/0006-3223(86)90145-9

Heffner HE, Heffner RS. 2007. Hearing ranges of laboratory animals. *J Am Assoc Lab Anim Sci* **46**:20–2. doi:http://dx.doi.org/10.1016/j.autrev.2015.04.014

Heike CL, Starr JR, Rieder MJ, Cunningham ML, Edwards KL, Stanaway IB, Crawford DC. 2010. Single nucleotide polymorphism discovery in TBX1 in individuals with and without 22q11.2 deletion syndrome. *Birth Defects Res A Clin Mol Teratol* **88**:54–63. doi:10.1002/bdra.20604

Hequembourg S, Liberman MC. 2001. Spiral ligament pathology: A major aspect of age-related cochlear degeneration in C57BL/6 mice. *JARO - J Assoc Res Otolaryngol* **2**:118–129. doi:10.1007/s101620010075

Hutson KA, Durham D, Imig T, Tucci DL. 2008. Consequences of unilateral hearing loss: cortical adjustment to unilateral deprivation. *Hear Res* **237**:19–31. doi:10.1016/j.heares.2007.12.007

Ishiguro H, Koga M, Horiuchi Y, Noguchi E, Morikawa M, Suzuki Y, Arai M, Niizato K, Iritani S, Itokawa M, Inada T, Iwata N, Ozaki N, Ujike H, Kunugi H, Sasaki T, Takahashi M, Watanabe Y, Someya T, Kakita A, Takahashi H, Nawa H, Arinami T. 2010. Supportive evidence for reduced expression of GNB1L in schizophrenia. *Schizophr Bull* **36**:756–765. doi:10.1093/schbul/sbn160

Ison JR, Allen PD. 2003. Low-Frequency Tone Pips Elicit Exaggerated Startle

Reflexes in C57BL/6J Mice with Hearing Loss. *JARO - J Assoc Res Otolaryngol* **4**:495–504. doi:10.1007/s10162-002-3046-2
Ison JR, Allen PD, O'Neill WE. 2007. Age-related hearing loss in C57BL/6J mice has both frequency-specific and non-frequency-specific components that produce a hyperacusis-like exaggeration of the acoustic startle reflex. *JARO - J Assoc Res Otolaryngol* **8**:539–550. doi:10.1007/s10162-007-0098-3
Jacquet H, Berthelot J, Bonnemains C, Simard G, Saugier-Veber P, Raux G, Campion D, Bonneau D, Frebourg T. 2003. The severe form of type I hyperprolinaemia results from homozygous inactivation of the PRODH gene. *J Med Genet* **40**:e7.
Ji XY, Zingg B, Mesik L, Xiao Z, Zhang LI, Tao HW. 2016. Thalamocortical Innervation Pattern in Mouse Auditory and Visual Cortex: Laminar and Cell-Type Specificity. *Cereb Cortex* **26**:2612–2625. doi:10.1093/cercor/bhv099
Jiramongkolchai P, Kumar MS, Chinnadurai S, Wootten CT, Goudy SL. 2016. Prevalence of hearing loss in children with 22q11.2 deletion syndrome. *Int J Pediatr Otorhinolaryngol* **87**:130–133. doi:10.1016/j.ijporl.2016.06.005
Jonas RK, Montojo CA, Bearden CE. 2014. The 22q11.2 deletion syndrome as a window into complex neuropsychiatric disorders over the lifespan. *Biol Psychiatry* **75**:351–360. doi:10.1016/j.biopsych.2013.07.019
Kallmann F. 1938. The Genetics of Schizophrenia.
Källstrand J, Lewander T, Baghdassarian E, Nielzén S. 2014. A new method for analyzing auditory brain-stem response waveforms using a moving-minimum subtraction procedure of digitized analog recordings. *Neuropsychiatr Dis Treat* **10**:1011–1016. doi:10.2147/NDT.S59178
Kandel ER, Schwartz JH, Jessell TM. 2000. Principles of Neural Science, Neurology. doi:10.1036/0838577016
Karayiorgou M, Simon TJ, Gogos JA. 2010. 22q11.2 microdeletions: linking DNA structural variation to brain dysfunction and schizophrenia. *Nat Rev Neurosci* **11**:402–416. doi:10.1038/nrn2841
Kato HK, Asinof SK, Isaacson JS. 2017. Network-Level Control of Frequency Tuning in Auditory Cortex. *Neuron* **95**:412–423.e4. doi:10.1016/j.neuron.2017.06.019
Keating P, Dahmen JC, King AJ. 2015. Complementary adaptive processes contribute to the developmental plasticity of spatial hearing. *Nat Neurosci* **18**:185–187. doi:10.1038/nn.3914
Keating P, King AJ. 2013. Developmental plasticity of spatial hearing following asymmetric hearing loss: context-dependent cue integration and its clinical implications. *Front Syst Neurosci* **7**:123. doi:10.3389/fnsys.2013.00123
Kempf L, Nicodemus KK, Kolachana B, Vakkalanka R, Verchinski BA, Egan MF, Straub RE, Mattay VA, Callicott JH, Weinberger DR, Meyer-Lindenberg A. 2008. Functional polymorphisms in PRODH are associated with risk and protection for schizophrenia and fronto-striatal structure and function. *PLoS Genet* **4**:e1000252. doi:10.1371/journal.pgen.1000252
Kim EJ, Jacobs MW, Ito-Cole T, Callaway EM. 2016. Improved Monosynaptic

Neural Circuit Tracing Using Engineered Rabies Virus Glycoproteins. *Cell Rep* **15**:692–699. doi:10.1016/j.celrep.2016.03.067
Korczak P, Smart J, Delgado R, M. Strobel T, Bradford C. 2012. Auditory Steady-State Responses. *J Am Acad Audiol* **23**:146–170. doi:10.3766/jaaa.23.3.3
Kotak VC, Fujisawa S, Lee FA, Karthikeyan O, Aoki C, Sanes DH. 2005. Hearing loss raises excitability in the auditory cortex. *J Neurosci* **25**:3908–18. doi:10.1523/JNEUROSCI.5169-04.2005
Kuchibhotla K V, Gill J V, Lindsay GW, Papadoyannis ES, Field RE, Sten TAH, Miller KD, Froemke RC. 2017. Parallel processing by cortical inhibition enables context-dependent behavior. *Nat Neurosci* **20**:62–71. doi:10.1038/nn.4436
Larsen KM, Pellegrino G, Birknow MR, Kjær TN, Baaré WFC, Didriksen M, Olsen L, Werge T, Mørup M, Siebner HR. 2018. 22q11.2 Deletion Syndrome Is Associated With Impaired Auditory Steady-State Gamma Response. *Schizophr Bull* **44**:388–397. doi:10.1093/schbul/sbx058
Lesh T a, Niendam TA, Minzenberg MJ, Carter CS. 2011. Cognitive control deficits in schizophrenia: mechanisms and meaning. *Neuropsychopharmacology* **36**:316–338. doi:10.1038/npp.2010.156
Lewandowski KE, Shashi V, Berry PM, Kwapil TR. 2007. Schizophrenic-like neurocognitive deficits in children and adolescents with 22q11 deletion syndrome. *Am J Med Genet B Neuropsychiatr Genet* **144B**:27–36. doi:10.1002/ajmg.b.30379
Lewis DA. 2014. Inhibitory neurons in human cortical circuits: substrate for cognitive dysfunction in schizophrenia. *Curr Opin Neurobiol* **26**:22–26. doi:10.1016/j.conb.2013.11.003
Lewis DA, Curley AA, Glausier JR, Volk DW. 2012. Cortical parvalbumin interneurons and cognitive dysfunction in schizophrenia. *Trends Neurosci* **35**:57–67. doi:10.1016/j.tins.2011.10.004
Lewis DA, Hashimoto T, Volk DW. 2005. Cortical inhibitory neurons and schizophrenia. *Nat Rev Neurosci* **6**:312–324. doi:10.1038/nrn1648
Li T, Ma X, Hu X, Wang Y, Yan C, Meng H, Liu X, Toulopoulou T, Murray RM, Collier DA. 2008. PRODH gene is associated with executive function in schizophrenic families. *Am J Med Genet B Neuropsychiatr Genet* **147B**:654–657. doi:10.1002/ajmg.b.30648
Liao J, Kochilas L, Nowotschin S, Arnold JS, Aggarwal VS, Epstein JA, Brown MC, Adams J, Morrow BE. 2004. Full spectrum of malformations in velo-cardio-facial syndrome/DiGeorge syndrome mouse models by altering Tbx1 dosage. *Hum Mol Genet* **13**:1577–85. doi:10.1093/hmg/ddh176
Libé-Philippot B, Michel V, Boutet de Monvel J, Le Gal S, Dupont T, Avan P, Métin C, Michalski N, Petit C. 2017. Auditory cortex interneuron development requires cadherins operating hair-cell mechanoelectrical transduction. *Proc Natl Acad Sci* **114**:201703408. doi:10.1073/pnas.1703408114
Lin S-C, Brown RE, Hussain Shuler MG, Petersen CCH, Kepecs A. 2015. Optogenetic Dissection of the Basal Forebrain Neuromodulatory Control of Cortical Activation, Plasticity, and Cognition. *J Neurosci* **35**:13896–13903. doi:10.1523/JNEUROSCI.2590-15.2015
Lindsay EA, Botta A, Jurecic V, Carattini-Rivera S, Cheah YC, Rosenblatt

HM, Bradley A, Baldini A. 1999. Congenital heart disease in mice deficient for the DiGeorge syndrome region. *Nature* **401**:379–383. doi:10.1038/43903

Linszen MMJJ, Brouwer RM, Heringa SM, Sommer IE. 2016. Increased risk of psychosis in patients with hearing impairment: Review and meta-analyses. *Neurosci Biobehav Rev* **62**:1–20. doi:10.1016/j.neubiorev.2015.12.012

Lodge DJ, Behrens MM, Grace AA. 2009. A loss of parvalbumin-containing interneurons is associated with diminished oscillatory activity in an animal model of schizophrenia. *J Neurosci* **29**:2344–2354. doi:10.1523/JNEUROSCI.5419-08.2009

Long JM, LaPorte P, Merscher S, Funke B, Saint-Jore B, Puech A, Kucherlapati R, Morrow BE, Skoultchi AI, Wynshaw-Boris A. 2006. Behavior of mice with mutations in the conserved region deleted in velocardiofacial/DiGeorge syndrome. *Neurogenetics* **7**:247–57. doi:10.1007/s10048-006-0054-0

Luck SJ (Steven J. 2014. An introduction to the event-related potential technique.

Ma G, Shi Y, Tang W, He Z, Huang K, Li Z, He G, Feng G, Li H, He L. 2007. An association study between the genetic polymorphisms within TBX1 and schizophrenia in the Chinese population. *Neurosci Lett* **425**:146–150. doi:10.1016/j.neulet.2007.07.055

Manolio TA, Collins file:///Volumes/Tara Z to add/Manolio et al 2009 F the missing heritability of complex diseases. pd. FS, Cox NJ, Goldstein DB, Hindorff LA, Hunter DJ, McCarthy MI, Ramos EM, Cardon LR, Chakravarti A, Cho JH, Guttmacher AE, Kong A, Kruglyak L, Mardis E, Rotimi CN, Slatkin M, Valle D, Whittemore AS, Boehnke M, Clark AG, Eichler EE, Gibson G, Haines JL, Mackay TFC, McCarroll SA, Visscher PM. 2009. Finding the missing heritability of complex diseases. *Nature* **461**:747–753. doi:10.1038/nature08494

Marín O. 2012. Interneuron dysfunction in psychiatric disorders. *Nat Rev Neurosci* **13**:107–120. doi:10.1038/nrn3155

Marissal T, Salazar RF, Bertollini C, Mutel S, De Roo M, Rodriguez I, Muller D, Carleton A. 2018. Restoring wild-type-like CA1 network dynamics and behavior during adulthood in a mouse model of schizophrenia. *Nat Neurosci* **21**:1412–1420. doi:10.1038/s41593-018-0225-y

Martin del Campo HN, Measor KR, Razak KA. 2012. Parvalbumin immunoreactivity in the auditory cortex of a mouse model of presbycusis. *Hear Res* **294**:31–9. doi:10.1016/j.heares.2012.08.017

Mason P, Rimmer M, Richman A, Garg G, Johnson J, Mottram PG. 2008. Middle-ear disease and schizophrenia: case-control study. *Br J Psychiatry* **193**:192–196. doi:10.1192/bjp.bp.108.052795

Maxwell CR, Liang Y, Weightman BD, Kanes SJ, Abel T, Gur RE, Turetsky BI, Bilker WB, Lenox RH, Siegel SJ. 2004. Effects of Chronic Olanzapine and Haloperidol Differ on the Mouse N1 Auditory Evoked Potential. *Neuropsychopharmacology* **29**:739–746. doi:10.1038/sj.npp.1300376

McCabe KL, Atkinson RJ, Cooper G, Melville JL, Harris J, Schall U, Loughland CM, Thienel R, Campbell LE. 2014. Pre-pulse inhibition and antisaccade performance indicate impaired attention modulation of

cognitive inhibition in 22q11.2 deletion syndrome 22q11DS. *J Neurodev Disord* **6**:38. doi:10.1186/1866-1955-6-38
McDonald-McGinn DM, Emanuel BS, Zackai EH. 2013. 22q11.2 Deletion Syndrome.
McDonald-McGinn DM, Sullivan KE, Marino B, Philip N, Swillen A, Vorstman JAS, Zackai EH, Emanuel BS, Vermeesch JR, Morrow BE, Scambler PJ, Bassett AS. 2015. 22q11.2 Deletion Syndrome. *Nat Rev Dis Prim* **1**. doi:10.1038/nrdp.2015.71
McEvoy JP. 2007. The Costs of Schizophrenia. *J Clin Psychiatry* **68**:1,478-7.
Meechan DW, Rutz HLH, Fralish MS, Maynard TM, Rothblat LA, LaMantia A-SS. 2015. Cognitive ability is associated with altered medial frontal cortical circuits in the LgDel mouse model of 22q11.2DS. *Cereb Cortex* **25**:1143–51. doi:10.1093/cercor/bht308
Meechan DW, Tucker ES, Maynard TM, LaMantia A-S. 2012. Cxcr4 regulation of interneuron migration is disrupted in 22q11.2 deletion syndrome. *Proc Natl Acad Sci* **109**:18601–18606. doi:10.1073/pnas.1211507109
Meechan DW, Tucker ES, Maynard TM, LaMantia A-SS. 2009. Diminished dosage of 22q11 genes disrupts neurogenesis and cortical development in a mouse model of 22q11 deletion DiGeorge syndrome. *Proc Natl Acad Sci U S A* **106**:16434–16439. doi:10.1073/pnas.0905696106
Miyamichi K, Shlomai-Fuchs Y, Shu M, Weissbourd BC, Luo L, Mizrahi A. 2013. Dissecting Local Circuits: Parvalbumin Interneurons Underlie Broad Feedback Control of Olfactory Bulb Output. *Neuron* **80**:1232–1245. doi:10.1016/j.neuron.2013.08.027
Moghaddam B, Javitt D. 2012. From revolution to evolution: the glutamate hypothesis of schizophrenia and its implication for treatment. *Neuropsychopharmacology* **37**:4–15. doi:10.1038/npp.2011.181
Moore AK, Wehr M. 2013. Parvalbumin-Expressing Inhibitory Interneurons in Auditory Cortex Are Well-Tuned for Frequency. *J Neurosci* **33**:13713–13723. doi:10.1523/JNEUROSCI.0663-13.2013
Moore AK, Weible AP, Balmer TS, Trussell LO, Wehr M. 2018. Rapid Rebalancing of Excitation and Inhibition by Cortical Circuitry. *Neuron* **97**:1341–+. doi:10.1016/j.neuron.2018.01.045
Moreau MP, Bruse SE, David-Rus R, Buyske S, Brzustowicz LM. 2011. Altered microRNA expression profiles in postmortem brain samples from individuals with schizophrenia and bipolar disorder. *Biol Psychiatry* **69**:188–193. doi:10.1016/j.biopsych.2010.09.039
Mowery TM, Kotak VC, Sanes DH. 2015. Transient Hearing Loss Within a Critical Period Causes Persistent Changes to Cellular Properties in Adult Auditory Cortex. *Cereb Cortex* **25**:2083–2094. doi:10.1093/cercor/bhu013
Nakazawa K, Zsiros V, Jiang Z, Nakao K, Kolata S, Zhang S, Belforte JE. 2012. GABAergic interneuron origin of schizophrenia pathophysiology. *Neuropharmacology* **62**:1574–1583. doi:10.1016/j.neuropharm.2011.01.022
Nelson A, Mooney R. 2016. The Basal Forebrain and Motor Cortex Provide Convergent yet Distinct Movement-Related Inputs to the Auditory Cortex. *Neuron* **90**:635–648. doi:10.1016/j.neuron.2016.03.031
Nelson A, Schneider DM, Takatoh J, Sakurai K, Wang F, Mooney R. 2013. A

circuit for motor cortical modulation of auditory cortical activity. *J Neurosci* **33**:14342–14353. doi:10.1523/JNEUROSCI.2275-13.2013
Nguyen PTH, Nakamura T, Hori E, Urakawa S, Uwano T, Zhao J, Li R, Bac ND, Hamashima T, Ishii Y, Matsushima T, Ono T, Sasahara M, Nishijo H. 2011. Cognitive and socio-emotional deficits in platelet-derived growth factor receptor-β gene knockout mice. *PLoS One* **6**:e18004. doi:10.1371/journal.pone.0018004
Nielzén S, Olsson O, Källstrand J, Nehlstedt S. 2008. Aberrant brain stem function in schizophrenia. *Eur Psychiatry* **23**:S135. doi:10.1016/J.EURPSY.2008.01.851
Oskarsdottir S, Persson C, Eriksson BO, Fasth A, Oskarsdóttir S, Persson C, Eriksson BO, Fasth A. 2005. Presenting phenotype in 100 children with the 22q11 deletion syndrome. *Eur J Pediatr* **164**:146–153. doi:10.1007/s00431-004-1577-8
Pachitariu M, Packer AM, Pettit N, Dalgleish H, Hausser M, Sahani M. 2013. Extracting regions of interest from biological images with convolutional sparse block coding. *Adv Neural Inf Process Syst* **1**:1745–1753.
Papaleo F, Crawley JN, Song J, Lipska BK, Pickel J, Weinberger DR, Chen J. 2008. Genetic dissection of the role of catechol-O-methyltransferase in cognition and stress reactivity in mice. *J Neurosci* **28**:8709–8723. doi:10.1523/JNEUROSCI.2077-08.2008
Papangeli I, Scambler P. 2013. The 22q11 deletion: DiGeorge and velocardiofacial syndromes and the role of TBX1. *Wiley Interdiscip Rev Dev Biol* **2**:393–403. doi:10.1002/wdev.75
Parham K. 1997. Distortion product otoacoustic emissions in the C57BL/6J mouse model of age-related hearing loss. *Hear Res* **112**:216–234. doi:10.1016/s0378-5955(97)00124-x
Paterlini M, Zakharenko SS, Lai W-S, Qin J, Zhang H, Mukai J, Westphal KGC, Olivier B, Sulzer D, Pavlidis P, Siegelbaum SA, Karayiorgou M, Gogos JA. 2005. Transcriptional and behavioral interaction between 22q11.2 orthologs modulates schizophrenia-related phenotypes in mice. *Nat Neurosci* **8**:1586–94. doi:10.1038/nn1562
Paylor R, Glaser B, Mupo A, Ataliotis P, Spencer C, Sobotka A, Sparks C, Choi C-HH, Oghalai J, Curran S, Murphy KC, Monks S, Williams N, O'Donovan MC, Owen MJ, Scambler PJ, Lindsay E. 2006. Tbx1 haploinsufficiency is linked to behavioral disorders in mice and humans-implications for 22q11 deletion syndrome. *Proc Natl Acad Sci U S A* **103**:7729–34. doi:10.1073/pnas.0600206103
Paylor R, Lindsay E. 2006. Mouse Models of 22q11 Deletion Syndrome. *Biol Psychiatry* **59**:1172–1179. doi:10.1016/j.biopsych.2006.01.018
Paylor R, McIlwain KL, McAninch R, Nellis A, Yuva-Paylor LA, Baldini A, Lindsay EA. 2001. Mice deleted for the DiGeorge/velocardiofacial syndrome region show abnormal sensorimotor gating and learning and memory impairments. *Hum Mol Genet* **10**:2645–2650. doi:10.1093/hmg/10.23.2645
Picton TW, Hillyard SA, Krausz HI, Galambos R. 1974. Human auditory evoked potentials. I: Evaluation of components. *Electroencephalogr Clin Neurophysiol* **36**:179–190. doi:10.1016/0013-4694(74)90155-2
Piskorowski RA, Nasrallah K, Diamantopoulou A, Mukai J, Hassan SI,

Siegelbaum SA, Gogos JA, Chevaleyre V. 2016. Age-Dependent Specific Changes in Area CA2 of the Hippocampus and Social Memory Deficit in a Mouse Model of the 22q11.2 Deletion Syndrome. *Neuron* **89**:163–176. doi:10.1016/j.neuron.2015.11.036

Polley DB, Thompson JH, Guo W. 2013. Brief hearing loss disrupts binaural integration during two early critical periods of auditory cortex development. *Nat Commun* **4**:2547. doi:10.1038/ncomms3547

Popescu M V., Polley DB. 2010. Monaural Deprivation Disrupts Development of Binaural Selectivity in Auditory Midbrain and Cortex. *Neuron* **65**:718–731. doi:10.1016/j.neuron.2010.02.019

Prasad SE, Howley S, Murphy KC. 2008. Candidate genes and the behavioral phenotype in 22q11.2 deletion syndrome. *Dev Disabil Res Rev* **14**:26–34. doi:10.1002/ddrr.5

Purves D, Augustine GJ, Fitzpatrick D, Katz LC, LaMantia A-S, McNamara JO, Williams SM. 2008. Neuroscience.

Qin ZB, Wood M, Rosowski JJ. 2010. Measurement of conductive hearing loss in mice. *Hear Res* **263**:93–103. doi:10.1016/j.heares.2009.10.002

Resnik J, Polley DB. 2017. Fast-spiking GABA circuit dynamics in the auditory cortex predict recovery of sensory processing following peripheral nerve damage. *Elife* **6**. doi:10.7554/eLife.21452

Reyes MRT, LeBlanc EM, Bassila MK. 1999. Hearing loss and otitis media in velo-cardio-facial syndrome. *Int J Pediatr Otorhinolaryngol* **47**:227–233. doi:10.1016/s0165-5876(98)00180-3

Rihs TA, Tomescu MI, Britz J, Rochas V, Custo A, Schneider M, Debbané M, Eliez S, Michel CM. 2013. Altered auditory processing in frontal and left temporal cortex in 22q11.2 deletion syndrome: A group at high genetic risk for schizophrenia. *Psychiatry Res - Neuroimaging* **212**:141–149. doi:10.1016/j.pscychresns.2012.09.002

Rosburg T, Boutros NN, Ford JM. 2008. Reduced auditory evoked potential component N100 in schizophrenia - A critical review. *Psychiatry Res* **161**:259–274. doi:10.1016/j.psychres.2008.03.017

Rossignol E. 2011. Genetics and function of neocortical GABAergic interneurons in neurodevelopmental disorders. *Neural Plast* **2011**:649325. doi:10.1155/2011/649325

Rudy B, Fishell G, Lee S, Hjerling-Leffler J. 2011. Three groups of interneurons account for nearly 100% of neocortical GABAergic neurons. *Dev Neurobiol* **71**:45–61. doi:10.1002/dneu.20853

Saha S, Chant D, McGrath J. 2007. A Systematic Review of Mortality in Schizophrenia Is the Differential Mortality Gap Worsening Over Time? *Arch Gen Psychiatry* **64**:1123–31. doi:10.1001/archpsyc.64.10.1123

Sanes DH, Kotak VC. 2011. Developmental plasticity of auditory cortical inhibitory synapses. *Hear Res* **279**:140–148. doi:10.1016/j.heares.2011.03.015

Scambler PJ. 2000. The 22q11 deletion syndromes. *Hum Mol Genet* **9**:2421–2426. doi:10.1093/hmg/9.16.2421

Schneider DM, Nelson A, Mooney R. 2014. A synaptic and circuit basis for corollary discharge in the auditory cortex. *Nature* **513**:189–94. doi:10.1038/nature13724

Scott KE, Schormans AL, Pacoli KY, De Oliveira C, Allman BL, Schmid S.

2018. Altered Auditory Processing, Filtering, and Reactivity in the Cntnap2 Knock-Out Rat Model for Neurodevelopmental Disorders. *J Neurosci* **38**:8588–8604. doi:10.1523/JNEUROSCI.0759-18.2018
Selemon LD. 2013. A role for synaptic plasticity in the adolescent development of executive function. *Transl Psychiatry* **3**:e238. doi:10.1038/tp.2013.7
Shad MU, Tamminga CA, Cullum M, Haas GL, Keshavan MS. 2006. Insight and frontal cortical function in schizophrenia: A review. *Schizophr Res* **86**:54–70. doi:10.1016/j.schres.2006.06.006
Shu Y, Hasenstaub A, McCormick DA. 2003. Turning on and off recurrent balanced cortical activity. *Nature* **423**:288–93. doi:10.1038/nature01616
Sigurdsson T, Stark KL, Karayiorgou M, Gogos JA, Gordon JA. 2010. Impaired hippocampal-prefrontal synchrony in a genetic mouse model of schizophrenia. *Nature* **464**:763–767. doi:10.1038/nature08855
Sinclair JL, Fischl MJ, Alexandrova O, Hess M, Grothe B, Leibold C, Kopp-Scheinpflug C, Heß M, Grothe B, Leibold C, Kopp-Scheinpflug C. 2017. Sound-Evoked Activity Influences Myelination of Brainstem Axons in the Trapezoid Body. *J Neurosci* **37**:8239–8255. doi:10.1523/jneurosci.3728-16.2017
Sivagnanasundaram S, Fletcher D, Hubank M, Illingworth E, Skuse D, Scambler P. 2007. Differential gene expression in the hippocampus of the Df1/+ mice: a model for 22q11.2 deletion syndrome and schizophrenia. *Brain Res* **1139**:48–59. doi:10.1016/j.brainres.2007.01.014
Slifstein M, Kolachana B, Simpson EH, Tabares P, Cheng B, Duvall M, Frankle WG, Weinberger DR, Laruelle M, Abi-Dargham A. 2008. COMT genotype predicts cortical-limbic D1 receptor availability measured with [11C]NNC112 and PET. *Mol Psychiatry* **13**:821–827. doi:10.1038/mp.2008.19
Sobin C, Kiley-Brabeck K, Karayiorgou M. 2004. Associations between prepulse inhibition and executive visual attention in children with the 22q11 deletion syndrome. *Mol Psychiatry* **10**:553–562. doi:10.1038/sj.mp.4001609
Sohal VS, Zhang F, Yizhar O, Deisseroth K. 2009. Parvalbumin neurons and gamma rhythms enhance cortical circuit performance. *Nature* **459**:698–702. doi:10.1038/nature07991
Sommer IE, Roze CM, Linszen MMJ, Somers M, van Zanten G a. 2014. Hearing loss; the neglected risk factor for psychosis. *Schizophr Res* **158**:266–267. doi:10.1016/j.schres.2014.07.020
Stark KL, Xu B, Bagchi A, Lai W-SS, Liu H, Hsu R, Wan X, Pavlidis P, Mills AA, Karayiorgou M, Gogos JA. 2008. Altered brain microRNA biogenesis contributes to phenotypic deficits in a 22q11-deletion mouse model. *Nat Genet* **40**:751–760. doi:10.1038/ng.138
Steel KP, Moorjani P, Bock GR. 1987. MIXED CONDUCTIVE AND SENSORINEURAL HEARING-LOSS IN LP/J MICE. *Hear Res* **28**:227–236. doi:10.1016/0378-5955(87)90051-7
Stefansson H, Rujescu D, Cichon S, Pietiläinen OPH, Ingason A, Steinberg S, Fossdal R, Sigurdsson E, Sigmundsson T, Buizer-Voskamp JE, Hansen T, Jakobsen KD, Muglia P, Francks C, Matthews PM, Gylfason A,

Halldorsson B V., Gudbjartsson D, Thorgeirsson TE, Sigurdsson A, Jonasdottir A, Jonasdottir A, Bjornsson A, Mattiasdottir S, Blondal T, Haraldsson M, Magnusdottir BB, Giegling I, Möller HJ, Hartmann A, Shianna K V., Ge D, Need AC, Crombie C, Fraser G, Walker N, Lonnqvist J, Suvisaari J, Tuulio-Henriksson A, Paunio T, Toulopoulou T, Bramon E, Di Forti M, Murray R, Ruggeri M, Vassos E, Tosato S, Walshe M, Li T, Vasilescu C, Mühleisen TW, Wang AG, Ullum H, Djurovic S, Melle I, Olesen J, Kiemeney LA, Franke B, Sabatti C, Freimer NB, Gulcher JR, Thorsteinsdottir U, Kong A, Andreassen OA, Ophoff RA, Georgi A, Rietschel M, Werge T, Petursson H, Goldstein DB, Nöthen MM, Peltonen L, Collier DA, St Clair D, Stefansson K, Kahn RS, Linszen DH, Van Os J, Wiersma D, Bruggeman R, Cahn W, De Haan L, Krabbendam L, Myin-Germeys I. 2008. Large recurrent microdeletions associated with schizophrenia. *Nature* **455**:232–236. doi:10.1038/nature07229

Stone JL, O'Donovan MC, Gurling H, Kirov GK, Blackwood DHR, Corvin A, Craddock NJ, Gill M, Hultman CM, Lichtenstein P, McQuillin A, Pato CN, Ruderfer DM, Owen MJ, St Clair D, Sullivan PF, Sklar P, Purcell SM, Korn J, Macgregor S, Morris DW, O'Dushlaine CT, Daly MJ, Visscher PM, Holmans PA, Scolnick EM, Williams NM, Georgieva L, Nikolov I, Norton N, Williams H, Toncheva D, Milanova V, Thelander EF, Sullivan P, Kenny E, Waddington JL, Choudhury K, Datta S, Pimm J, Thirumalai S, Puri V, Krasucki R, Lawrence J, Quested D, Bass N, Curtis D, Crombie C, Fraser G, Leh Kwan S, Walker N, Muir WJ, McGhee KA, Pickard B, Malloy P, Maclean AW, Van Beck M, Pato MT, Medeiros H, Middleton F, Carvalho C, Morley C, Fanous A, Conti D, Knowles JA, Paz Ferreira C, Macedo A, Helena Azevedo M, McCarroll SA, Daly M, Chambert K, Gates C, Gabriel SB, Mahon S, Ardlie K. 2008. Rare chromosomal deletions and duplications increase risk of schizophrenia. *Nature* **455**:237–241. doi:10.1038/nature07239

Sumitomo A, Horike K, Hirai K, Butcher N, Boot E, Sakurai T, Jr FCN, Bassett AS, Sawa A, Tomoda T. 2018. A mouse model of 22q11.2 deletions: Molecular and behavioral signatures of Parkinson's disease and schizophrenia 1–10. doi:10.1126/sciadv.aar6637

Swerdlow NR, Geyer MA. 1998. Using an animal model of deficient sensorimotor gating to study the pathophysiology and new treatments of schizophrenia. *Schizophr Bull* **24**:285–301.

Swerdlow NR, Geyer MA, Braff DL. 2001. Neural circuit regulation of prepulse inhibition of startle in the rat: current knowledge and future challenges. *Psychopharmacology (Berl)* **156**:194–215. doi:10.1007/s002130100799

Swerdlow NR, Stephany N, Wasserman LC, Talledo J, Shoemaker J, Auerbach PP. 2003. Amphetamine effects on prepulse inhibition across-species: replication and parametric extension. *Neuropsychopharmacology* **28**:640–650. doi:10.1038/sj.npp.1300086

Swerdlow NR, Weber M, Qu Y, Light GA, Braff DL. 2008. Realistic expectations of prepulse inhibition in translational models for schizophrenia research. *Psychopharmacol* **199**:331–388. doi:10.1007/s00213-008-1072-4

Takesian AE, Kotak VC, Sanes DH. 2012. Age-dependent effect of hearing

loss on cortical inhibitory synapse function. *J Neurophysiol* **107**:937–47. doi:10.1152/jn.00515.2011
Takesian AE, Kotak VC, Sanes DH. 2009. Developmental hearing loss disrupts synaptic inhibition: implications for auditory processing. *Futur Neurol* **4**:331–349. doi:10.2217/FNL.09.5
Teichert M, Liebmann L, Hubner CA, Bolz J. 2017. Homeostatic plasticity and synaptic scaling in the adult mouse auditory cortex. *Sci Rep* **7**:14. doi:10.1038/s41598-017-17711-5
Thornton JL, Anbuhl KL, Tollin DJ. 2014. Unilateral conductive hearing loss causes impaired auditory information processing in neurons in the central auditory system. *Proc ISAAR 2013 Audit Plast – List with Brain 4th Symp Audit Audiol Res*.
Tomescu MI, Rihs TA, Becker R, Britz J, Custo A, Grouiller F, Schneider M, Debbane M, Eliez S, Michel CM, Debbané M, Eliez S, Michel CM. 2014. Deviant dynamics of EEG resting state pattern in 22q11.2 deletion syndrome adolescents: A vulnerability marker of schizophrenia? *Schizophr Res* **157**:175–181. doi:10.1016/j.schres.2014.05.036
Tomlin D, Rance G, Graydon K, Tsialios I. 2006. A comparison of 40 Hz auditory steady-state response (ASSR) and cortical auditory evoked potential (CAEP) thresholds in awake adult subjects. *Int J Audiol* **45**:580–588. doi:10.1080/14992020600895170
Tong L, Altschuler RA, Holt AG. 2005. Tyrosine hydroxylase in rat auditory midbrain: Distribution and changes following deafness. *Hear Res* **206**:28–41. doi:10.1016/j.heares.2005.03.006
Torres F, Barbosa M, Maciel P. 2016. Recurrent copy number variations as risk factors for neurodevelopmental disorders: critical overview and analysis of clinical implications. *J Med Genet* **53**:73–90. doi:10.1136/jmedgenet-2015-103366
Turetsky BI, Calkins ME, Light GA, Olincy A, Radant AD, Swerdlow NR. 2007. Neurophysiological endophenotypes of schizophrenia: The viability of selected candidate measures. *Schizophr Bull* **33**:69–94. doi:10.1093/schbul/sbl060
Tyrer HE, Crompton M, Bhutta MF. 2013. What have we learned from murine models of otitis media? *Curr Allergy Asthma Rep* **13**:501–511. doi:10.1007/s11882-013-0360-1
Uhlhaas PJ, Singer W. 2010. Abnormal neural oscillations and synchrony in schizophrenia. *Nat Rev Neurosci* **11**:100–113. doi:10.1038/nrn2774
Umlauf MG. 2008. 22q11 deletion syndrome is that what they used to call. *Perspect Psychiatr Care* **44**:259–66. doi:10.1111/j.1744-6163.2008.00185.x
Usiskin SI, Nicolson R, Krasnewich DM, Yan W, Lenane M, Wudarsky M, Hamburger SD, Rapoport JL. 1999. Velocardiofacial syndrome in childhood-onset schizophrenia. *J Am Acad Child Adolesc Psychiatry* **38**:1536–1543. doi:10.1097/00004583-199912000-00015
Vasquez-Lopez SA, Weissenberger Y, Lohse M, Keating P, King AJ, Dahmen JC. 2017. Thalamic input to auditory cortex is locally heterogeneous but globally tonotopic. *Elife* **6**. doi:10.7554/eLife.25141
Verheij E, Derks LSM, Stegeman I, Thomeer H. 2017. Prevalence of hearing loss and clinical otologic manifestations in patients with 22q11.2 deletion

syndrome: A literature review. *Clin Otolaryngol* **42**:1319–1328. doi:10.1111/coa.12874
Vila PM, Lieu JEC. 2015. Asymmetric and unilateral hearing loss in children. *Cell Tissue Res* **361**:271–8. doi:10.1007/s00441-015-2208-6
Weinberger DR, Harrison PJ, editors. 2010. Schizophrenia. Oxford, UK: Wiley-Blackwell. doi:10.1002/9781444327298
Whitton JP, Polley DB. 2011. Evaluating the perceptual and pathophysiological consequences of auditory deprivation in early postnatal life: A comparison of basic and clinical studies. *JARO - J Assoc Res Otolaryngol* **12**:535–546. doi:10.1007/s10162-011-0271-6
Wickersham IR, Lyon DC, Barnard RJO, Mori T, Finke S, Conzelmann KK, Young JAT, Callaway EM. 2007. Monosynaptic Restriction of Transsynaptic Tracing from Single, Genetically Targeted Neurons. *Neuron* **53**:639–647. doi:10.1016/j.neuron.2007.01.033
Williams NM, Glaser B, Norton N, Williams H, Pierce T, Moskvina V, Monks S, Del Favero J, Goossens D, Rujescu D, Giegling I, Kirov G, Craddock N, Murphy KC, O'Donovan MC, Owen MJ. 2008. Strong evidence that GNB1L is associated with schizophrenia. *Hum Mol Genet* **17**:555–566. doi:10.1093/hmg/ddm330
Willott JF. 2006. Measurement of the Auditory Brainstem Response (ABR) to Study Auditory Sensitivity in Mice. *Curr Protoc Neurosci* **Chapter 8,**:1–12. doi:10.1002/0471142301.ns0821bs34
Willott JF. 2001. Handbook of Mouse Auditory Research: From Behavior to Molecular Biology. CRC Press.
Willott JF, Kulig J, Satterfield T. 1984. The acoustic startle response in DBA/2 and C57BL/6 mice: relationship to auditory neuronal response properties and hearing impairment. *Hear Res* **16**:161–167. doi:10.1016/0378-5955(84)90005-4
Willyard C. 2018. Send in the germs. *Nature* **556**:16–18.
Wolpaw JR, Penry JK. 1977. Hemispheric differences in the auditory evoked response. *Electroencephalogr Clin Neurophysiol* **43**:99–102.
Wu EQ, Birnbaum HG, Shi L, Ball DE, Kessler RC, Moulis M, Aggarwal J. 2005. The Economic Burden of Schizophrenia in the United States in 2002. *J Clin Psychiatry* **66**:1,478-1129.
Xu H, Kotak VC, Sanes DH. 2007. Conductive Hearing Loss Disrupts Synaptic and Spike Adaptation in Developing Auditory Cortex. *J Neurosci* **27**:9417–9426. doi:10.1523/jneurosci.1992-07.2007
Yao JD, Sanes DH. 2018. Developmental deprivation-induced perceptual and cortical processing deficits in awake-behaving animals. *Elife* **7**:30. doi:10.7554/eLife.33891
Yost WA. 2007. Fundamentals of Hearing: An Introduction. Academic Press.
Zebardast N, Crowley MJ, Bloch MH, Mayes LC, Wyk B Vander, Leckman JF, Pelphrey KA, Swain JE. 2013. Brain mechanisms for prepulse inhibition in adults with Tourette syndrome: initial findings. *Psychiatry Res* **214**:33–41. doi:10.1016/j.pscychresns.2013.05.009
Zheng QY, Johnson KR, Erway LC. 1999. Assessment of hearing in 80 inbred strains of mice by ABR threshold analyses. *Hear Res* **130**:94–107.